Acta Pharmaceutica Sinica B 2026;16(6):3425−3472

Chinese Pharmaceutical Association
Institute of Materia Medica, Chinese Academy of Medical Sciences

Acta Pharmaceutica Sinica B

www.elsevier.com/locate/apsb
www.sciencedirect.com

REVIEW

Smart responsive hydrogels combined with AI design for tumor therapy

Qingquan Wang, Jiaqi Li, Nianping Feng*, Yongtai Zhang*

School of pharmacy, Shanghai University of Traditional Chinese Medicine, Shanghai 201203, China

Received 1 October 2025; received in revised form 8 December 2025; accepted 11 December 2025

KEY WORDS

Functionalised hydrogels;
Smart responsive materials;
Cancer;
Characterization methods;
Combination therapy;
Precision medicine;
AI;
Clinical translation

Abstract Advances in cancer therapy have underscored the critical need for multifunctional platforms that enable precise targeting, controlled drug release, and immunomodulation. Hydrogels, as transformative tools with programmable drug release capabilities, microenvironmental responsiveness, and immunoregulatory properties, demonstrate broad application prospects. This review focuses on the design and application of functionalized hydrogels, emphasizing their responsiveness to multiple stimuli, including temperature, pH, reactive oxygen species (ROS), and enzymes. It provides an in-depth analysis of their multimodal synergistic therapeutic mechanisms, including photothermal therapy, immunotherapy, starvation therapy, intelligent detection, targeted capture, and tumor microenvironment (TME) simulation. Meanwhile, recent developments in machine learning-enabled intelligent hydrogel technologies have driven the transformation of materials into intelligent systems with "smart design-perception-decision" capabilities. Although the literature on smart hydrogels has made significant progress in exploring mechanisms and optimizing performance, systematic reviews of artificial intelligence (AI)-driven platforms remain notably lacking. This paper systematically summarizes the regulatory strategies of material-derived intelligent hydrogels, AI-enabled mechanisms, and practical application cases, revealing core challenges and future development directions, thereby providing theoretical guidance and practical pathways for next-generation hydrogels in personalized and multimodal cancer therapy.

*Corresponding authors.
E-mail addresses: analysisdrug@126.com (Yongtai Zhang), npfeng@shutcm.edu.cn (Nianping Feng).

Peer review under the responsibility of Chinese Pharmaceutical Association and Institute of Materia Medica, Chinese Academy of Medical Sciences.

https://doi.org/10.1016/j.apsb.2026.02.019

1. Introduction

According to The Cancer Atlas, 4th edition, published by the International Agency for Research on Cancer, over 18 million new cancer cases were diagnosed globally in 2022, with lung, breast, colorectal, and prostate cancers being the most common types (Fig. 1A and B)[1–5]. In the United States specifically, as of January 1, 2025, there were approximately 18.6 million cancer survivors, a number projected to exceed 22 million by 2035[3]. Although conventional therapies, including surgery, chemotherapy, and radiotherapy, remain the cornerstone interventions, their clinical utility is limited by inherent limitations[6]. Surgical resection is adequate in debulking tumors but cannot eradicate disseminated cancer cells. Chemotherapeutic agents have systemic antitumor activity but also induce off-target cytotoxicity in normal tissues, and their long-term effectiveness is frequently compromised by chemotherapy resistance[7]. Radiotherapy precisely targets tumors, but carries the risk of lung inflammation and heart damage. Treatment success is commonly compromised by radiotherapy resistance, driven by factors such as tumor hypoxia, enhanced DNA damage repair pathways, and resilient cancer stem cell populations, which often lead to local recurrence and metastatic progression[8].

With the advancement of science and technology, new strategies such as nanoparticles, cancer vaccines, antibody–drug conjugates, and hydrogel-based drug delivery systems are reshaping therapeutic paradigms[9–11]. Hydrogels offer significant advantages: (1) their injectable porous matrix enables localised drug encapsulation and sustained release kinetics, minimising systemic toxicity while maintaining therapeutic efficacy; (2) biodegradability ensures complete metabolic clearance without residual foreign body effects[12]; and (3) functional modifications by ligand conjugation or microenvironment responsive design allow precise targeting of neoplastic cells and tumor-specific niches[13].

Hydrogels are a class of polymeric materials formed by the chemical or physical crosslinking of hydrophilic polymers. They can swell rapidly in an aqueous environment while maintaining their structural integrity and mechanical properties. These hydrophilic polymer matrices are broadly classified into natural and synthetic types based on their precursor origin (Table 1)[14]. Natural hydrogels-including gelatin (GA), alginate (ALG), chitosan (CS) and agar-are derived from biopolymers with inherent advantages in biocompatibility and biodegradability. Synthetic hydrogels are artificially synthesised polymers produced by methods such as radical polymerisation or ionic crosslinking. Common examples include polyvinyl alcohol, polyacrylamide, polyvinyl pyrrolidone, and polyethylene glycol (PEG)[15]. Artificial synthesis methods can precisely control the polymer chain

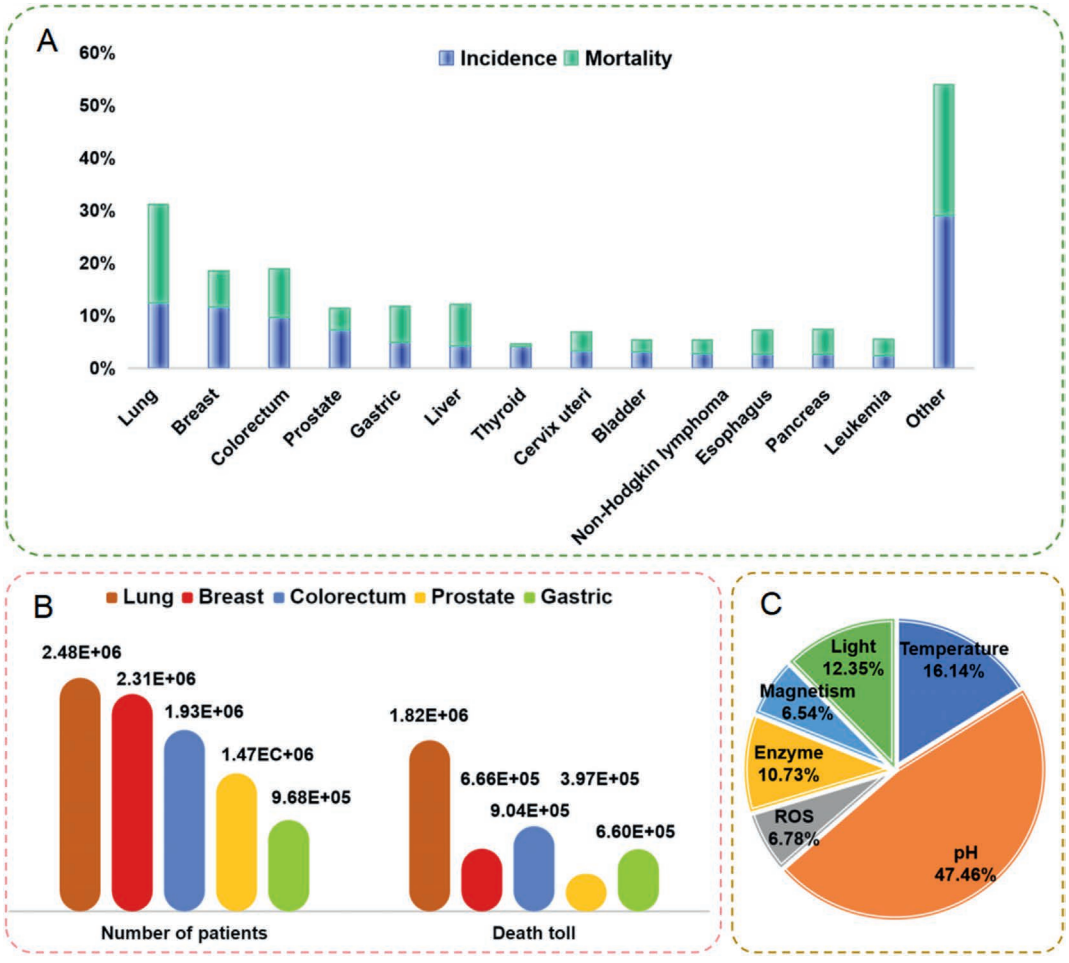

Figure 1 Analysis of global cancer prevalence data for 2022 and preclinical research statistics of hydrogels for cancer treatment up to 2025. (A) Incidence and mortality rates for the 10 most commonly diagnosed cancers worldwide in 2022. (B) The number of cases and deaths from the five most common cancers worldwide in 2022. (C) Research statistics of different responsive hydrogels used in cancer treatment up to 2025[1–5].

Table 1 The advantages and disadvantages of natural and synthetic polymer hydrogels.

	Natural polymer hydrogels	Synthetic polymer hydrogels	Ref.
Advantages	Excellent biocompatibility; intrinsic bioactivity; biodegradability; abundant sources; easy chemical modification	Superior mechanical properties; highly customizable; good batch-to-batch consistency; excellent processability; well-defined structure	17,18
Disadvantages	Weak mechanical strength; significant batch variations; poor stability; potential biological risks; difficult performance control	Low bioactivity; limited biocompatibility; restricted degradability; reliance on chemical modification	19,20

structure at the molecular level, allowing systematic optimisation of key hydrogel parameters such as mechanical strength, swelling rate, degradation kinetics, and host compatibility[16]. This molecular engineering paradigm has created smart hydrogels with new capabilities (Fig. 1C) (Table 1[17−20]).

With the advent of the Fourth Industrial Revolution and profound transformations in materials science, the exploration of human-machine interaction, machine learning, and neural network technologies is driving a revolutionary change in the field of materials[21−23]. The application of AI in hydrogel research has increasingly become a forefront topic in academia. In particular, machine learning (ML) methods have gradually been integrated into the design and performance optimization of hydrogels[24]. Leveraging big data-driven material property prediction and intelligent regulation, AI has not only significantly accelerated the development of intelligent hydrogels but also enhanced their responsiveness and therapeutic efficacy in complex biological environments[25]. By constructing mathematical models, AI can systematically describe the structure-property relationships of hydrogels and predict their behavior under various conditions, thereby providing a scientific basis for material design[26]. These AI-enabled intelligent hydrogel systems can achieve precise sensing and dynamic modulation of the TME, promoting the innovation and implementation of multimodal cancer therapy strategies. Moreover, the application of AI effectively reduces research and development costs and enables precise manufacturing of materials, facilitating the translation of hydrogel materials into clinical use[27]. Introducing AI technology into the design of cancer treatment hydrogels not only represents a significant direction in the development of intelligent biomaterials but also demonstrates broad scientific value and promising application prospects.

With the continuous advancement of cancer treatment technologies, functionalized hydrogels have emerged as cutting-edge materials in antitumor research due to their unique stimuli-responsive properties and multifunctionalities. This review explores the design strategies and preparation methods for functionalized hydrogels and their applications in various antitumor therapeutic approaches, aiming to provide new insights and techniques for cancer therapy. In addition, we focus on integrating hydrogels with AI to develop intelligent systems, in which data-driven design and deep behavioral analysis endow hydrogels with novel intelligent functionalities.

2. Design and preparation of responsive hydrogels

Stimuli-responsive hydrogels have emerged as promising candidates for intelligent drug delivery systems due to their specific responsiveness to the TME[28,29]. The unique pathophysiological characteristics of TME provide ideal targets for the development of innovative materials. For example, thermoresponsive hydrogels can exploit local hyperthermia induced by rapid tumor cell proliferation and by the effects of radiotherapy to achieve site-specific drug release[30,31]. pH-sensitive hydrogels can exploit the markedly lower pH of the TME to swell or degrade specifically in the acidic tumor milieu, thereby achieving precise drug release[32]. Furthermore, aberrant metabolic activity, hypoxic conditions, and chronic inflammation within the TME synergistically create an ROS-rich microenvironment, with concentrations typically 10−100 times higher than physiological levels. Based on this, some ROS-responsive hydrogels can achieve controlled drug release by cleaving oxidation-sensitive bonds within their molecular structures[33]. These intelligent, responsive mechanisms enhance tumor targeting efficiency and minimise systemic toxicity, thereby establishing a new therapeutic paradigm in precision oncology.

2.1. *Thermoresponsive hydrogels*

Thermoresponsive hydrogels exhibit distinct phase-transition behaviour upon thermal stimulation (Table 2). The temperature threshold that induces this transition is known as the critical solution temperature. Based on their transition patterns, hydrogels can be classified into two categories: lower critical solution temperature (LCST) hydrogels and upper critical solution temperature (UCST) hydrogels[34]. The characteristic behaviour of LCST hydrogels exists in the sol state when the ambient temperature is below the LCST. When the ambient temperature exceeds the LCST, they dehydrate and collapse into a gel-like state due to enhanced hydrophobic interactions between the polymer chains (Fig. 2A). A prominent example is poly(*N*-isopropyl acrylamide) (PNIPAM), which exhibits LCST properties near physiological temperature (approximately 32 °C)[35]. UCST hydrogels show the opposite behaviour, swelling above their critical temperature and contracting below it. UCST dominant phase transitions are relatively rare in thermoresponsive hydrogel systems.

A variety of thermoresponsive hydrogel matrix materials have been developed. Both PNIPAM and poly(*N*,*N*-diethylacrylamide) exhibit temperature-driven phase transitions governed by the competitive interplay between hydrophilic and hydrophobic moieties. In PNIPAM, hydration is mediated by hydrogen bonding between the amide groups (−CONH−) and water molecules. Below the LCST, hydrogen bonding predominates, maintaining PNIPAM in a swollen and dissolved state. Above this threshold, thermal disruption of hydrogen bonding allows the hydrophobic isopropyl groups, $-CH(CH_3)_2$, to induce dehydration-induced contraction *via* interchain aggregation[36]. Similarly, in poly(*N*,*N*-diethylacrylamide) systems, stabilisation is mainly achieved by hydrogen bonding between amide groups and water molecules. As the temperature increases, the hydrogen bonds are broken. Meanwhile, interactions between the hydrophobic ethyl groups

Table 2 Types and properties of thermoresponsive hydrogels.

Materials	Responsiveness	Intermolecular forces	Phase transition conditions	Ref.
Poly(*N*-isopropylacrylamide)	LCST	Hydrogen bonding and hydrophobic interactions	32 °C	35
Poly(*N*,*N*-diethylacrylamide)	LCST	Hydrogen bonding and hydrophobic interactions	33 °C	37
Poly(lactic-*co*-glycolic acid)	LCST	Hydrogen bonding and hydrophobic interactions	>30 °C, explicitly determined by the polymerisation ratio of the compound.	39
Poly(sulfobetaine) hydrogel	UCST	Electrostatic adsorption	20−60 °C, explicitly determined by the degree of sulfonation of the groups.	46
Poly(acrylamide-*co*-acrylic acid)	UCST	Hydrogen bonding and hydrophobic interactions	20 −70 °C, explicitly determined by the polymerisation ratio of the compound.	48
poly(*N*-npropylmethacrylamide)	LCST	Hydrogen bonding and hydrophobic interactions	28 °C	53
Poloxamers	LCST	Hydrogen bonding and hydrophobic interactions	>20 °C, explicitly determined by the polymerisation ratio of the compound.	54
CS and β-GP	LCST	Proton transfer and electrostatic repulsion	37 °C	55
Hydroxybutylchitosan	LCST	Hydrogen bonding and hydrophobic interactions	50 °C	56
Arg-Gly-Asp modified hydroxybutylchitosan	LCST	Hydrogen bonding and hydrophobic interactions	37 °C	57
Elastin-like polypeptide	LCST	Hydrogen bonding and hydrophobic interactions	25−60 °C, explicitly determined by the polymerisation ratio of the compound.	58
Poly(*N*-vinyl caprolactam)	UCST	Hydrogen bonding and hydrophobic interactions	34 °C	59

LCST, lower critical solution temperature; UCST, upper critical solution temperature; CS,chitosan; β-GP, β-glycerophosphate; Arg, arginine; Gly, glycine; Asp, aspartic acid.

($-C_2H_5$) are enhanced, causing the polymer chains to aggregate and lose their hydration layers[37,38].

Poly(lactic-*co*-glycolic acid) (PLGA), a copolymer synthesised *via* ester bonds between lactic acid and glycolic acid, exhibits phase transition behaviour and physical properties that are determined by the lactic acid/glycolic acid ratio. Higher lactic acid content increases the LCST due to the increased hydrophobicity and crystallinity of the lactic acid units[39,40]. Similarly, thermoresponsive polymers derived from 2-(2-methoxyethoxy)ethyl methacrylate and oligo(ethylene glycol) methacrylate undergo conformational rearrangements upon heating. At low temperatures, the ethylene glycol side chains adopt a twisted conformation that positions the hydrophilic ether oxygen groups (−O−) outwards while minimising the exposure of the hydrophobic backbone, thereby increasing hydrophilicity. At the same time, the multiple ethoxy ($-CH_2CH_2O-$) units in 2-(2-methoxyethoxy)ethyl methacrylate and oligo(ethylene glycol) methacrylate form strong hydrogen bonds with water molecules, stabilising the extended polymer chains. These hydrogen bonds weaken upon heating, allowing hydrophobic backbones to aggregate into micellar structures *via* intermolecular interactions, thereby driving the sol−gel phase transition[41,42].

The mixture of CS and β-glycerophosphate (β-GP) exhibits temperature-sensitive gelation ability. Below the LCST, the protonated amino groups ($-NH_3^+$) on CS form hydration shells *via* hydrogen bonding with H_2O, and the glycerol hydroxyls provide steric stabilisation. Above the LCST, deprotonation reduces the electrostatic repulsion between the chains. The glycerol hydroxyl groups competitively sequester H_2O, and the hydrophobic groups aggregate to form intramolecular hydrogen bonds, driving the gelation process[43]. In addition, chemical modification of CS can confer thermoresponsiveness. Hydroxybutylchitosan is a derivative of CS obtained by reacting the hydroxyl groups (−OH) of CS with 1,2-epoxybutane to introduce hydrophobic hydroxybutyl groups. When the temperature exceeds the LCST, the hydrophobic interactions between the hydroxybutyl groups are enhanced, leading to aggregation of the hydroxybutylchitosan polymer chains and subsequent gelation[44].

Hydrogels with UCST properties exhibit inverse phase transition mechanisms. They remain insoluble below the UCST and dissolve above the UCST. This behaviour is caused by strong intermolecular interactions, such as covalent bonds, electrostatic attractions, and hydrophobic associations, which stabilise the collapsed polymer network[45]. A typical example is the polysulfobetaine hydrogel, whose backbone contains positively charged quaternary ammonium groups and negatively charged sulfonic acid groups. At low temperatures, these oppositely charged groups form strong electrostatic interactions (such as ion pairs or dipole-dipole interactions), thereby forming a cross-linked gel network[46,47]. Another UCST system, the poly(acrylamide-*co*-acrylic acid) hydrogel, exhibits thermoresponsiveness driven by hydrogen bonding. The copolymer contains both carboxylic acid (−COOH) and amide ($-CONH_2$) groups. Under acidic conditions (pH $<$ 3) and temperatures below UCST, protonated carboxyl groups form interchain hydrogen bonds with amide groups, inducing crosslinking and stabilising the gel phase[48,49].

In particular, the phase transition temperature (LCST or UCST) of thermoresponsive hydrogels can be precisely tailored to meet specific application requirements using a variety of strategies. Firstly, the phase transition temperature of hydrogels can be

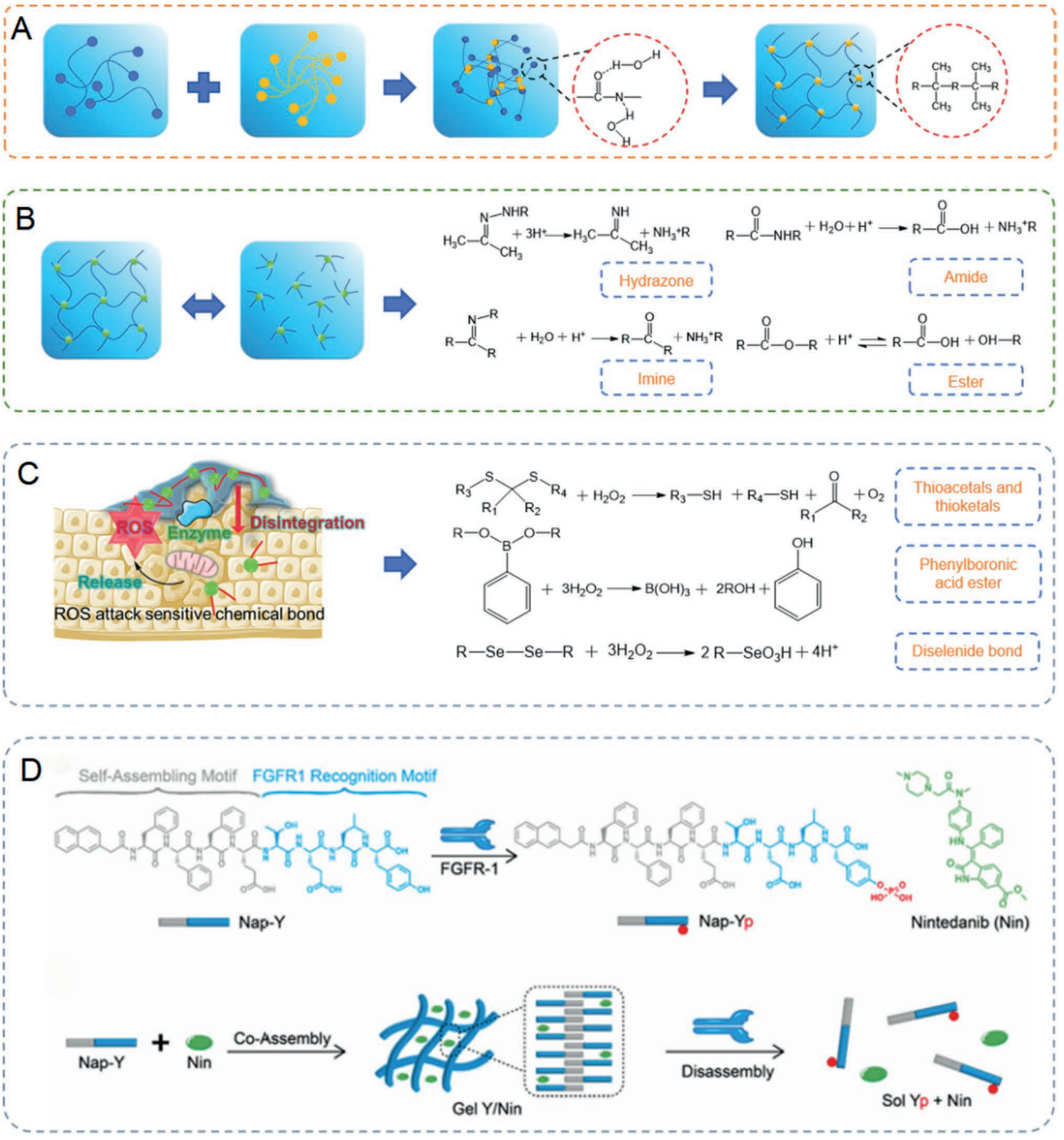

Figure 2 Phase transition mechanism of the responsive hydrogels. (A) The simple phase transition mechanism of thermoresponsive hydrogels-PNIPAM. (B) The simple phase transition mechanism of pH-responsive hydrogels. (C) The simple phase transition mechanism of ROS-responsive hydrogels. (D) Structural diagram of hydrogel and enzyme-responsive hydrolysis mechanism. Reprinted with permission from Ref. 108. Copyright © 2024 American Chemical Society.

precisely controlled by modifying the chemical structures of the polymers. This can be achieved by several strategies, including the introduction of hydrophilic or hydrophobic groups, adjustment of the copolymer monomer ratio, design of block or graft structures, and control of molecular weight[50,51]. The presence of salts, ionic strength, and pH can significantly influence interpolymer chain interactions and thereby modulate the phase transition temperature. For example, the salting-out effect can lower the LCST[52].

2.2. *pH-responsive hydrogels*

pH-responsive hydrogels are a class of intelligent polymeric materials that can swell, contract, or dissolve in response to changes in environmental pH (Table 3)[60]. This responsiveness is primarily due to the ionisable functional groups incorporated into their polymer chains, including hydrazone, imine, ester, and amide linkages (Fig. 2B). Hydrazone (C═NNHR) is a class of

Table 3 Components and properties of some pH-responsive hydrogels.

Reactive groups	Intermolecular forces	Reaction mechanism	Typical hydrogels	Ref.
Azine bond (C═NNHR)	Ionisation effect	Under acidic conditions, the C═N double bond is susceptible to proton attack, leading to bond cleavage.	Acyl hydrazone hyaluronic acid hydrogel	61
Imine bond (−C═N−)	Ionisation effect	Under acidic conditions, the C═N double bond is susceptible to proton attack, leading to bond cleavage.	Oxidised sodium ALG carboxymethyl chitosan hydrogel	62
Ester linkage (R−COO−R′)	Ionisation effect	Ortho esters are hydrolysed under acidic conditions to produce carboxylic acids and alcohols.	Polyacrylate hydrogel; Polyethylene glycol-polylactic acid hydrogel	63
Amino group ($-NH_2$)	Electrostatic and hydrogen bonding interactions.	Hydrogel swelling is caused by electrostatic repulsion between protonated $-NH_3^+$ groups, while contraction arises from hydrogen bonding and hydrophobicity in deprotonated $-NH_2$ states.	Polyethyleneimine hydrogel.	67
Amide linkage (−CONH)	Ionisation effect	The nitrogen atom in the amide linkage can accept a proton (H^+) to form an amide cation, which can then be attacked by a nucleophile, leading to cleavage.	3-Aminophenylboronic acid modified human-like collagen hydrogel	72
Carboxyl group (−COOH)	Electrostatic and hydrogen bonding interactions.	Hydrogel swelling is triggered by electrostatic repulsion between deprotonated −COO− groups, while contraction results from hydrogen bonding and hydrophobicity in protonated −COOH states.	Polyacrylic acid hydrogel and polymethacrylic acid hydrogel.	73,74

Abbreviations: ALG, alginate.

compounds formed by the condensation of hydrazine with an aldehyde or ketone. Their C═N double bond is readily broken by protonation under acidic conditions. Notably, hydrazone bonds are more stable under physiological conditions (pH 7.4) than ester, vinyl ether, or imine bonds[61]. The imine linkage (−C═N−) is formed by condensation of the aldehyde with the primary amine. As a dynamic bond, it remains stable under physiological pH conditions, but is highly susceptible to cleavage in acidic environments[62]. The ester linkage is formed by dehydration condensation between alcohol and acid. Under acidic conditions, it can be hydrolysed to form carboxylic acid and alcohol[63]. Amide bonds (−CONH−), formed from reactions between carboxylic acids and amines, hydrolyse in acidic environments *via* a two-step mechanism. Protonation of the amide nitrogen produces a cationic intermediate, which is subsequently subjected to nucleophilic attack to form a tetrahedral transition state, which finally decomposes into carboxylic acid and amine products[64]. Based on the specific degradation pathways of these bonds, pH-responsive hydrogels can exhibit targeted stimulus-responsive behaviour under pathophysiological conditions.

Protonation is a common mechanism for pH-triggered drug release from hydrogels. Common protonatable functional groups include carboxyl (−COOH), amino ($-NH_2$), sulphonate ($-SO_3H$), and imidazole moieties. Protonation or deprotonation of these groups at varying pH induces significant changes in molecular chain conformation, charge distribution, stability, and solubility[65,66]. In particular, when the functional groups on the polymer chains carry similar charges, increased electrostatic repulsion drives hydrogel swelling. Conversely, when the functional groups are uncharged, hydrogen bonding and hydrophobic interactions enhance hydrogel contraction. For example, poly(acrylic acid) (PAA) and poly(methacrylic acid) hydrogels, which are rich in −COOH groups, exhibit swelling behaviour at high pH and contraction at low pH. Polyethyleneimine hydrogels, which are rich in $-NH_2$ groups, show an opposite swelling pattern[67,68].

In some cases, hydrogels made from a single polymer have minor shortcomings, such as insufficient pH responsiveness, poor mechanical properties, and instability[69]. To address these shortcomings, researchers have developed block copolymer-based hydrogels that exploit precise molecular design and microphase-separated architectures to provide flexibility and adaptability for practical applications. One notable example is poly(lactic-*co*-glycolic acid)-*block*-PAA, which is composed of a hydrophobic PLGA block (providing mechanical reinforcement) and a hydrophilic PAA block (containing −COOH groups). Below pH 4.5−5.0, protonated −COOH groups increase intra-chain hydrogen bonding and hydrophobic interactions, causing the hydrogel to collapse[70]. In addition to synthetic polymers, engineered peptide hydrogels such as L5 (Ac−KPVFQFLFHE−NH_2) exhibit pH-triggered self-assembly behaviour. Under neutral conditions, L5 assembles *via* $\pi-\pi$ stacking, electrostatic forces, and hydrogen bonding. In acidic environments (pH $<$ 5.5), lysine and histidine residues protonate, generating positive charges that disrupt supramolecular organisation and induce gel dissolution[71].

2.3. *ROS-responsive hydrogels*

ROS play dual physiological and pathological roles in cellular signalling, immune responses, and oxidative stress pathways in biological systems[75]. The molecular structures of ROS-responsive hydrogels typically contain ROS-sensitive groups or chemical bonds that can undergo selective degradation or chemical modification in the presence of ROS, thereby inducing structural changes in the hydrogel (Fig. 2C)[76].

Hydrogels containing thiol functional groups within their polymer networks exhibit significant ROS responsiveness because these functional groups undergo preferential oxidative cleavage when attacked by ROS[77]. For example, thioether groups (−S−) are progressively oxidised to sulfoxide (−SO−) and sulfone ($-SO_2-$) moieties under H_2O_2 exposure, whereas thioacetal/thioketal bonds undergo oxidative cleavage in ROS-rich environments to yield ketones/aldehydes and free thiols (−SH)[78,79]. Disulfide bonds, although stable under oxidative conditions, undergo reductive cleavage in glutathione (GSH)-mediated reducing environments to regenerate sulfhydryl groups[80].

Compounds with phenylboronic acid functional groups can form ROS-responsive hydrogels with diol-containing compounds (*e.g.*, glucose, sorbitol, and polyvinyl alcohol) through reversible boronate ester bonds. These boronate ester bonds undergo H_2O_2-mediated redox reactions in ROS-rich microenvironments, yielding phenolic derivatives and boronic acid. This structural transition converts the trigonally coordinated boronate to a tetrahedrally configured boronic acid, culminating in network disintegration through permanent bond rupture[77,81,82].

The ROS sensitivity of hydrogels using selenides as crosslinking sites is primarily dependent on the ROS sensitivity of selenium[83]. In these hydrogels, crosslinking is predominantly facilitated by intermolecular diselenide bonds, with common cross-linkers including selenocysteine and selenocysteine[84]. Under the influence of ROS, selenium atoms within diselenide bonds undergo oxidation to form selenoxides, which can be further converted to selenones[85].

In addition to the ROS-responsive functional groups mentioned above, some components remain underexplored. Zhang et al.[86] pioneered a ROS-labile polymer system using poly(deca-4,6-diynedioic acid), which undergoes ROS-triggered cleavage to yield biocompatible succinic acid. Robby's group[87] developed a hydrogel containing MnO_2 nanoparticles and PAA, in which the MnO_2 nanoparticles initially suppress hydrogen-bond-mediated crosslinking through carboxylate coordination. GSH present in cancer cells can reduce MnO_2 to Mn^{2+} ions, thereby removing the hydrogen bond inhibition. Subsequently, Ca^{2+}-phosphate complexation between the $CaCl_2$ and Na_2HPO_4 components within the system drives rapid reconstitution of the hydrogel network *via* supramolecular coordination.

Hydrogel nanoparticles circulating *in vivo* combine the high drug-loading capacity of hydrogels with the prolonged circulation and targeting capabilities of nanocarriers, making them a recent research focus[88–91]. The targeting ability of such hydrogel nanoparticles often relies on elevated ROS levels in the TME[92]. However, ROS is not a tumor-specific marker, as high ROS levels are also present in non-cancerous lesions such as inflammation and infection, resulting in a lack of exclusivity for tumor-triggered activation[93,94]. To address this challenge, current strategies mainly involve synergistic responsiveness and active targeting. By exploiting multiple pathological features specific to the TME, such as acidic pH, elevated GSH levels, and overexpression of MMP-2/9, multi-responsive hydrogel nanoparticles are designed to require the simultaneous activation of multiple stimuli for drug release, thereby enabling more precise, targeted therapy[95]. Additionally, physical enrichment and isolation are achieved through tumor ligand modification, cell membrane camouflage, or intratumoral *in situ* injection, ensuring that the hydrogel is activated exclusively at the target site[96,97]. Such integrated designs significantly enhance the spatiotemporal specificity of drug release, effectively minimizing off-target release and associated toxicity in non-target tissues.

2.4. *Enzyme-responsive hydrogels*

During cancer progression, the expression of several matrix metalloproteinases (MMPs) is significantly upregulated[98]. These enzymes are zinc-dependent proteases that can specifically hydrolyse a variety of proteins in the extracellular matrix (ECM), thereby degrading ECM components, disrupting cell-cell adhesion, and promoting cancer cell invasion and metastasis[99]. The key to designing MMP-responsive hydrogels is to introduce specific cleavage sites for MMPs into the hydrogel system, which can be achieved by incorporating the appropriate responsive peptide sequences[100,101]. Gelatinase B (MMP-9), a secreted type of collagenase within the MMP superfamily, exhibits preferential proteolytic activity towards denatured collagen and gelatinous ECM components during pathological tissue remodelling[102]. Common response sequences for MMP-9 include GPLG/IAGQ and PLG/LAG[103,104]. Lin et al.[105] developed an MMP-9 responsive hydrogel consisting mainly of oxidised hyaluronic acid and hydrazide-functionalised gelatin. Collagen-derived peptide sequences in hydrazide-functionalised gelatin confer hydrogel responsiveness to MMP-9.

Transglutaminase is a protein crosslinking enzyme that is widely distributed in humans, animals, plants, and microorganisms. This enzyme catalyses crosslinking reactions between or within protein molecules, thereby improving the structural and mechanical properties of the ECM[106]. Davis and colleagues[107] developed a two-component hydrogel system consisting of lysine-rich and glutamine-rich peptide polymers that undergo rapid enzymatic crosslinking upon transglutaminase activation. Rheological characterisation by frequency sweep analysis after 1 h of gelation revealed stabilised storage moduli of around 10 kPa, demonstrating the rapid establishment of mechanically robust network structures. Scanning electron microscopy imaging confirmed the development of interconnected porous architectures by spontaneous assembly after crosslinking. Fibroblast growth factor receptor 1 is an attractive molecular target for the treatment of non-small cell lung cancer. Tang et al.[108] rationally designed an octapeptide gelator, Nap-Phe−Phe−Phe−Glu−Thr−Glu−Leu−Tyr-OH, which was co-assembled with nintedanib to form a supramolecular hydrogel. Upon local microinjection into the A549 tumor site, the gelator in the hydrogel can be specifically recognised and phosphorylated by the highly expressed fibroblast growth factor receptor 1 on the A549 cell membrane, thereby triggering the degradation of the hydrogel and the local, sustained release of nintedanib. Both cellular and animal experiments showed that this kinase-responsive supramolecular hydrogel significantly enhanced the therapeutic efficacy of nintedanib against A549 tumors (Fig. 2D).

Enzyme-responsive hydrogels are primarily constructed from peptides and their derivatives that use endogenous enzymes as biological triggers to control hydrogel formation or degradation. These systems exhibit high sensitivity to enzymatic activity, allowing precise control of material behaviour through hydrophobicity adjustment, charge modification, and disassembly of self-assembling units. Such responsiveness enables dynamic phase transitions in disease-specific contexts, making them promising candidates for targeted therapy and controlled drug release[109,110].

2.5. *Photoresponsive hydrogels*

Photoresponsive hydrogels are smart materials that incorporate light-sensitive groups or photothermal nanoparticles, and their light-penetration depth and response mechanisms vary with the

wavelength of the light source. Ultraviolet (UV) light has a penetration depth on the micrometer scale and high energy, capable of inducing bond cleavage, isomerization, and crosslinking reactions, making it suitable for surface-level applications[111,112]. Visible light can penetrate up to the millimeter scale and exhibits low toxicity, making it appropriate for applications in shallow tissues[113]. Near-infrared (NIR) light, especially within the second NIR window, can penetrate tissues on the centimeter scale, demonstrating great potential for photothermal therapy and photoacoustic imaging[114,115]. The primary photoresponse mechanisms include photothermal effects and photochemical effects. The photothermal effect converts light energy into heat through materials such as gold nanoparticles, carbon nanotubes, graphene, or photothermal dyes. This heat generation induces volumetric phase transitions or changes in crosslinking density in temperature-sensitive hydrogels, such as PNIPAM[116]. Photochemical hydrogels instead leverage non-thermal photochemical processes to directly tune their network structure, with primary mechanisms including molecular isomerization, photocleavage of caged molecules, and light-triggered polymerization[117]. For example, azobenzene undergoes reversible *cis*−*trans* isomerization under UV light, altering the rigidity of the polymer network[118]. Spiropyran exhibits reversible ring-opening and closing under UV irradiation, triggering sol−gel transitions[119]. Photocleavable molecules such as coumarin and *o*-nitrobenzyl alcohol break chemical bonds upon light exposure, releasing reactive groups, such as thiols or aldehydes, that initiate crosslinking or degradation[120].

2.6. Multiresponsive hydrogel

Due to the complexity of the physiological environment, single-responsive hydrogels often fail to achieve the desired therapeutic effects. Deep tumor therapy has set higher requirements for tissue penetration depth and the targeting accuracy of response mechanisms (Table 4). In contrast, multi-responsive hydrogels can more effectively target patient lesions for treatment. By integrating multiple stimulus-responsive mechanisms or nanofunctional units, these hydrogels enable synergistic responses to various signals, including temperature, pH, light, and ionic strength. For example, Kharkar et al.[121] prepared thiol- and photosensitive-degradable hydrogels *via* a Michael-type addition reaction between maleimide and thiol-terminated 4-arm polyethylene glycol to control the release of a model drug from fluorescent nanoadsorbents. The central degradable functional units of the prepared hydrogel are ortho-nitrobenzyl acetate and a thiol-cleavable phenylacetic acid based on a thioether-succinimide linkage, which undergo irreversible cleavage upon light irradiation and reaction with GSH, respectively. These changes trigger rapid degradation of the hydrogel, subsequently leading to the release of the model drug. Huang et al.[122] constructed a pH/redox dual-responsive hydrogel, LPL-CDE, by crosslinking poly(L-lysine) isophthalamide with disulfide-containing L-cystine dimethyl ester dihydrochloride *via* an EDC/NHS coupling reaction. After loading the hydrogel with a magnesium nanoemulsion, approximately 20.4% of magnesium ions were released in simulated gastric fluid and 30.8% in simulated intestinal fluid. When 1,4-dithiothreitol was added to the simulated intestinal fluid as a reducing trigger, the release rate significantly increased to 72.5%, confirming its dual-responsive properties. Liang et al.[123] prepared a pH/glucose dual-responsive hydrogel by crosslinking phenylboronic acid/benzaldehyde-modified polyethylene glycol-poly(glycerol sebacate) copolymer with dihydrocaffeic acid/L-arginine-modified CS derivative *via* Schiff base and boronate ester bonds. Under acidic conditions, the Schiff base bonds in the network dissociate, while glucose competitively disrupts the boronate ester bonds, and the two mechanisms synergistically regulate drug release.

3. Characterization methods of smart responsive hydrogels

The performance of hydrogels is determined by multiscale factors, including chemical composition, crosslinking density, network structure, and swelling state[132]. However, with the rapid development of new materials, traditional single-characterization techniques have become insufficient to comprehensively elucidate their complex structure−property relationships. Therefore, establishing a multiscale characterization system spanning from the molecular level to macroscopic properties is of great significance for revealing the structure-property relationships of hydrogels and optimizing design criteria.

3.1. Swelling

The swelling behavior of hydrogels is quantitatively evaluated through mass swelling ratio, water content, and volume swelling

Table 4 Comparison of response mechanisms for deep tumor treatment.

Response mechanism	Trigger conditions	Efficacy in deep tumors	Key challenges	Ref.
pH	TME pH 6.5−6.8	Moderate to good	Small pH difference (0.2−0.4 units); tumor heterogeneity; irreversibility issues	124,125
Thermoresponsive	40−42 °C	Good (with deep-penetrating energy sources)	Requires external heating equipment; temperature control precision, and safety concerns	126,127
ROS-responsive	Intracellular GSH 2−10 mmol/L; ROS levels 10−100 × higher than normal	Moderate	Complex biological environment; tumor heterogeneity; difficult controllability	128
Enzyme-responsive	Overexpressed enzymes (glycosidases, proteases, etc.)	Moderate	Difficult response time control; enzyme activity regulation; heterogeneity	129
Light-responsive	Specific wavelength irradiation (UV/NIR)	Poor (penetration depth <1 cm)	Limited tissue penetration; clinical translation barriers	130,131

Abbreviations: TME, tumor microenvironment; GSH, glutathione; ROS, reactive oxygen species; UV, ultra-violet; NIR, near infra-red.

ratio[133]. Swelling kinetics are fitted using the Schott or Peleg models[134]. The crosslinking density (Ve, number of effective crosslinks per unit volume) is inversely proportional to the molecular weight of the network chains[135]. This relationship is quantitatively described by the Flory-Rehner theory[136].

3.2. Mechanical properties

3.2.1. Macroscopic mechanical properties

Compression Testing: Used to evaluate the load-bearing capacity of hydrogels, with a strain rate typically set at 10−100 mm/min. For highly hydrated gels, low-stress loading should be employed to prevent water extrusion[137].

Tensile Testing: Characterizes fracture strength, elongation, and toughness. High-toughness hydrogels (*e.g.*, double-network gels) can exhibit elongations exceeding 1000%[138].

3.2.2. Rheology

Dynamic rheology is the gold standard for characterizing hydrogel viscoelasticity, enabling comprehensive analysis of network structure through multi-mode collaborative testing. In curing process monitoring, time-sweep mode facilitates *in-situ* tracking of sol-gel transition kinetics, accurately capturing the crossover point between storage modulus (G′) and loss modulus (G″)-the gel point-which marks the initial formation of three-dimensional networks and the critical transition from liquid-like to solid-like behavior[139,140]. Frequency sweep evaluates gel stability; for an ideal hydrogel, the G′ in the plateau region should be essentially frequency-independent and significantly higher than G″, reflecting the permanence and structural uniformity of the chemical crosslinking network. In contrast, weak gels or physically crosslinked systems typically exhibit a decline in G′ and an increase in tanδ in the low-frequency region[141]. Strain sweep determines the linear viscoelastic region by progressively increasing oscillation amplitude; the maximum critical strain value at which G′ remains constant within this region directly reflects the gel's toughness limit and reversible deformation capacity, with network structure suffering irreversible damage beyond this threshold[142−144]. Building on this, step-strain cycles (low→high→low) enable systematic evaluation of self-healing performance, with the criterion being the percentage of G′ recovery to its initial value. After high-strain damage-recovery rates exceeding 80%, self-healing is generally considered excellent[145]. This property originates from the network's ability to rebuild through the reconstruction of dynamic covalent bonds and reversible non-covalent interactions[146].

Temperature sweep precisely determines the gelation temperature and phase-transition behavior; by monitoring abrupt modulus changes under programmed temperature control, it reveals polymer chain collapse-aggregation mechanisms and assembly-disassembly reversibility, making it particularly valuable for intelligent responsive design of thermosensitive hydrogels[147]. Rheometers equipped with photocuring modules further enable *in situ* monitoring of photo-responsive behavior, capturing in real time the modulus growth kinetics during photo-crosslinking[148]. Additionally, rotational test mode serves as a crucial complement to oscillatory mode, systematically characterizing shear-thinning behavior under increasing shear rates (0.001−100 s^{-1})[149]. The criterion is a significant decrease in viscosity with increasing shear rate, indicating reversible network dissociation under shear, a critical indicator of extrudability in 3D printing[150].

3.3. Microscopic morphology and structure

Multi-scale characterization techniques for hydrogel microstructure and nanostructure encompass scanning electron microscope (SEM), atomic force microscope (AFM), confocal laser scanning microscope (CLSM), each offering unique advantages and complementarity. SEM employs liquid nitrogen rapid vitrification freezing to suppress ice crystal nucleation, followed by freeze-drying sublimation to remove water, thereby maximizing preservation of the porous network skeleton[151]. Environmental scanning electron microscopy enables direct imaging of hydrated gels through high-humidity environments, circumventing drying stress but at the cost of limited resolution[152]. AFM can perform *in situ* scanning of three-dimensional gel surface topography in liquid environments such as PBS or deionized water, eliminating the need for drying and thereby altogether avoiding dehydration-induced damage to the microstructure[153]. This allows for an accurate reflection of *in situ* topological features in the swollen state, making it suitable for studies on mechanical matching at cell-material interfaces. CLSM uses fluorescence labeling to reconstruct swollen-state gels in 3D with high fidelity[154]. Multi-channel imaging clearly separates covalent and physical crosslinks and calculates connectivity even when porosity >90%[155].

3.4. Chemical structure characterization

The chemical and surface structural characterization of hydrogels primarily relies on the synergistic analysis of fourier transform infrared spectroscopy, nuclear magnetic resonance spectroscopy (NMR), small-angle X-ray scattering, and small-angle neutron scattering. Fourier transform infrared spectroscopy tracks the crosslinking reaction process and verifies functional group consumption and new bond formation through characteristic peak intensity changes and shifts[156]. Quantitative liquid-state NMR can calculate the crosslinking conversion rate and effective crosslinking density of hydrogels[157]; solid-state MAS NMR can evaluate the network uniformity of insoluble gels using relaxation times[158]; low-field NMR can non-destructively differentiate bound, restricted, and free water, analyze pore connectivity, and, when combined with PFG-NMR, accurately determine the self-diffusion coefficient of drug molecules[159]. Small-angle X-ray scattering uses electron density differences to study chain entanglements and nanofiller dispersion at sizes of 1−100 nm[160]. Small-angle neutron scattering uses deuterated solvents to improve contrast and reveal details about crosslink distribution and chain elasticity[161]. Together, these two techniques help build a multiscale model linking crosslink density, chain structure, and material properties.

3.5. Stimulus responsiveness characterization

The core of characterizing thermosensitive hydrogels lies in accurately capturing their phase-transition critical temperature, typically determined systematically using variable-temperature UV−Vis or dynamic light scattering[162]. In UV−Vis testing, the thermosensitive gel solution is heated at a programmed rate while monitoring transmittance changes at 500 nm; the temperature at which transmittance abruptly drops by 50% is defined as LCST[163]. Dynamic light scattering technology defines LCST by tracking the abrupt change in hydrodynamic radius of nanoparticles or molecular chains near the LCST. At temperatures near the LCST, particle size increases sharply by tens to hundreds of

nanometers[164]. The combined use of both techniques enables mutual validation. It reveals the multiscale transition mechanism of molecular chain collapse, aggregation, and macroscopic phase separation, providing key thermodynamic parameters for predicting the temperature-controlled behavior of thermosensitive hydrogels in applications such as smart drug delivery and tissue engineering scaffolds.

Systematic evaluation of pH-responsive hydrogels centers on establishing swelling profiles and apparent p*K*a values[165]. Hydrogel samples are incubated in a pH 2−10 buffer series at 37 °C until equilibrium, followed by precise gravimetric or volumetric measurements to construct Q-pH curves. The inflection point approximates the apparent p*K*a of network ionizable groups, with deviations from monomeric p*K*a indicating microenvironmental polarity and charge shielding within the crosslinked architecture[166]. Subsequent analysis incorporates charge-to-mass ratios to determine pH-dependent charge densities, which can be correlated with mechanical testing to elucidate electrostatic crosslinking effects on network rigidity[167]. This characterization paradigm is essential for the rational design of hydrogels in oral colon-targeted delivery (leveraging gastrointestinal pH gradients) and TME-responsive applications (acidic pH).

Characterization of ROS-responsive hydrogels centers on their specific recognition and scavenging capacity of ROS[168]. First, responsiveness is verified and molecular mechanisms elucidated by applying exogenous ROS to recapitulate oxidative stress microenvironments, while monitoring the kinetics of oxidative cleavage or structural transformation of characteristic functional groups (*e.g.*, boronic esters, thioketals, selenoethers, polyphenols) *via* ^{1}H NMR or UV−Vis[169]. Macroscopic performance responses were subsequently quantified through swelling ratio or degradation rate tests, constructing dose−response sensitivity curves complemented by rheological time-sweep measurements to track G′ decay, with the time required for 50% modulus reduction defined as the response half-life[170].

The characterization of enzyme-responsive hydrogels primarily focuses on the specific recognition of substrates and the precise quantification of enzymatic degradation kinetics[171,172]. Initially, gel electrophoresis or mass spectrometry is employed to verify changes in the molecular weight of enzymatically cleaved peptide substrates within the hydrogel network, confirming both the accessibility of enzyme recognition sites and reaction specificity[173]. Subsequently, enzyme kinetic parameters (K_m, V_{max}) are determined using fluorophore-labeled peptide substrates. Macroscopic degradation behavior is quantified by monitoring the swelling ratio or mass loss over time in enzyme-containing buffer[174,175]. Degradation half-life profiles at varying enzyme concentrations have been established. At the same time, time-sweep oscillatory rheometry is used to track the real-time decay kinetics of G′, where the rate of modulus reduction reflects the efficiency of crosslink cleavage[176]. For systems loaded with drugs or growth factors, high-performance liquid chromatography or ELISA kits are used to model enzyme-triggered release kinetics and verify the hydrogel's capability to achieve spatiotemporally precise "on-demand" release in pathological microenvironments[177].

The functional validation of light-responsive hydrogels relies on *in situ* monitoring of photochemical reaction kinetics by UV−Vis spectroscopy[178]. When a hydrogel containing photosensitive groups is placed in a spectrophotometer equipped with a light irradiation accessory, changes in the intensity or shift of characteristic absorption peaks can be continuously recorded under illumination at a specific wavelengt[179]. By fitting the data to first- or second-order kinetic models, key parameters such as the photo-isomerization/photo-cleavage rate constant and reaction conversion can be quantitatively determined[180]. Additionally, photo-rheometry can be used to track the increase in G′ during irradiation in real time, establishing a quantitative correlation between photocrosslinking kinetics and the resulting enhancement in mechanical strength of the hydrogel network[181,182].

4. Functionalised hydrogels in anti-tumor applications

4.1. Photothermal therapy

Photothermal therapy (PTT) is a minimally invasive oncological intervention that uses NIR light to activate photothermal agents, generating local hyperthermia. At temperatures above 50 °C, this modality induces irreversible protein denaturation and mitochondrial dysfunction in malignant cells[183,184]. With further development, functionalised hydrogels have become a therapeutic platform for PTT applications in tumors. By integrating efficient photothermal nanomaterials (such as metal nanoparticles and organic semiconductors) into the polymer matrix, these engineered hydrogels can precisely convert NIR energy into local hyperthermia, thereby enhancing the specificity of thermal ablation therapy (Fig. 3)[185]. In addition, by incorporating thermoresponsive polymers into their structure, these hydrogels acquire NIR-triggered properties (*i.e.*, they undergo sol-gel phase transition under NIR irradiation), enabling on-demand drug encapsulation and controlled release[186].

The quest for advanced photothermal hydrogel systems has focused on two critical components: chromophores with exceptional photon-to-thermal conversion efficiency and thermoresponsive matrices capable of rapid phase transitions in response to physiological temperature variations (Table 5). The combination of β-GP with CS hydrogels imparts thermoresponsive properties to CS. When combined with a carbon nanoparticle suspension (0.30 mg/mL), this system could reach a temperature of 60 °C under 808 nm laser irradiation (1.0 W/cm^2). This system showed proliferation inhibition rates of 26.75% against B16 cells and 84.60% against 4T1 cells[187]. Yu et al.[188] developed a β-GP/CS hydrogel platform to disrupt the tumor DNA repair machinery. Olaparib-loaded liposomes (which induce DNA damage in tumor cells) and gold nanoparticles were co-encapsulated in the hydrogel to achieve a synergistic effect of thermal and DNA damage[189]. Red blood cells are considered ideal biomaterials due to their natural origin and excellent biocompatibility. When autologous red blood cells are injected subcutaneously into mice, they can spontaneously form a hydrogel *in situ*, triggered by physiological signals such as those from platelets and thrombin. Due to the deep red colour of red blood cells, the red blood cells hydrogel formed *in situ* can be heated by near-infrared light (808 nm, 1 W/cm^2 laser irradiation), raising the temperature to 50 °C within 10 min, effectively ablating the tumor (Fig. 4A)[190].

The high local recurrence rate of tumors remains a critical issue in clinical practice. In addition, the potential risk of surgical infection in postoperative patients and those with compromised immunity increases the likelihood of bacterial infection. This can lead to difficulties in wound healing and serious complications[191]. Recent studies have shown that PTT can effectively eradicate bacterial infection and continuously improve the oxidative and inflammatory microenvironment of wounds[192]. Multi-element-

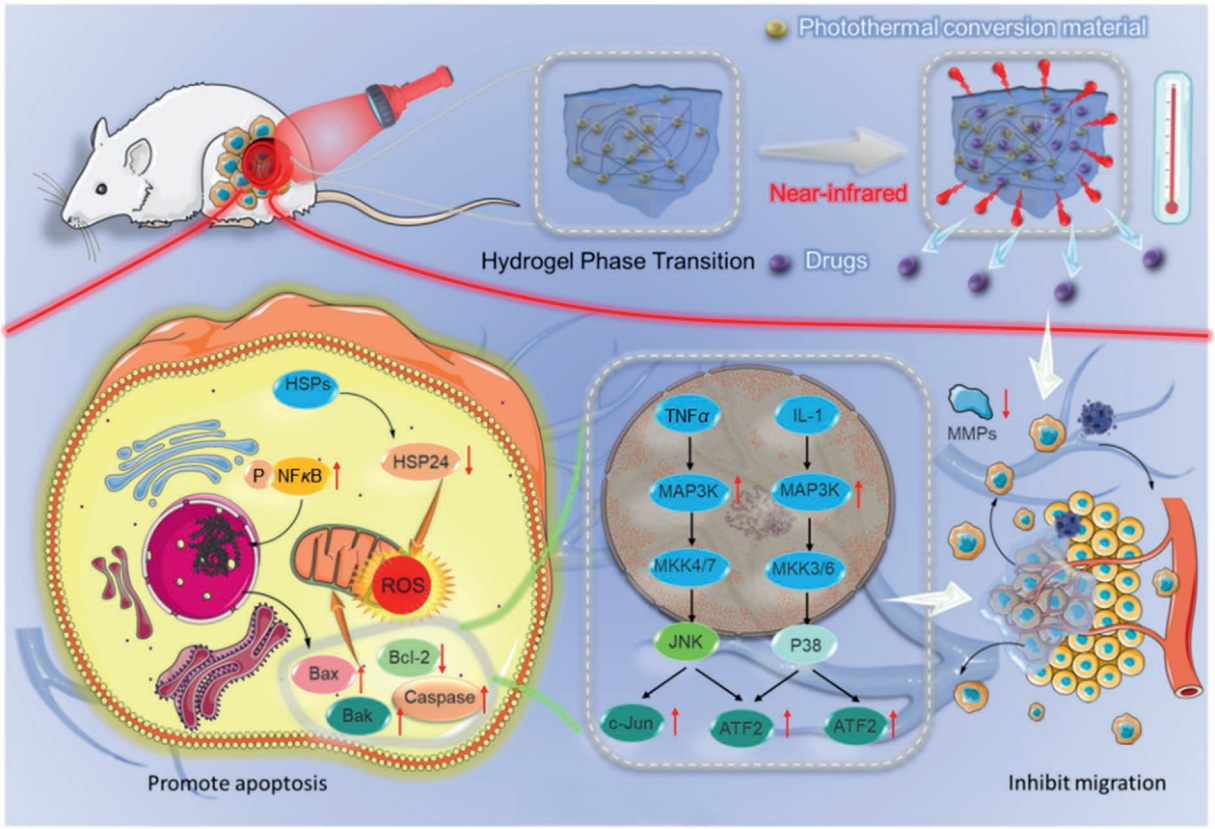

Figure 3 Photothermal hydrogels integrate photothermal conversion nanomaterials within a three-dimensional polymeric network, exhibiting antitumor effects through mechanisms including oxidative stress induction, promotion of apoptosis, and inhibition of cell migration.

doped bioactive glass nanoparticles (BGNs, Ag/Au/Zn/B/Ca/Ti/Cu) exhibit remarkable pro-healing capacities by stimulating epithelial migration, fibroblast proliferation, and angiogenesis[193]. Liu et al.[194] developed a hydrogel of ALG and manganese-doped bioactive glass nanoparticles (Mn-BGN), an adaptable platform for melanoma postoperative wound healing and anti-tumor immunotherapy. Mn^{2+} released from Mn-BGN can activate the cyclic GMP−AMP synthase-stimulator of interferon genes (cGAS−STING) immune pathway, leading to NK cell aggregation. In addition, Mn-BGN imparts excellent photothermal properties to the system and demonstrates strong angiogenic and tissue-regenerative potential (Fig. 4B).

ALG is a natural polysaccharide extracted from the cell walls and intercellular matrix of brown algae. ALG molecules are composed of three distinct regions: the mannuronic acid-rich "M-block", the guluronic acid-rich "G-block", and the "MG-block", which contains both acids. Divalent cations such as Ca^{2+} readily bind to the G-blocks, forming a three-dimensional network through cross-linking of these specific segments[195]. Due to its simple phase transition mechanism, ALG has been widely used[196,197]. The combination of ALG with photothermal materials shows excellent anticancer activities. A multifunctional hydrogel integrating ALG, bismuth sulfide nanorods (Bi_2S_3 NRs), and allantoin achieves simultaneous tumor suppression and wound healing. Under 808 nm laser irradiation (1.5 W/cm^2), a concentration of 200 μg/mL Bi_2S_3 NRs could raise the system temperature to 45.3 °C (Fig. 4C). The Bi^{3+} released from Bi_2S_3 NRs disrupted bacterial and tumor metabolism by inhibiting the tricarboxylic acid cycle. At the same time, allantoin accelerates tissue repair by modulating inflammatory responses, stimulating fibroblast proliferation, and promoting ECM deposition[198]. Research has shown that Ca^{2+} can induce mitochondrial calcium overload, reducing ATP levels and mitochondrial respiratory dysfunction[199]. Based on this, Yang et al.[200] developed an ALG hydrogel containing melittin and polyaniline nanofibres. Under 1064 nm laser irradiation, polyaniline nanofibres rapidly heated the hydrogel to 50 °C within 10 min. Melittin disrupted tumor cell membranes and enhanced sustained Ca^{2+} release from the ALG-Ca^{2+} hydrogel. The combined effects of Ca^{2+}-induced mitochondrial dysfunction and polyaniline nanofibres-induced GSH depletion improve oxidative stress in cancer cells, resulting in potent anti-tumor activity[201].

In summary, PTT based on hydrogels primarily relies on integrating highly efficient photothermal nanomaterials with temperature-responsive polymers. However, current systems still face challenges such as limited optical penetration depth, potential damage to healthy tissues due to localized overheating, and difficulties in precise temperature control[202]. Furthermore, the lack of standardized evaluation criteria across studies, particularly in metrics such as photothermal conversion efficiency and cell inhibition rates, leads to inconsistencies in reported therapeutic outcomes[203]. Future research should focus on exploring novel combinations of nanomaterials and polymers to optimize the material system and enhance synergistic photothermal and immune effects. In parallel, systematic studies on long-term safety and efficacy, along with the establishment of standardized preclinical evaluation protocols, are urgently needed. PTT utilizes hydrogels as carriers for photothermal agents to achieve tumor

Table 5 Composition, properties, and efficacy of photothermal therapy hydrogels.

Hydrogel matrix materials	Drug	Photothermal transduction agents	Crosslinking agent	Crosslinking method	Crosslinking mechanism	Curative effect	Ref.
CS and HA	Imiquimod	Indocyanine green	β-GP	Physical crosslinking	Above the LCST (37 °C), proton transfer from the amino groups on the CS molecules reduces the electrostatic repulsion. At the same time, bound water molecules are displaced by the hydroxyl groups of glycerol, causing the hydrophobic groups to aggregate and form intramolecular hydrogen bonds, resulting in gelation.	Photothermal toxicity and immune activation.	187
CS	Olaparib-liposomes	Gold nanoparticles	β-GP	Physical crosslinking	Above the LCST (37 °C), proton transfer from the amino groups on the CS molecules reduces the electrostatic repulsion. At the same time, bound water molecules are displaced by the hydroxyl groups of glycerol, causing the hydrophobic groups to aggregate and form intramolecular hydrogen bonds, resulting in gelation.	Photothermal toxicity and oxidative stress.	188
ALG	Melittin	Polyaniline nanofibers	Ca^{2+}	Physical crosslinking	The carboxylate groups (−COO−) in the ALG polymer chains form ionic bonds with Ca^{2+}, forming an "egg box" structure and resulting in crosslinking.	Photothermal toxicity and oxidative stress	200
Carboxymethyl chitosan	–	Polyphenol (Tannic acid)-metal nanoparticle	Oxidized fucoidan	Chemical crosslinking	The amino groups in carboxymethyl chitosan react with the aldehyde groups in oxidized fucoidan to form Schiff base bonds, resulting in crosslinking.	Photothermal toxicity, bactericidal activity, anti-inflammatory effects, and promotion of wound healing.	204
PEGDA	Fe-doped bioactive glass nanoparticles	Ag_2S nanodots	AIPH	Chemical crosslinking	The photothermal effect mediated by Ag_2S nanoparticles induces the decomposition of AIPH, generating alkyl radicals that trigger the gelation of PEGDA.	Photothermal toxicity, bactericidal activity, and wound-healing promotion.	205
ALG and AIPH	–	TiO nanosheets	Ca^{2+}	Physical crosslinking	The carboxylate groups (−COO−) in the ALG polymer chains form ionic bonds with Ca^{2+}, forming an "egg box" structure and resulting in crosslinking.	Photothermal toxicity and oxidative stress.	206
ALG	Programmed death ligand-1 antibody prodrug nanoparticles	Protoporphyrin IX-modified iron oxide nanoparticles	Ca^{2+}	Physical crosslinking	The carboxylate groups (−COO−) in the ALG polymer chains form ionic bonds with Ca^{2+}, forming an "egg box" structure and resulting in crosslinking.	Photothermal toxicity, immune activation, and oxidative stress	207

ALG	Glucose oxidase	MoS_2 nanosheets.	Fe^{3+}	Physical crosslinking	The carboxylate groups (−COO−) in the ALG polymer chains form ionic bonds with Ca^{2+}, forming an "egg box" structure and resulting in crosslinking.	Photothermal toxicity, starvation therapy, and oxidative stress	208
Polyacrylamide and acrylic acid modify the DAN chain.	Doxorubicin	Ti_3C_2TX-based MXene	PAM	Chemical crosslinking	The photothermal effect of MXene nanosheets induces the degradation of the cross-linked structure of DNA double chains in the hydrogel matrix.	Photothermal toxicity	209
Guanosine	−	Polydopamine -functionalized AuNPs	Sodium borate	Chemical crosslinking	Guanosine and polydopamine form dynamic borate ester bonds with the borate ions of sodium borate through the diol and catechol groups in their molecules, promoting the formation of the cross-linked network.	Photothermal toxicity	210
Methylcellulose	PLGA porous microspheres	Indocyanine green	PLGA	Physical crosslinking	As the temperature increases, the hydrophobic moieties (lactic acid moieties) in PLGA increase their repulsive interactions with water molecules, causing the molecular chains to contract and aggregate, inducing gelation.	Photothermal toxicity	211
CS and cyanuric chloride	−	PBI-DOPA	PBI-DOPA	Chemical crosslinking	In an alkaline environment, the deprotonated catechol groups of PBI-DOPA react with the grafted cyanuric chloride on cyanuric chloride-*g*-CS to form cross-linked covalent bonds.	Photothermal toxicity and oxidative stress	212
PLGA-PEG-PLGA and arachidonic acid	Ferromagnetic inducer	Ferromagnetic $Zn_{0.4}Fe_{2.6}O_4$ nanocubes	Arachidonic acid	Chemical crosslinking	As the temperature (37 °C) increases, the repulsive interaction between the hydrophobic segments (lactic acid moieties) of PLGA and water molecules increases, leading to contraction and aggregation of the molecular chains, thereby inducing gelation.	Photothermal toxicity and oxidative stress	213
Silk fibroin	−	Iron oxide nanocubes	−	Physical crosslinking	Ultrasound-induced self-assembly of silk fibroin molecules forms β-sheets and cross-linked networks.	Photothermal toxicity and oxidative stress	214

Note: −, Not applicable.

Abbreviations: HA, hyaluronic acid; CS, chitosan; β-GP, β-glycerophosphate; LCST, lower critical solution temperature; ALG, alginate; PEGDA, poly(ethylene glycol) double acrylates; AIPH, 2,2′-azobis [2-(2-imidazolin-2-yl) propane]-dihydrochloride; PAM, polyacrylamide; AuNPs, Au nanoparticles; PLGA, poly(lactic-*co*-glycolic acid); PBI-DOPA, perylene bisimide dopamine.

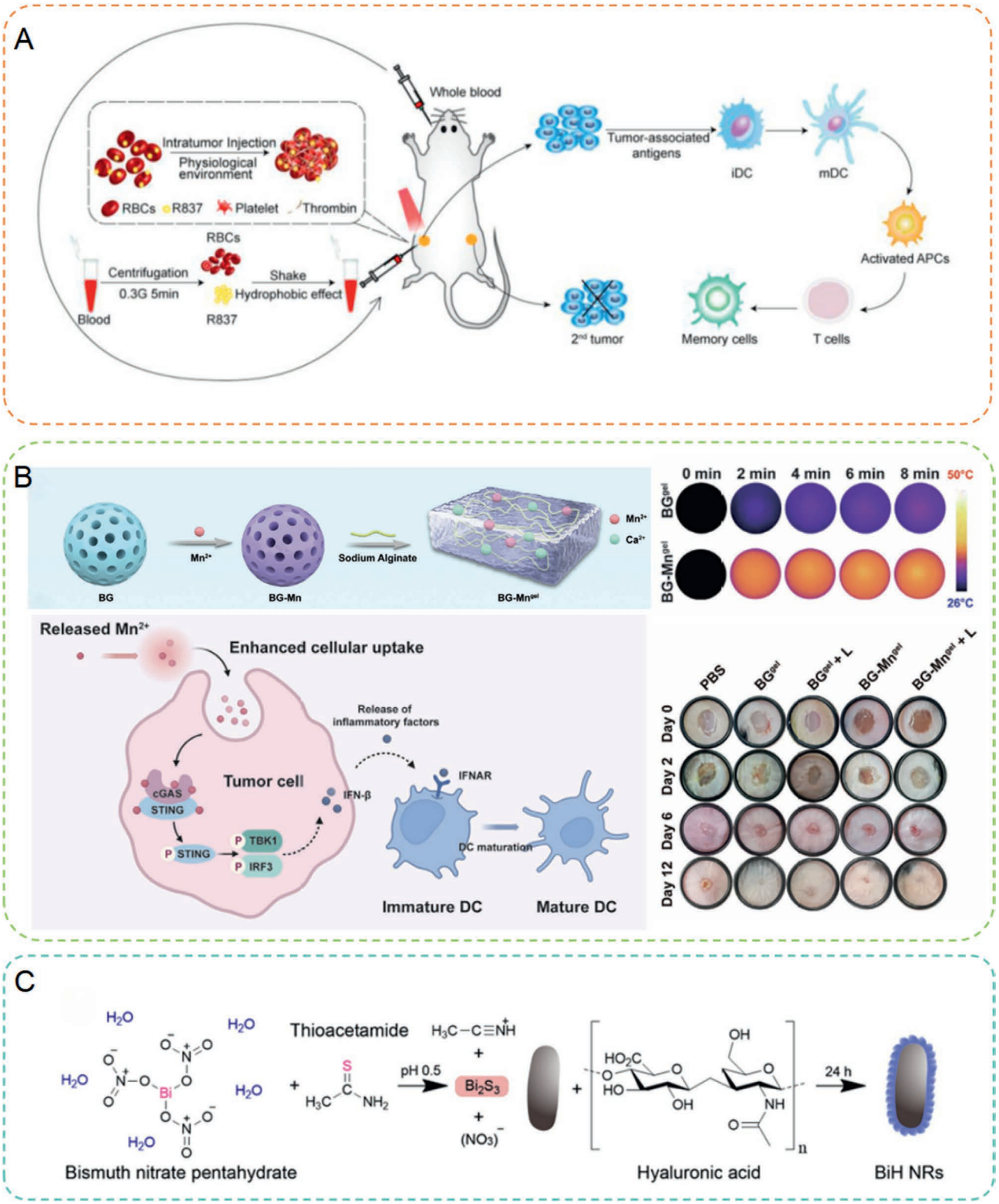

Figure 4 Examples of multi-level cancer therapy using hydrogels with photothermal conversion effects. (A) Preparation, characterization, and photoimmunotherapy mechanism of erythrocyte hydrogel. Reprinted with permission from Ref. 190. Copyright © 2021 Elsevier. (B) Schematic illustration of the composition of Mn-BGN hydrogel system, pharmacological mechanism, photothermal effect, and therapeutic efficacy in promoting wound healing. Reprinted with permission from Ref. 194. Copyright © 2024 John Wiley and Sons. (C) Construction of ALG-BIH hydrogel and its photothermal conversion efficiency. Reprinted with permission from Ref. 198. Copyright © 2023 The Royal Society of Chemistry.

thermal ablation upon light irradiation. Beyond hyperthermia, light energy can be harnessed to activate photodynamic therapy that generates ROS, while magnetic field-induced magnetic hyperthermia offers an alternative physical therapeutic modality for deep-seated tumors.

4.2. Photodynamic therapy and magnetic hyperthermia

Photodynamic therapy (PDT) is a novel therapeutic approach that combines photosensitizers, light sources of specific wavelengths, and oxygen[215]. It is primarily used to treat malignant tumors, vascular lesions, and microbial infections. When photosensitizers are irradiated with light of specific wavelengths (visible light, near infrared, or ultraviolet), photon absorption induces a transition between the ground and excited states of the photosensitiser molecules. This process generates chemical energy that is transferred to oxygen molecules, causing them to ionise into cytotoxic ROS[183,216–218]. A CS-based hydrogel containing perylene bisimide dopamine (PBI-DOPA) and cyanuric chloride showed improved PDT efficacy. Under alkaline conditions, the deprotonated catechol groups of PBI-DOPA react with the Cy functional groups in the Cs polymer chains to form cross-linked covalent bonds. PBI-DOPA efficiently generates $^1O_2$ under near-infrared light. However, the tendency for intermolecular $\pi-\pi$ interactions within its molecular structure reduces the production of $^1O_2$. Interestingly, when incorporated into a hydrogel, the random distribution of PBI-DOPA molecules within the three-dimensional network reduces $\pi-\pi$ stacking and self-quenching, thereby increasing the quantum efficiency of $^1O_2$ generation[212].

Magnetic hyperthermia therapy (MHT) enables non-invasive, localised cancer treatment without limitations on penetration depth. This approach relies on magnetic nanoparticles that generate heat *via* magnetic loss mechanisms (*e.g.*, hysteresis and Brownian relaxation) under alternating magnetic fields[219]. When such nanoparticles accumulate in tumor tissue and are exposed to an electromagnetic field, they convert electromagnetic energy into localised thermal ablation energy[220]. Hydrogel immobilisation is an effective strategy to prevent nanoparticle leakage. Some injectable thermosensitive hydrogels have been investigated for the delivery of magnetic nanoparticles. Chen et al.[213] developed an iron-supplemented hydrogel using PLGA-PEG-PLGA copolymer, arachidonic acid, $Zn_{0.4}Fe_{2.6}O_4$ ferromagnetic nanocubes, and the ferroptosis inducer RAS-selective lethal small molecule 3 (RSL3). The $Zn_{0.4}Fe_{2.6}O_4$ nanocubes played a dual role: (1) as magnetothermal transducers and (2) as iron donors promoting intracellular Fe^{2+} overload and inducing ferroptosis. The release of RSL3 further enhanced the antitumor effect by increasing intracellular lipid peroxidation. Hydrophilic iron oxide nanocubes (IONCs) are recently discovered magnetic heat-conversion materials with efficient cancer-ablative properties. Under an alternating magnetic field of 35 kA/m, a solution of IONCs at 2.0 mg/mL can reach a temperature of 55.8 °C within 10 min. Qian et al.[214] developed an injectable hydrogel by integrating IONCs with silk fibroin. Ultrasound induced the silk fibroin to self-assemble into β-sheet structures and cross-linked networks, while hydrogen bonding between the IONCs and the fibroin matrix provided nanoparticle encapsulation.

In PDT, hydrogel platforms help suppress photosensitizer self-quenching, thereby enhancing singlet oxygen generation and strengthening the efficacy of photodynamic killing. MHT relies on heat generated by magnetic nanoparticles under an alternating magnetic field to achieve precise thermal ablation of tumors. Although both approaches exhibit innovation in material design and therapeutic mechanisms, challenges remain, such as photosensitizer stability, biosecurity of magnetic nanoparticles, and optimization of carrier performance[221,222]. Future research should focus on synergistic multifunctional material systems to improve photothermal conversion efficiency and controlled release performance, thereby enhancing targeting capability and biocompatibility. While PDT and MHT rely on external physical stimuli for therapeutic activation, Chemodynamic therapy (CDT) offers a self-sufficient alternative by exploiting the intrinsic chemical properties of the TMEt. By catalyzing Fenton or Fenton-like reactions to convert endogenous hydrogen peroxide into cytotoxic hydroxyl radicals, this modality achieves tumor-specific oxidative damage without external energy input[223].

4.3. Chemodynamic therapy

CDT uses tumor-specific chemical reactions to generate high concentrations of ROS that directly damage cellular DNA, proteins, and lipids. Although ROS induces oxidative stress-mediated tumor cell death, the hypoxic microenvironment in deep-seated tumor regions limits ROS generation[224]. The use of hydrogels (Table 6) to deliver toxic free radicals has facilitated the development of this therapeutic approach (Fig. 5). Xing et al.[206] developed an injectable hydrogel that integrates photothermal and thermodynamic therapies using ALG, TiO nanosheets, and AIPH as raw materials. Under infrared light irradiation, TiO nanosheets release heat *via* electron transitions, which rapidly catalyse AIPH to produce alkyl free radicals, thereby inducing oxidative stress in cancer cells.

Ferroptosis, an iron-dependent, non-apoptotic, and regulated mode of cell death, has become a central therapeutic target in oncology[225]. Dysregulated iron metabolism increases intracellular labile Fe^{2+} levels, which drives $-OH$ generation *via* Fenton reaction-mediated H_2O_2 decomposition, thereby accelerating lipid peroxidation[226,227]. The accumulation of lipid peroxidation products disrupts the integrity of tumor cell membranes by oxidising polyunsaturated fatty acids and compromising structural stability. At the same time, ferroptosis triggers ER stress, which promotes surface exposure of ecto-calreticulin (CRT) to induce immunogenic cell death (ICD) (Fig. 5). The development of iron-loaded hydrogel systems has become a favoured therapeutic approach to promote oxidative stress in tumor cells. These hydrogels not only effectively release iron ions locally to enhance oxidative stress in tumor cells, but also improve treatment targeting. Ding et al.[207] developed a multifunctional hydrogel system integrating PTT and CDT. The composite achieved NIR-responsive ROS release by incorporating protoporphyrin IX-functionalised Fe_3O_4 nanoparticles into an ALG hydrogel matrix. Under 660 nm laser irradiation, protoporphyrin IX-functionalised Fe_3O_4 nanoparticles catalysed Fenton-like reactions to generate cytotoxic $-OH$ and O^{2-}[228,229]. These ROS-induced ICD and tumor ablation cleaved ROS-labile chemical bonds within co-encapsulated aPDL1 prodrug nanoparticles, thereby triggering spatiotemporally controlled antibody release. The released aPDL1 antibodies synergistically block tumor immune checkpoints while amplifying CRT-mediated "eat-me" signals[230].

The incorporation of iron-based metal-organic framework (Fe-MOF) into hydrogels is a practical approach to induce oxidative stress in tumors. Zhuang et al.[231] developed a hydrogel incorporating paclitaxel/chlorin e6 and Fe-MOF. Fe-MOF facilitates the generation of $-OH$ *via* Fenton reactions. Adjuvant ultrasound

Table 6 Composition, properties, and efficacy of hydrogel-based chemical dynamic therapy.

Hydrogel matrix materials	Drug	Responsiveness	Crosslinking agent	Crosslinking method	Crosslinking mechanism	Curative effect	Ref.
ALG	MoS_2 nanosheets, glucose oxidase	Metal ions	Fe^{3+}	Physical crosslinking	The carboxylate groups (−COO−) in the ALG polymer chains form ionic bonds with Fe^{3+}, forming an "egg-box" structure.	Ensured a continuous Fenton reaction.	208
ALG	Paclitaxel/chlorin e6-loaded iron-based metal-organic framework	Metal ions	Ca^{2+}	Physical crosslinking	The carboxylate groups (−COO−) in the ALG polymer chains form ionic bonds with Ca^{2+}, forming an "egg box" structure.	FeMOF has peroxidase/GSH oxidase mimicking properties that can accelerate the generation of −OH by activating the Fenton reaction and promoting GSH consumption.	231
ALG	Tannins and RSL3 coordination nanoparticles	Metal ions	Ca^{2+}	Physical crosslinking	The carboxylate groups (−COO−) in the ALG polymer chains form ionic bonds with Ca^{2+}, forming an "egg box" structure.	Induce ferroptosis in cancer cells and reverse the immunosuppressive TMEt.	233
Catechol functionalised hyaluronic acid	indocyanine green	Metal ions	Cu^{2+}	Physical crosslinking	Cu^{2+} formed coordination bonds with catechol groups, facilitating the polymerization of hyaluronic acid into a cross-linked network.	Cu^{2+} is used instead of Fe^{3+} to mediate a Fenton-like reaction.	238
Poloxamer 407, cystamine-linked carrageenan-eicosapentaenoic acid, and ferrocene	−	Temperature	Poloxamer 407	Physical crosslinking	As the temperature increases, the thermal energy breaks the hydrogen bonds formed between the hydrophilic poly(ethylene oxide) segments of Poloxamer 407 and water molecules. As a result, the hydrophobic poly(propylene oxide) segments in the centre begin to aggregate and form hydrogen bonds, facilitating the formation of a cross-linked network.	Ferrocene catalyses the production of −OH from H_2O_2 *via* the Fenton reaction. Eicosapentaenoic acid promotes lipid peroxidation in cells, triggering ferroptosis.	246

Note: −, not applicable.
Abbreviations: ALG, alginate; GSH, glutathione.

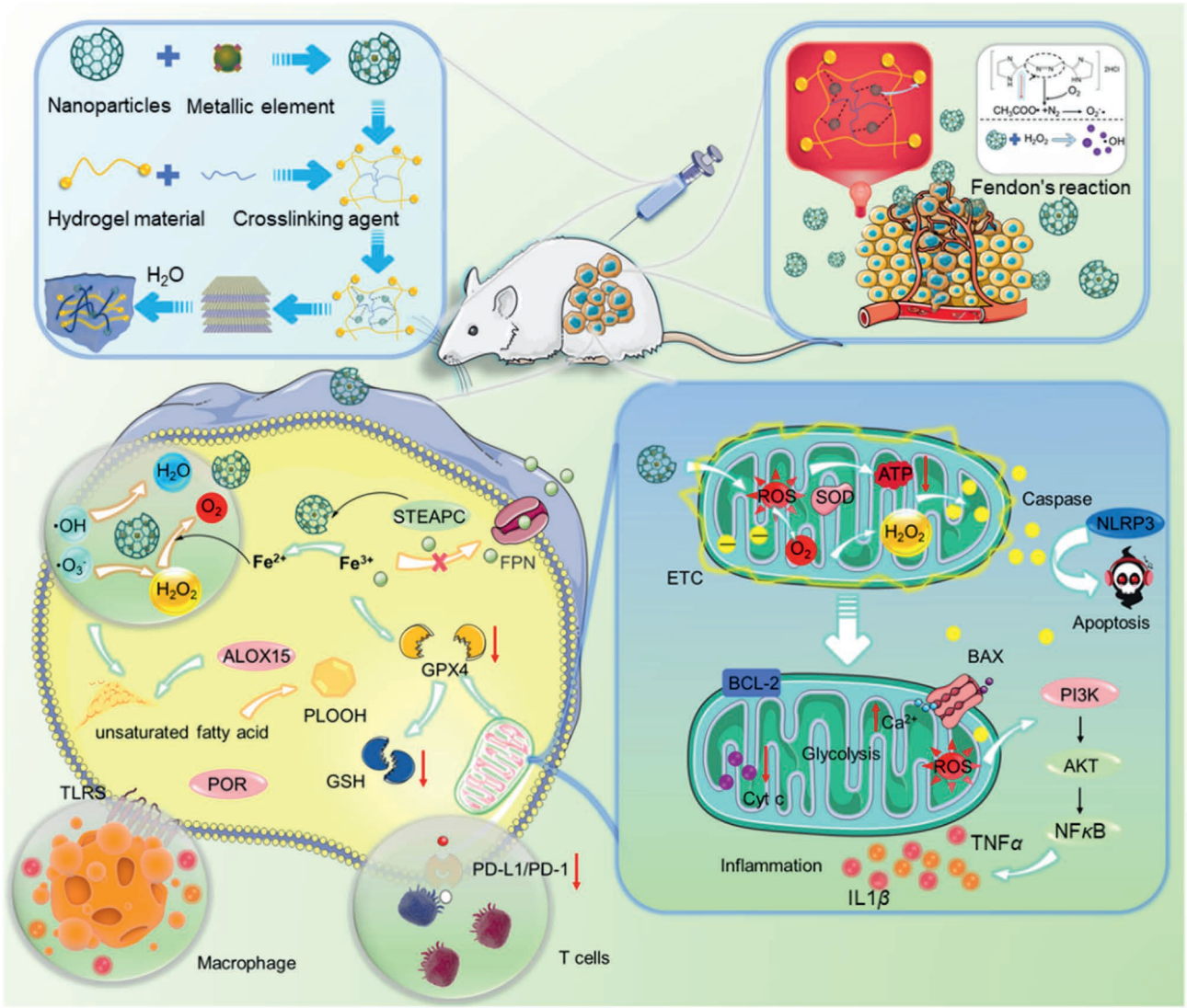

Figure 5 CDT uses tumor-specific chemical reactions to generate high concentrations of ROS that directly damage cellular DNA, proteins, and lipids.

therapy may further activate the sonosensitiser chlorin e6, thereby promoting the generation of toxic $^1O_2$. Low-dose paclitaxel can reduce glutathione peroxidase 4 (GPX4) levels by downregulating SLC7A11, further enhancing the catalytic activity of Fe-MOFs. RSL3, an irreversible inhibitor of GSH synthetase, drives ferroptosis by depleting the antioxidant GSH and suppressing GPX4 activity, thereby crippling cellular redox defence systems[232]. Building on this mechanism, a recent study developed tannic acid-stabilized Fe^{3+}—RSL3 coordination nanoparticles and co-encapsulated them with glucose oxidase (GOX) in an ALG hydrogel. This composite system exploits the Fe^{3+}/GOX synergy to enhance ROS production through glucose-driven H_2O_2 generation and Fenton reaction, while tannic acid-stabilized Fe^{3+}-RSL3 coordination nanoparticles sustain RSL3 release to enforce GPX4 inhibition in tumor cells. By localising these cytotoxic cascades within the hydrogel matrix, this platform minimises off-target effects while maximising therapeutic specificity[233].

To address the limited sustainability of Fenton reactions in the TME, Zhou et al.[208] developed a multifunctional hydrogel system integrating MoS_2 nanosheets, GOx, and ALG. The Fe^{3+} ions acted as crosslinkers to polymerise the ALG matrix. The MoS_2 nanosheets exhibited exceptional photothermal conversion efficiency, rapidly raising the hydrogel temperature to 72 °C within 5 min of 808 nm laser irradiation. Beyond their photothermal performance, these nanosheets engaged in redox cycling with Fe^{3+}, generating Fe^{2+} and molybdate ions (MoO_4^{2-}), which triggered hydrogel degradation and subsequent GOX release. The released GOX catalysed glucose oxidation to produce H_2O_2, which reacted with Fe^{2+} *via* Fenton chemistry to regenerate Fe^{3+} and hydroxyl radicals. The regenerated Fe^{3+} responds again with the remaining MoS_2, creating a self-sustaining loop that ensures prolonged Fenton activity[234,235]. This cascade mechanism synergistically combines photothermal ablation, glucose starvation therapy, and oxidative damage into a single platform, reflecting a multimodal approach to cancer therapy. Although the Fenton reaction exhibits potent antitumor efficacy, its practical application is limited by the narrow acidic pH requirement (2.0—4.5) of Fe^{2+} activation, which conflicts with the near-neutral TMEt (pH 6.5—7.0)[236]. Copper ions (Cu^+) have emerged as promising alternatives for Fenton-like reactions due to their broad pH adaptability and low toxicity.

These ions not only catalyse the conversion of endogenous H_2O_2 to −OH over physiological pH ranges, but also deplete GSH through redox cycling between Cu^{2+} and Cu^{+} to exacerbate oxidative stress[237]. Capitalising on these properties, Kim et al.[238] developed a tumor-targeted hydrogel system using $CuSO_4$-mediated crosslinking of catechol-functionalised hyaluronic acid. Incorporation of indocyanine green imparted photothermal capabilities to the hydrogel. Dang et al.[239] incorporated CuO nanoparticles into hydrogels. Under acidic conditions, CuO could continuously release Cu^{2+} and generate intracellular ROS through Fenton-like reactions. Notably, the CuO-mediated PTT effect further enhanced the efficiency of the Fenton-like reactions. These copper-based platforms exemplify the rational engineering design of metal−ligand coordination systems and a synergistic therapeutic approach combining photothermal therapy and oxidative stress therapy.

The metabolic cycle of metal ions is closely coupled with the regulation of the hydrogel microenvironment, thereby breaking the bottleneck of traditional CDT limited by tumor hypoxia and acidic pH. Unlike photodynamic therapy or starvation therapy, the unique value of CDT hydrogel lies in the recyclability of the catalytic reaction and the accuracy of metabolic pathway interference, such as systematically destroying the redox defense of tumor cells by iron death, driving lipid peroxidation, and GSH depletion[240].

However, there is a lack of systematic toxicological evaluation on the long-term metabolic toxicity, liver and kidney accumulation risk, and off-target oxidative damage of metal ions[241]. Existing research has focused chiefly on the local toxicity of cells and tumors, and a systemic metal-ion metabolic kinetics model has not yet been established[242]. The Fenton/Fenton-like reaction rate is highly dependent on local H_2O_2 concentration, metal ion valence state stability, and pH microenvironment. Differences in the microenvironment in metastatic lesions, fibrotic tumors, or blood-rich areas may cause catalytic efficiency to fluctuate by more than 10-fold. Still, existing research lacks multi-model head-to-head comparison data[243,244]. Beyond direct tumor ablation, cancer cell death can release tumor antigens and damage-associated molecular patterns, thereby inducing immunogenic cell death[245]. This immunogenic effect provides a mechanistic basis for combining them with immunotherapy, a strategy increasingly enabled by hydrogel platforms that co-deliver immunomodulatory agents to elicit systemic anti-tumor immunity.

4.4. Immunotherapy

Cancer immunotherapy (CIT) is a transformative therapeutic strategy with high specificity and low systemic toxicity. It exerts anticancer effects by modulating key steps in the immune cycle, including antigen-presenting cell recruitment, tumor-associated antigen release, and T-cell activation (Fig. 6)[247,248]. Currently, most CIT methods rely on the intravenous injection of cancer vaccines and immunomodulatory factors. Although exogenous cancer therapeutic vaccines have great potential, traditional intravenous administration causes problems such as off-target and low delivery efficiency, resulting in the need for high doses and frequent injections in patients[249,250]. In contrast, intratumoral or peritumoral administration significantly enhances local drug accumulation in tumors[251]. Hydrogels have emerged as ideal platforms for localised CIT due to their tunable swelling behaviour, biocompatibility, and lack of immune rejection. Their three-dimensional porous networks facilitate cellular infiltration and sustained release of immunomodulators[252]. These systems allow spatio-temporally controlled delivery of therapeutic payloads while minimising off-target effects (Table 7).

Some proteins on the surface of tumor cells are closely linked to the immune response. During ICD, tumor cells expose surface danger signals known as damage-associated molecular patterns, including CRT, secreted high-mobility group box-1 protein, and MHC class I molecules, which together send “eat-me” signals to immune cells (Fig. 6)[253]. However, tumor cells also express immune-evading proteins such as PDL1 and CD47. PDL1 binds to PD1 on T cells to suppress their activation, whereas CD47 binds to SIRPα on macrophages to block phagocytic clearance, effectively counteracting DAMP-mediated immunogenicity[254,255]. For example, $CCR9^{+}CD8^{+}$ T cells induce robust antitumor responses[256]. However, these cells also exhibit increased PD1 expression as they mount an immune response. This interacts with the upregulated expression of PDL1 in tumor cells to inhibit the effector functions of these T cells[257,258]. An ALG hydrogel containing β-CD in its molecular structure can overcome this challenge. The hydrogel recruited $CCR9^{+}$ $CD8^{+}$ T cells into the pores by releasing CCL25. Meanwhile, the encapsulated adamantane-modified anti-PD1 antibody blocked PD1 on the surface of $CCR9^{+}$ $CD8^{+}$ T cells, thereby inhibiting the immune checkpoint. Interestingly, the fixation of the PD1 antibody relied on the supramolecular host−guest interactions between β-CD and adamantane. Therefore, by injecting an anti-PD1 antibody *in vitro*, the hydrogel could achieve repeated accumulation of the anti-PD1 antibody (Fig. 7A)[25.9]. In particular, hypoxia drives adaptive and genetic reprogramming in tumor cells, characterized by upregulation of hypoxia-inducible factor subunit alpha (HIF1A) expression, which induces transcriptional activation of the CD47 gene, thereby evading phagocytic clearance. To counteract this immunosuppressive mechanism, Liang et al.[260] incorporated biocompatible $CaCO_3$ nanoparticles into a hydrogel matrix composed of Pluronic F-127 and HA and simultaneously encapsulated Tuni (an endoplasmic reticulum stress inducer) using a double-emulsion technique. Pluronic F127 undergoes a temperature (37 °C) induced sol-gel transition under physiological conditions, ensuring localised retention and sustained release of Tuni[261]. The sustained release of Tuni effectively induces ER stress in tumor cells and upregulates the expression of the pro-phagocytic signal CRT on the tumor cell surface. At the same time, $CaCO_3$ nanoparticles catalyze the decomposition of endogenous H_2O_2 into oxygen, thereby alleviating tumor hypoxia, suppressing HIF1A-mediated CD47 upregulation, and reprogramming the immunosuppressive niche into a phagocytosis-permissive microenvironment.

In addition to expressing surface immune resistance proteins, tumor cells actively secrete immunosuppressive factors (*e.g.*, IL10, TGFβ, IL4, and IL35) to establish an immune-evasive niche that undermines phagocytic clearance. These cytokines directly impair the functions of cytotoxic $CD8^{+}$ T cells and natural killer (NK) cells by suppressing effector proliferation and cytotoxic granule polarisation. This immunosuppressive mechanism, which simultaneously desensitises immune recognition and turns off cytotoxic responses, fundamentally limits the efficacy of current immunotherapies[262]. To overcome the immunosuppressive TMEt, researchers have encapsulated various immune adjuvants in hydrogels to enhance cross-presentation of antigens and thereby promote immune cell infiltration into tumors[263,264]. Fu et al.[265] developed an ROS-responsive hydrogel-PIVOT using mannan, methyl 3-mercaptopropionate, and chondroitin sulphate to co-deliver oxaliplatin, αTIM-3 antibodies, and FMS-like tyrosine

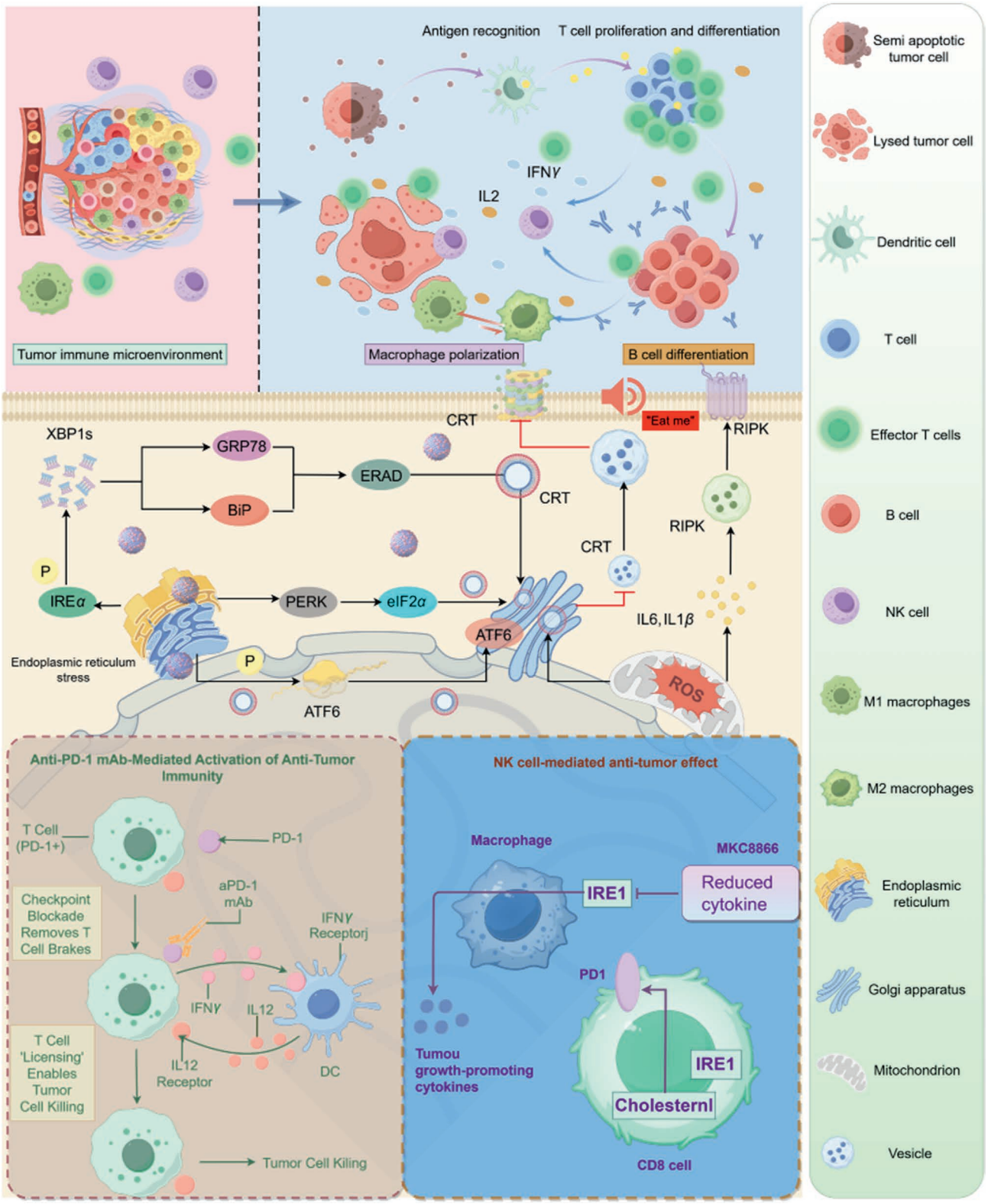

Figure 6 Tumor cells evade immune surveillance by downregulating antigen presentation, activating checkpoint pathways such as PD-1/PDL1, and secreting inhibitory factors, thereby forming an immunosuppressive TME. Cancer immunotherapy, in contrast, restores anti-tumor immune responses by blocking checkpoint molecules or genetically engineering T cells (such as CAR-T) to relieve this suppression.

Table 7 Composition, properties, and efficacy of immunotherapy hydrogels.

Hydrogel matrix materials	Drug	Responsiveness	Crosslinking agent	Crosslinking method	Crosslinking mechanism	Curative effect	Ref.
ALG and β-CD	Adamantine-labelled anti-PD1 and CCL25 antibodies	Metal ions	Ca^{2+}	Physical crosslinking	The carboxylate groups (−COO−) in the ALG polymer chains form ionic bonds with Ca^{2+}, forming an "egg box" structure.	Capture CCL25 to recruit CCR9+CD8+ T cell populations and to silence immune cell PD1 antibodies.	259
Pluronic F-127 and HA	Granulocyte-macrophage colony-stimulating factor, $CaCO_3$ nanoparticles and PD1 antibody	Temperature	−	Physical crosslinking	As the temperature rises, thermal energy breaks the hydrogen bonds between water molecules and the poly(ethylene oxide) chains in Pluronic F-127. The interactions between the hydrophobic poly (propylene oxide) segments become stronger, leading to polymer chain aggregation and loss of the hydration layer.	Trigger ER stress in tumor cells.	260
Polyvinyl alcohol and benzoboric acids	Gemcitabine and STING agonist DMXAA	ROS	N^1-(4-boronobenzyl)-N^3-(4-boronophenyl)-N^1,N^1,N^3,N^3-tetramethylpropane-1,3-diaminium	Chemical crosslinking	The diol groups of polyvinyl alcohol form borate ester bonds with phenylboronic acid on N^1-(4-boronobenzyl)-N^3-(4-boronophenyl)-N^1,N^1,N^3,N^3-tetramethylpropane-1,3-diaminium.	Recruit immune cells and promote inflammatory responses.	267
Pluronic F-127	Toll like receptors 7/8/9 and STING	Temperature	−	Physical crosslinking	As the temperature rises, thermal energy breaks the hydrogen bonds between water molecules and the poly(ethylene oxide) chains in Pluronic F-127. The interactions between the hydrophobic poly (propylene oxide) segments increase, and the polymer chains begin to aggregate.	Trigger effective systemic innate and adaptive anti-tumor memory immunity.	270
Fibrinogen	Doxorubicin -loaded mesoporous polydopamine and M1 macrophage-derived nanovesicles.	Enzyme	Thrombin	Chemical crosslinking	Thrombin cleaves the peptide bonds on the Aα and Bβ chains of fibrinogen, releasing fibrinopeptides A and B. The two monomers self-assemble into fibrin polymers through non-covalent interactions, which clotting factor XIIIa then cross-links to form a stable fibrin clot.	M2-type TAMs transform into M1-type TAMs.	277

PLGA-PEG-PLGA	Oxaliplatin and resiquimod	Temperature	−	Physical crosslinking	As the temperature increases, the repulsive interactions between the hydrophobic segments (lactic acid moieties) in PLGA and water molecules increase, leading to contraction and aggregation of the molecular chains, inducing gelation.	Promote dendritic cell maturation and induce the formation of central memory T cells.	284
Arginine-glycine-aspartic acid modified elastin-like protein	Gemcitabine and aPDL1	−	Tetrakis (hydroxymethyl) phosphonium chloride	Chemical crosslinking	Tetrakis (hydroxymethyl) phosphonium chloride reacts mainly through its hydroxymethyl groups with amino, carboxyl, and other functional groups in arginine-glycine-aspartic acid modified elastin-like protein molecules to form a cross-linked network.	Promote the expression of PDL1 on the surface of tumor cells and extend the retention time of aPDL1.	285
ALG	Nanoparticle albumin-bound paclitaxel and an immunostimulatory agent R83	Metal ions	Ca^{2+}	Physical crosslinking	The carboxylate groups (−COO−) in the ALG polymer chains form ionic bonds with Ca^{2+}, forming an "egg box" structure.	Induce apoptosis in tumor cells and promote DC maturation.	286
AMPA-THMA and HA	Kynurenine hydrolase	−	−	Physical crosslinking	Matrix crosslinking is driven by synergistic dynamic interactions between the amine groups of APMA and the carboxyl groups of HA, coupled with a triple-hydrogen-bonding network formed by the three hydroxyl groups of THMA.	Disrupt kynurenine-mediated immune suppression pathways in TME.	287
Fdodecyl-modified hydroxypropylmethylcellulose, poly(ethylene glycol)-*block*-poly(lactic acid) nanoparticles	Immunostimulatory CD40 agonist	−	−	Physical crosslinking	The entropy-driven non-covalent interactions between fdodecyl-modified hydroxypropylmethylcellulose and nanoparticles facilitate the formation of a cross-linked network.	Reduce the dose-limiting toxicity of immunostimulatory CD40 agonist while maintaining its practical anti-cancer efficacy.	288
Tetra-PEG-SS	Glutaminyl cyclase isoenzyme	pH	BSA	Chemical crosslinking	Under alkaline conditions (pH > 10), the SS groups in Tetra-PEG-SS react with the amino groups in alkaline bovine serum albumin to form amide bonds, forming a three-dimensional cross-linked network.	Downregulate CD47 expression on the tumor surface to enhance antigen-presenting cell function.	289
PLGA-PEG-PLGA	ROCK inhibitorY27632	Temperature	−	Physical crosslinking	As the temperature increases, the repulsive interactions between the hydrophobic segments (lactic acid moieties) in PLGA and water molecules increase, leading to contraction and aggregation of the molecular chains, inducing gelation.	Enhance the phagocytic function of DCs and activate T cell-mediated anti-tumor immune responses.	290

Note: −, not applicable.

Abbreviations: ALG, alginate; β-GP, β-glycerophosphate; HA, hyaluronic acid; TAMs, tumor-associated macrophages; PLGA, poly(lactic-*co*-glycolic acid); PEG, polyethylene glycol; TME, tumor microenvironment; AMPA-THMA, poly(*N*-(3-aminopropyl)methacrylamide)-*co*-(*N*-[tris(hydroxymethyl)methyl]acrylamide); Tetra-PEG-SS, tetra-armed PEG succinimidyl succinate; BSA, alkaline bovine serum albumin.

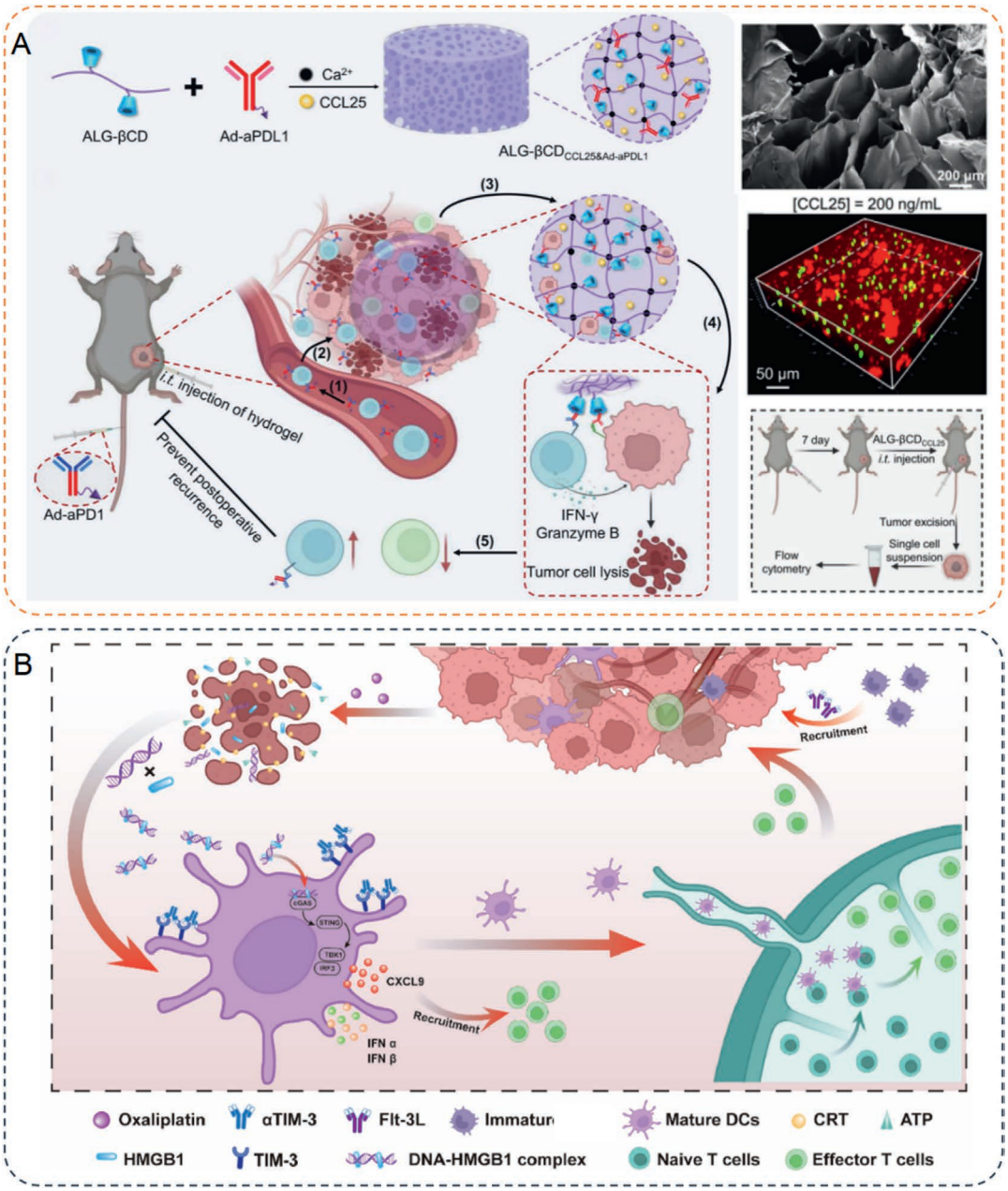

Figure 7 Hydrogels in synergy with immune adjuvants for cancer therapy. (A) Schematic illustration of the recruitment, engagement, and reinvigoration effects of the ALG-*β*CD hydrogel system to enhance T cell-mediated immunotherapy. Reprinted with permission from Ref. 259. Copyright © 2023 John Wiley and Sons. (B) Schematic illustration of PIVOT for enhancing antitumor immune responses by shaping tumor immunogenicity and reversing tolerogenic DCs. Reprinted with permission from Ref. 265. Copyright © 2024 Elsevier.

kinase 3 ligand (Flt-3L). Oxaliplatin can induce the cleavage and release of tumor DNA. The released DNA fragments form complexes with the high-mobility group box-1 protein in NK cells, thereby activating the nucleic acid-sensing pathway to initiate innate immunity. At the same time, Flt-3L recruits dendritic cells (DCs), particularly conventional type 1 DCs, into the tumor environment. Internalised *α*TIM-3 antibodies disrupted high-mobility group box-1 protein-TIM3 complex formation, reversed DCs' tolerance, and licensed cDC1s for antigen presentation. This process activates the cGAS−STING axis in cDC1s, driving IFN production and amplifying anti-tumor innate immune responses (Fig. 7B). The cGAS−STING signalling axis is the primary pathway by which DCs recognise and respond to cytosolic double-stranded DNA. Once activated, this pathway orchestrates a robust innate immunity by inducing IFN-type and pro-inflammatory cytokines[266]. The use of hydrogels to deliver STING agonists is an effective strategy to enhance tumor-specific immune responses. Wang et al.[267] developed a ROS-responsive hydrogel by covalent crosslinking of poly(vinyl alcohol) and boronic acid derivatives using N^1-(4-boronobenzyl)-N^3-(4-boronophenyl)-N^1,N^1,N^3,N^3-tetramethylpropane-1,3-diaminium. This platform was co-encapsulated with gemcitabine and a synthetic STING agonist. STING promotes the production of type I interferons by binding to cyclic dinucleotides, thereby recruiting $CD8^+$ T cells[268].

Gemcitabine synergistically enhances tumor immunogenicity by inducing damage-associated molecular patterns and facilitating DC-mediated antigen presentation and T cell priming[269]. Cheng et al.[270] developed a thermoresponsive hydrogel co-loaded with immune checkpoint blockade antibodies, toll like receptor 7/8/9 agonists, and STING agonists. In several poorly immunogenic tumor models, this combinatorial approach dismantled the multi-layered immunosuppressive TME and induced durable systemic antitumor memory through coordinated activation of innate and adaptive immunity.

In addition to immune cells that promote phagocytosis, the TME harbours immune cells that facilitate tumor proliferation, including tumor-associated macrophages (TAMs), regulatory T cells, and myeloid-derived suppressor cells. TAMs exhibit functional plasticity and dynamically switch between pro-inflammatory M1 and immunosuppressive M2 polarisation states[271,272]. Although M1-polarised TAMs exert antitumor activity through phagocytic clearance and antigen presentation, the TME predominantly enriches M2-like TAMs that drive malignant tumor progression[273]. These M2 TAMs establish feedforward immunosuppression by secreting IL-4 and IL-13 to expand Treg populations while simultaneously producing TGFβ and IL-10 to blunt cytotoxic T cell effector functions, thereby reinforcing an immune-evasive niche (Fig. 6)[274]. Recent studies have demonstrated that extracellular vesicles (EVs) derived from M1-polarised TAMs can reprogram immunosuppressive M2-like TAMs into antitumorigenic M1 phenotypes. However, achieving sustained delivery and functional retention of these EVs in the TME is a significant challenge. Studies have shown that specific biodegradable hydrogel systems (such as fibrin- and tannic acid-based matrices) can stably encapsulate EVs while maintaining their bioactivity. Furthermore, the PTT effect can inhibit the polarisation of TAM towards the M2 phenotype[275]. The integration of M1 TAM-derived EVs with PTT-functionalised hydrogel systems can establish a self-enhancing immunotherapeutic platform. At the same time, PTT-enhanced heat shock protein expression enhances T cell infiltration and effector functions[276]. This dual-action strategy simultaneously inhibits the recruitment of immunosuppressive myeloid-derived suppressor cells and regulatory T cells, thereby generating potent antitumor immunity in preclinical models[277].

In particular, the TME often has acidic properties that can reduce T-cell activity and recruit immunosuppressive cells, thereby promoting the formation of an immunosuppressive TME[278,279]. The combination of alkaline metal salt nanoparticles with locally injected hydrogels can neutralise the acidity. Furthermore, while neutralising the acidic environment, the metal ions produced by the nanoparticles can generate peroxidase-like catalytic activity, promoting the decomposition of endogenous H_2O_2 into ROS, which subsequently downregulates the expression of the anti-phagocytic signal CD47[265]. In addition, the TME can suppress immune cell-mediated antitumor immunity *via* physical mechanisms[280]. Neutrophil extracellular traps, consisting of neutrophil nuclear DNA, can coat tumor cells and form a physical barrier that prevents immune cell infiltration. Cheng et al.[281] have developed a dual pH-responsive hydrogel containing a tumor acidity neutraliser (mesoporous bioactive glass nanoparticles) and a neutrophil extracellular traps-cleaving enzyme, deoxyribonuclease 1, to prevent liver cancer recurrence after hepatectomy. GODM gel can be sprayed onto surgical margins to form an adhesive gel that rapidly stops bleeding. It also neutralised the acidic TMEt, reduced local infiltration of immunosuppressive cells, and facilitated NET degradation by releasing DNase I.

Hydrogel-based immunotherapy exemplifies the convergence of material innovation and immunobiology in dismantling the immunosuppressive TME. These systems enhance antitumor immunity by enabling spatiotemporal delivery of immunomodulators, neutralising acidic niches, and disrupting physical barriers. However, the dense ECM of desmoplastic tumors often restricts hydrogel distribution and immune cell infiltration. Injectable, *in situ*-forming hydrogels enable minimally invasive administration but suffer from rapid, uncontrolled degradation. While stimuli-responsive designs achieve on-demand drug release, contradictions persist in the literature-some studies correlate accelerated hydrogel erosion with enhanced T cell activation. In contrast, others argue that prolonged retention is crucial for maintaining efficacy[282,283]. Future research must harmonize release kinetics with tumor immune dynamics, establish comprehensive quality standards for hydrogels, and define clear immunogenicity benchmarks, all of which are imperative for resolving these discrepancies and accelerating the clinical translation of hydrogel immunotherapies.

4.5. Starvation therapy

Tumor recurrence is critically dependent on vascular nutrient supply to sustain the proliferative and metabolic demands of malignant cells, which has led to interest in "starvation therapy", a therapeutic paradigm that induces tumor cell apoptosis by disrupting metabolic pathways or nutrient access[291]. Thrombin, which promotes platelet aggregation and catalyzes the conversion of fibrinogen to fibrin to induce vascular occlusion, represents a promising starvation strategy[292]. However, systemic thrombin administration carries significant risks that can be circumvented by hydrogel-mediated localised delivery. Wang et al.[293] developed an injectable, photoresponsive hydrogel using polydopamine-crosslinked collagen/silk fibroin composites for thrombin delivery to block tumor vasculature. In a weakly acidic environment, dopamine self-polymerises to polydopamine and simultaneously induces amine-mediated crosslinking of silk fibroin to form a gel matrix. Upon near-NIR irradiation, polydopamine generated photothermal heating, destabilising thrombin−DNA base-pairing interactions within the hydrogel and triggering thrombin release. This photothermal effect simultaneously suppresses vascular endothelial growth factor (VEGF) secretion, thereby inhibiting compensatory angiogenesis in peritumoral tissues.

While permanent vascular occlusion promotes ischaemic tumor necrosis, it also exacerbates hypoxia-driven adaptive responses in tumors. Hypoxia upregulates HIF1A and VEGF synthesis, paradoxically accelerating compensatory angiogenesis[294,295]. To address this challenge, Fan et al.[296] used a precipitation method to copolymerise the thermoresponsive monomer *N*-isopropylacrylamide with catechol group-containing dopamine methacrylamide and encapsulate Mn^{2+} to produce an injectable thermoresponsive hydrogel. This hydrogel can crosslink into a semi-solid gel at body temperature, thereby achieving embolization. Mn^{2+} can convert H_2O_2 produced by tumor cells into hydroxyl radicals through the Fenton reaction. Meanwhile, hydroxyl radicals rapidly oxidise the catechol groups into highly reactive quinones, further enhancing the hydrogel's and vessel wall's adhesion properties. Therefore, this hydrogel can simultaneously embolize and inhibit hypoxic environments. Separately, Liu et al.[297] addressed the hydrophobicity-driven delivery limitations of clinical angiogenesis inhibitors by developing a Cu-nanodot functionalized 2D layered double hydroxide system to

load sorafenib. 2D layered double hydroxide features brucite-like positively charged metal hydroxide layers ('host sheets') interspersed with exchangeable anions and water molecules ('guest interlayers'), providing substantial surface area and intercalation capacity for hydrophobic drug loading *via* ion exchange or adsorption[298]. Secondly, hydroxyl-rich 2D layered double hydroxide interacts with amide linkages in thermoresponsive poly(*N*-isopropyl acrylamide) matrices to form hydrogels that undergo rapid photothermal contraction under 1064 nm laser irradiation, achieving vascular blockade[299]. Evidence suggests that nutrient-deprived tumor cells rewire their metabolic pathways by downregulating IGF-1/IGF-1R signalling to activate pro-survival autophagy. While autophagy transiently increases $CD8^+$ T cell infiltration, it simultaneously enhances Treg-mediated immunosuppression[300,301]. Hypoxia caused by starvation therapy may promote the creation of an immunosuppressive environment[302]. Zhang et al.[303] have developed a microbial therapy hydrogel (ACG gel) that simultaneously enhances hypoxia-restricted tumor starvation treatment and immunotherapy. The ACG gel consists of ALG, chlorella, and glucose oxidase. The chlorella encapsulated in the ACG gel produces an abundant oxygen supply through photosynthesis, thereby increasing glucose consumption.

Hydrogel-mediated tumor starvation therapy centers on the localized delivery of thrombin, angiogenesis inhibitors, or metabolic interference agents *via* smart-responsive hydrogels, thereby enabling precise blockade of the tumor blood supply while minimizing the bleeding risks associated with systemic administration. However, starvation-induced activation of the HIF1A/VEGF pathway and autophagy-mediated formation of an immunosuppressive microenvironment may lead to therapeutic resistance. Second, systematic long-term evaluations are lacking regarding the safety of material degradation products and the long-term stability of thrombi.

4.6. Others

Facilitating wound healing is critical to prolonging the post-operative survival of cancer patients. Some hydrogel-based matrices have effective wound healing properties. For example, acrylate-grafted CS exhibits haemostasis by attracting red blood cells through electrostatic interactions and stimulating platelets to release clotting factors. Oxidised hyaluronic acid exhibits haemostatic properties closely associated with keratinocyte proliferation and migration[304]. In addition, natural or metabolically derived products that promote wound healing can be encapsulated in hydrogels to enhance their healing properties[305,306]. In particular, the endogenous metabolite biliverdin not only has a high photothermal conversion efficiency but also possesses antioxidant, anti-inflammatory, and cytoprotective effects. Therefore, it can be used as a biodegradable photothermal agent for PTT and as a bioactive drug for subsequent wound healing processes[307].

In recent years, the therapeutic potential of siRNA and mRNA drugs in the fight against cancer has been recognised[308]. However, compared to DNA therapeutics, mRNA and siRNA are more susceptible to nucleases *in vivo*[309]. The emergence of hydrogel delivery systems provides a nuclease-free environment, allowing precise and targeted *in vivo* delivery of siRNA and mRNA[310]. A drug delivery system comprising methacrylated gelatin and lipid nanoparticles encapsulating siRNA and mRNA allows localised and sustained drug release in the intestine. In this system, the lipid nanoparticles mask the siRNA's charge, thereby protecting it from RNase degradation. Upon mixing, the methacrylate groups within the gelatin scaffold cross-link under 405 nm blue light irradiation, encapsulating the nanoparticles and forming an *in situ* delivery system. This delivery scaffold prolongs drug release for up to 7 days[311]. Yin et al.[312] discovered that low-molecular-weight polyethyleneimine can bind the mRNA encoding ovalbumin *via* electrostatic interactions. The introduction of graphene oxide into the system resulted in unique behaviour distinct from that of traditional (chemically cross-linked) hydrogels: some liquid-solution hydrogels spontaneously transformed into nanoparticles due to interfacial instability, further facilitating controlled drug release.

5. Functionalized hydrogels in cancer diagnosis and TMEt simulation

5.1. Intelligent monitoring

Recent advances in detection technologies have propelled the development of ultrasensitive biosensors for early cancer screening and postoperative surveillance[313]. Hydrogel materials have emerged as an ideal platform for constructing wearable and implantable biosensing systems due to their exceptional biocompatibility, tunable microarchitecture, and versatile functionalization capabilities. By integrating colorimetric, spectroscopic, and fluorescence-based signal transduction mechanisms, hydrogel-based sensors now enable *in situ*, real-time monitoring of tumor-associated proteins and metabolites with high sensitivity[314].

Cancer cells can promote their own proliferation and adaptation to the TME by regulating metabolic pathways and altering metabolite levels. Fluctuations in metabolite concentrations directly mirror oncogenic activity and TME dynamics, often preceding radiologically detectable lesions[315,316]. The key point is that these metabolite concentration changes occur much earlier than visible lesions on imaging and are not affected by intertumoral heterogeneity, making them the next golden biomarker for "liquid biopsy"[315]. Sarcosine has emerged as a clinically significant biomarker for prostate cancer. The biosynthesis and catabolism of sarcosine are tightly regulated by key metabolic enzymes, notably glycine-*N*-methyltransferase and sarcosine dehydrogenase, whose dysregulation leads to pathological sarcosine accumulation. In contrast, sarcosine concentrations remain undetectable or minimal in benign prostatic hyperplasia and healthy control cohorts[317,318]. Capitalizing on this differential expression, Passornraprasit et al.[319] developed a colorimetric biosensor employing cellulose nanofiber (CNF)/PAA hydrogel matrices for direct quantification of sarcosine in urine samples from prostate cancer patients. The sensing mechanism relies on the HRP−H_2O_2−TMB interaction principle. The hydrogel is loaded with a TMB-HRP-sarcosine oxidase solution, in which enzymatic sarcosine demethylation, triggered upon sarcosine exposure, generates glycine, formaldehyde, and hydrogen peroxide (H_2O_2), inducing a visible colorimetric shift. Furthermore, the researchers integrated CNF/PAA hydrogels with 3D-printed test strips and embedded them into diapers. Upon contact with urine, the hydrogel exhibits a distinct color change, enabling real-time monitoring of creatinine concentration in the body through visual observation and comparison with a color chart. Additionally, the hydrogel can be retrieved for more accurate quantitative analysis using a spectrophotometer[320] (Fig. 8A). Surface-enhanced Raman spectroscopy (SERS) exhibits exceptional sensitivity, enabling detection at ultralow concentrations

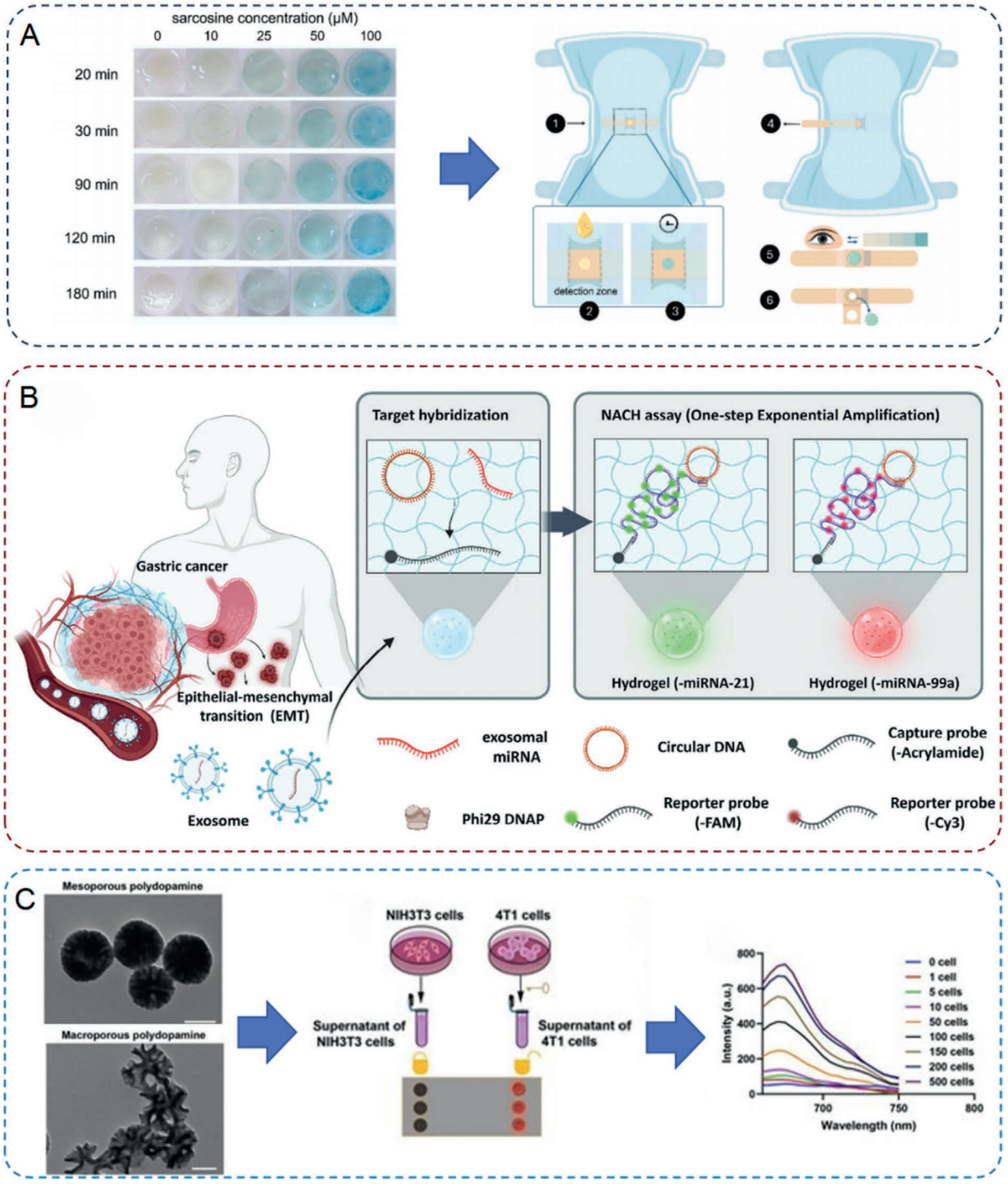

Figure 8 Hydrogel-based platform integrating AI for ultrasensitive cancer biomarker detection in early screening and postoperative monitoring. (A) Hydrogel platform for prostate cancer screening *via* sarcosine detection. Reprinted with permission from Ref. 319. Copyright © 2025 Elsevier. (B) Nucleic acid amplification circuit-based hydrogel for the detection of metastatic gastric cancer exosomal miRNA. Reprinted with permission from Ref. 329. Copyright © 2024 John Wiley and Sons. (C) Implantable hydrogel sensor for postoperative detection of carcinoembryonic antigen and rapid ablation of recurrent cancer cells *via* photothermal therapy. Reprinted with permission from Ref. 331. Copyright © 2024 John Wiley and Sons.

down to the single-molecule level. This remarkable capability facilitates noninvasive cancer screening by identifying trace tumor biomarkers in bodily fluids, including blood, saliva, and sweat[321]. Numerous studies have established strong correlations between cancer progression and metabolic byproducts such as uric acid, creatinine, glucose, and various aldehydes[322]. Chen et al.[323] developed a SERS-integrated hydrogel wearable sensor for noninvasive monitoring of tumor progression through sweat

analysis. This detection module comprises a polyvinyl alcohol-sucrose hydrogel integrated with silver dendritic nanostructures that serve as a SERS substrate. Through surface functionalization with molecular receptors, these dendritic nanostructures enable selective capture of cancer biomarkers in sweat. For example, grafting with 4-mercaptophenylboronic acid facilitates glucose sensing. The charge transfer between glucose and 4-mercaptophenylboronic acid enhances the characteristic SERS signal. Functionalization with 4-mercaptobenzoic acid imparts pH-responsiveness, as the protonation/deprotonation of its carboxyl groups ($COOH \leftrightarrow COO^-$) induces measurable Raman shifts at 1187 cm^{-1} (ν_{C-O}) and 1420 cm^{-1} (ν_{COO-}), thereby enabling precise pH monitoring. After modification with 4-mercaptopyridine, it can interact with α-dicarbonyl metabolites (such as glyoxal and methylglyoxal) *via* proton transfer, and the intensity ratio $I_{1611}/I_{1583}3$ quantitatively reflects the degree of protonation and carbonyl metabolite concentration. These enhanced Raman signals are wirelessly transmitted to smartphones *via* Bluetooth or Wi-Fi. After specific data processing, the signals are uploaded to cloud servers for analysis, enabling automatic disease diagnosis.

Compared to blood or other biofluids, interstitial fluid (ISF) from tumor sites represents a richer source of biomarkers, offering superior diagnostic accuracy and sensitivity for detecting residual microtumors before clinical recurrence. During EMT, tumor-derived ISF becomes enriched with microRNAs (miRNAs) that serve as master regulators of EMT[324,325]. Specifically, miRNA-21 and miRNA-99a downregulate E-cadherin while activating transcription factors (Twist, Snail, ZEB) to drive cytoskeletal remodeling and MMP expression[326,327]. Conversely, the miRNA-200 family suppresses ZEB1 and ZEB2, thereby preserving epithelial phenotypes. Monitoring these EMT-associated miRNA dynamics in ISF thus provides a powerful strategy for early tumor detection, intervention, and improved therapeutic outcomes[328]. Seo et al.[329] developed a nucleic acid-amplified hydrogel biosensor for the sensitive detection of exosomal miRNA-21 and miRNA-99a, biomarkers associated with metastatic gastric cancer. The system comprises two key components: (1) a capture probe with a 3′-acrylamide modification for covalent immobilization within a polyethylene glycol diacrylate hydrogel network *via* photopolymerization; (2) a circular DNA template for isothermal rolling circle amplification. Upon target miRNA binding, the capture probe, tethered at one end to the hydrogel matrix, hybridizes with one segment of the miRNA. At the same time, the circular DNA binds to the complementary region, forming a bridged hybridization complex. This structure primes isothermal rolling circle amplification catalyzed by Phi29 DNA polymerase, using the miRNA as a primer and the circular DNA as a template. The resulting long, repetitive DNA products are then detected by sequence-specific fluorescent probes, generating an amplified signal proportional to the target concentration (Fig. 8B). Fluorescence signals were collected using the ChemiDoc imaging system and subsequently analyzed for fluorescence intensity using ImageJ, enabling rapid evaluation of clinical samples. Wang et al.[330] developed an instrument-free miRNA detection platform by coupling an entropy-driven dynamic DNA network hydrogel membrane with a gold nanoparticle (AuNP). In this system, the target miRNA initiates a toehold-mediated strand-displacement reaction, triggering cyclic amplification within the dynamic DNA network cascade. This process releases abundant output DNA strands (S2), which disrupt the hydrogel matrix, thereby liberating entrapped AuNPs. The resulting dispersion shifts the solution color from colorless to red *via* changes in localized surface plasmon resonance (LSPR). By quantifying the RGB values of this colorimetric transition *via* smartphone imaging, the platform achieves semi-quantitative miRNA analysis without specialized equipment. Carcinoembryonic antigen (CEA) in tumor ISF serves as a well-established biomarker for predicting and monitoring tumor recurrence. This approach combines the programmability of DNA circuits with the visual readout of nanoplasmonics, enabling point-of-care miRNA profiling in resource-limited settings. Geng et al.[331] have developed an innovative implantable hydrogel sensor system for ultrasensitive detection of carcinoembryonic antigen (CEA) in tumor interstitial fluid, coupled with real-time photothermal therapeutic capabilities. The platform employs a methacrylated ALG hydrogel matrix incorporating three functionally integrated components: macroporous polydopamine nanoparticles (MPDA) loaded with molecular beacon probes, an MMP-responsive exonuclease I delivery system (exo I@TGMS), and embedded fibroblasts. Through fluorescence resonance energy transfer (FRET), the MPDA nanoparticles effectively quench the fluorescence of Cy5-labeled hairpin DNA (Cy5-hDNA) probes until target recognition occurs. CEA binding induces conformational changes in Cy5-hDNA that disrupt FRET quenching, restoring fluorescent signals. The TME's characteristic MMP overexpression triggers the controlled release of exonuclease I, which selectively cleaves CEA−DNA complexes, enabling continuous target recycling and signal amplification. Furthermore, the incorporated fibroblasts enhance detection sensitivity by chemotaxis of CXCR4-expressing tumor cells *via* CXCL12. Beyond diagnostic functionality, the system leverages MPDA's exceptional photothermal conversion efficiency to provide precise, image-guided tumor ablation upon near-infrared irradiation when residual microtumors are detected (Fig. 8C). This integrated theranostic platform represents a significant advancement in post-operative cancer management, seamlessly combining early recurrence monitoring through ultrasensitive biomarker detection with on-demand therapeutic intervention in a single implantable device.

Hydrogel-based biosensors have demonstrated remarkable potential to translate tumor metabolic fingerprints and recurrence biomarkers into readable, real-time signals, enabling noninvasive screening, intraoperative navigation, and postoperative recurrence prevention for comprehensive cancer management. However, critical challenges-including enzyme activity drift, long-term nanomaterial toxicity, interference from complex biofluid matrices, and cross-reactivity during multiplexed biomarker detection-must be addressed before clinical translation[332,333]. Moreover, as biomarker concentrations fluctuate with medication, inflammation, and dietary factors, establishing region-specific dynamic reference ranges coupled with AI-powered error-correction algorithms becomes imperative[334]. Only by overcoming these limitations can hydrogel-based "liquid sentinels" evolve from proof-of-concept prototypes into reliable, pocket-sized life-alert systems for cancer patients.

5.2. *Cancer cell capture*

Hydrogels have demonstrated significant potential for cancer cell capture, primarily due to their ability to mimic the three-dimensional structure and high water content of the ECM. These properties promote the natural proliferation and aggregation of cancer cells, enabling key applications such as three-dimensional cell culture platforms, targeted cancer cell capture, sorting and enrichment, biosensing and diagnostics[335,336].

The tunable pore size and flexible structure of hydrogel materials enable excellent performance in cell sorting and enrichment, particularly when combined with microfluidic technology for isolating and enriching circulating tumor cells (CTCs), which is of great importance for early cancer detection[337,338]. Despite these advances, achieving target specificity in CTC capture in the complex haematological environment of peripheral blood remains an ongoing challenge. Recent research has identified sialylated glycans on CTC surfaces as viable biomarkers for hepatocellular carcinoma screening[339,340]. Capitalising on this discovery, hydrogels prepared from histidine-based receptors combined with poly(ethylene glycol) methacrylate exhibited high affinity for sialylated glycoproteins, achieving capture efficiencies of up to 93% even when assaying 10 CTCs. Notably, CTCs captured by the hydrogels could be released using trypsin-EDTA solution (0.25% trypsin and 0.02% EDTA), and the released CTCs remained viable. Clinical studies have confirmed that this method can accurately differentiate between liver cancer, cirrhosis, and healthy groups, with an accuracy of 94%[341]. However, enzymatic treatment methods can lead to excessive exposure of cells to enzyme solutions, which may cause functional impairment of the captured cancer cells[342,343]. To overcome this limitation, chemically stable aptamers have emerged as precision molecular tools for CTC recognition, offering antibody-like specificity and enhanced resistance to nucleases. Lin et al.[342] synthesised two polymeric DNA chains (R1 and R2) *via* rolling circle amplification: the R1 chain contains repeated aptamer sequences that specifically recognise CTC surface markers and DNAzyme sequences. The R2 chain contains the corresponding DNAzyme substrate sequence. R1 and R2 can form a DNAzyme hydrogel (MA-RCA) *in situ*, encapsulating the target cells in three dimensions. Captured cells can be released by Zn^{2+}-induced specific cleavage of the DNAzyme hydrogel, avoiding cell damage caused by enzymatic lysis (Fig. 9A). Ye et al.[344] developed a three-dimensional porous DNA hydrogel containing promoter DNA with aptamer-to-hold blocks that specifically bind to the epithelial cell adhesion molecule on CTC surfaces, forming a hydrogel to encapsulate CTCs. This hydrogel can disintegrate under mild chemical stimulation, releasing CTCs[345].

Following surgical treatment, residual glioblastoma (GBM) cells, including therapy-resistant glioblastoma stem-like cells (GSC), are highly likely to infiltrate healthy brain parenchyma and form secondary tumors[346]. Vascular co-option, the predominant invasion mechanism in GBM progression, is driven by the chemokine CXCL12 secreted from perivascular niches, which engages the CXCR4 receptor overexpressed on GBM/GSC membranes to mediate tumor-endothelial interactions[347]. To disrupt this pathological crosstalk, Khan et al.[348] developed an injectable thiol-functionalised hydrogel capable of electrostatically immobilising cationic CXCL12 *via* stable anionic thiolate bonds. This *in situ*-forming matrix creates a synthetic chemotactic sink that sequesters migrating GBM/GSC populations within its porous architecture, effectively diverting tumor cells from hemogenic dissemination pathways (Fig. 9B). Despite the widespread adoption of ligand-based capture strategies targeting surface biomarkers for CTC isolation, the dynamic phenotypic shifts induced by EMT present a fundamental limitation-epithelial marker loss (*e.g.*, EpCAM) coupled with mesenchymal marker upregulation (*e.g.*, vimentin) generates substantial heterogeneity that eludes conventional single-marker approaches[349,350]. To address this challenge, Zuo et al.[351] engineered an innovative dual-recognition platform that leverages a three-dimensional wrinkled cellulose hydrogel substrate, which synergistically combines EpCAM-specific and vimentin-targeting aptamers to achieve phenotype-agnostic CTC capture. The system's diagnostic utility is further enhanced by an elegantly designed glucose-encapsulated signaling probe, in which aminated mesoporous silica nanoparticles (MSNs) loaded with glucose are sealed by L-cysteine-modified gold nanoparticles *via* Au−S bonds, forming Au-G-MSN-Apt conjugates functionalized with both aptamer types. Crucially, CTC binding triggers gold nanoparticle displacement and glucose release, enabling instrument-free quantification *via* portable glucose meter readouts-a robust signal transduction mechanism that circumvents the need for complex analytical instrumentation (Fig. 9C).

5.3. *Mimicking TME*

Unravelling the dynamic interplay between the TME and malignant progression is central to advancing precision oncology. Traditional two-dimensional tumor models, while experimentally tractable, impose non-physiological constraints by exposing cells to hyper-rigid substrates that disrupt critical cell−cell and cell−ECM communication networks[352,353]. Although multicellular spheroids partially recapitulate the three-dimensional tumor architecture, their homogeneous spherical geometry does not mimic the biomechanical and biochemical complexity of native TME niches. Hydrogel-based 3D culture systems overcome this limitation by replicating tissue-specific viscoelasticity and ECM ligand density, thereby preserving tumor-stromal crosstalk, which is essential for modelling metastatic behaviour, pathway activation, and pharmacodynamic responses (Fig. 10)[354]. Gel, derived from animal connective tissue, promotes cell adhesion and growth through its RGD sequence (Arg-Gly-Asp, a cell adhesion signal corresponding to the integrin $\alpha V\beta 1$, $\alpha V\beta 3$, $\alpha V\beta 5$, $\alpha V\beta 6$, $\alpha V\beta 8$, $\alpha 8\beta 1$, and $\alpha 5\beta 1$ binding domains). It is therefore commonly used to construct TMEt hydrogels. De Lorenzi et al.[355] developed a bioprinted tumor-on-chip platform using gel hydrogels to pattern multicellular tumor organoids within a spatially vascularised microenvironment. The endothelial and stromal compartments were co-printed and self-organised into perfusable microvascular networks *via* angiogenic sprouting. This architecture supports mesoscale tumor expansion while preserving malignant cell-endothelial interactions.

Dynamic stiffening and rapid stress relaxation (viscoelasticity) are two physical properties that characterise the tumor stromal microenvironment and critically influence tumor growth, progression, and therapeutic response[356]. During tumor invasion and progression, the ECM exhibits dynamic stiffening that modulates intracellular signalling pathways, gene expression profiles, and cellular behaviour, collectively shaping a microenvironment conducive to tumor cell proliferation[357]. To replicate this stromal stiffening process *in vitro*, Nguyen et al.[358] developed a hydrogel (GelNB). Pendant functional groups (hydroxyphenylacetic acid and carboxyhydrazide) within the polymer chains allowed secondary crosslinking and dynamic stiffening of the initially soft hydrogels. In addition, two GelNB-based copolymers, GelNB-hydroxyphenylacetic acid and GelNB-boronic acid, were crosslinked with 4-arm poly(ethylene glycol) thiol to impart hydrogel elasticity. Specifically, the addition of fungal tyrosinase oxidises the hydroxyphenylacetic acid and boronic acid moieties to form hydroxyphenylacetic acid dimers and boronic acid diols. This oxidation process induces the stiffening of cell-laden hydrogels, mimicking the desmoplastic response observed in the TMEt. In

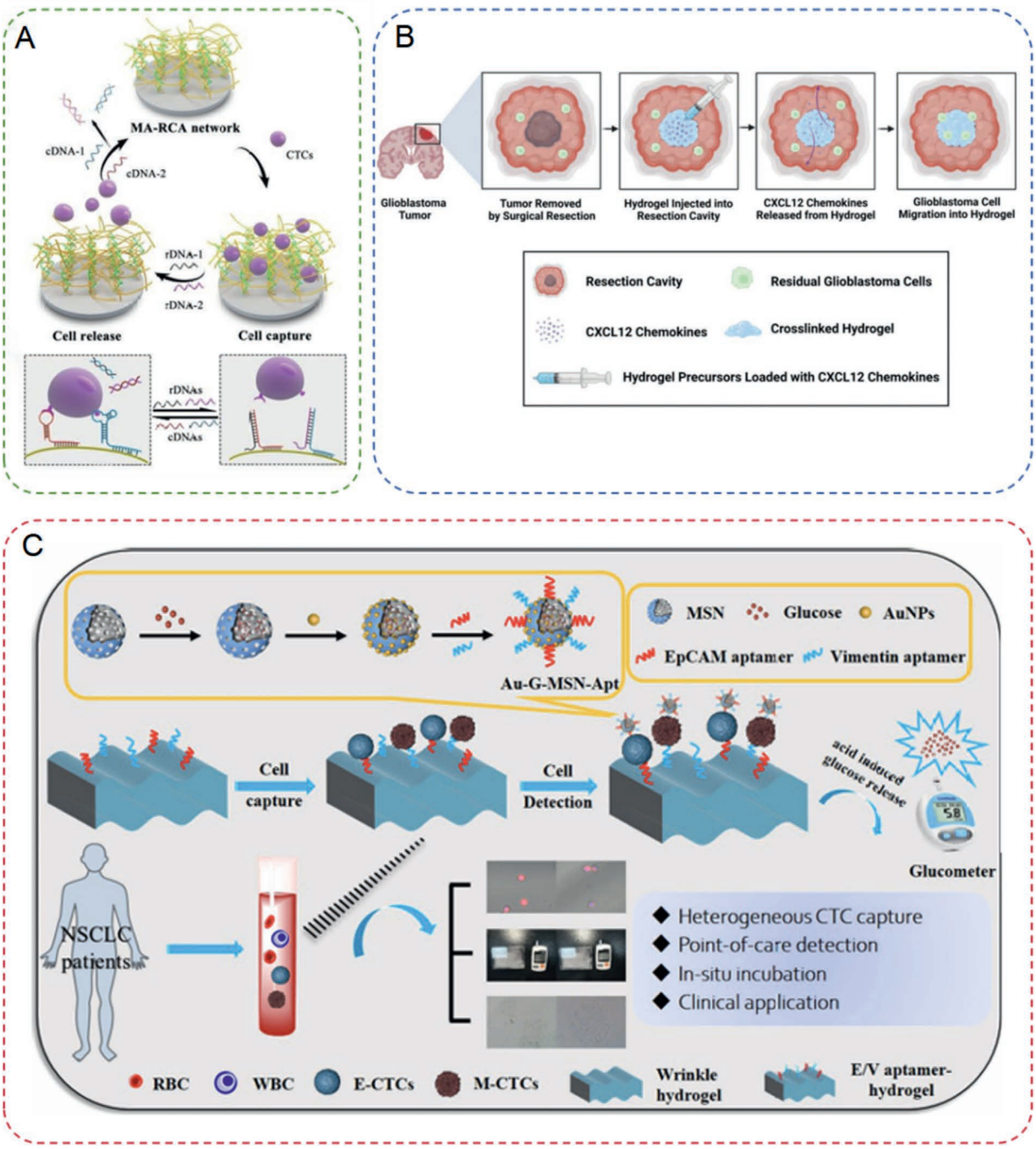

Figure 9 Specific capture and sequestration of cancer cells by hydrogels. (A) Schematic illustration of the MA-RCA hydrogel for CTC capture and release. Reprinted with permission from Ref. 342. Copyright © 2019 Royal Society of Chemistry (B) Schematic overview of the proposed CXCL12-mediated chemotaxis of residual GBM cells. Reprinted with permission from Ref. 348. Copyright © 2023 John Wiley and Sons. (C) Fabrication of E/V aptamer-hydrogel and Au-G-MSN-Apt nanoprobes and applications in capture, detection, and *in situ* culture of CTCs in NSCLC patients. Reprinted with permission from Ref. 351. Copyright © 2023 American Chemical Society.

addition, boronic acid groups facilitate the binding of boronic acid diols to newly formed hydroxyphenylacetic acid dimers generated by fungal tyrosinase-mediated stiffening, thereby enhancing the stress-relaxation capacity of the hydrogel.

Stress relaxation in the ECM refers to the gradual release of perceived mechanical stress by cells over time under external or internal forces. Enhanced stress relaxation promotes diverse biological processes, including stem cell lineage specification, tissue patterning, and maintenance of progenitor cell plasticity, while contributing to the formation of proto-oncogenic and chemo-resistant microenvironments[359]. To engineer stress-relaxing properties within 3D hydrogels, recent studies have employed hydrazone crosslinking (R−HC═NH−NH−R), a dynamic covalent chemistry strategy involving condensation reactions between carbonyl electrophiles (*e.g.*, aldehydes) and nucleophilic hydrazines[360]. Hydrazone bonds exhibit reversible properties, with their

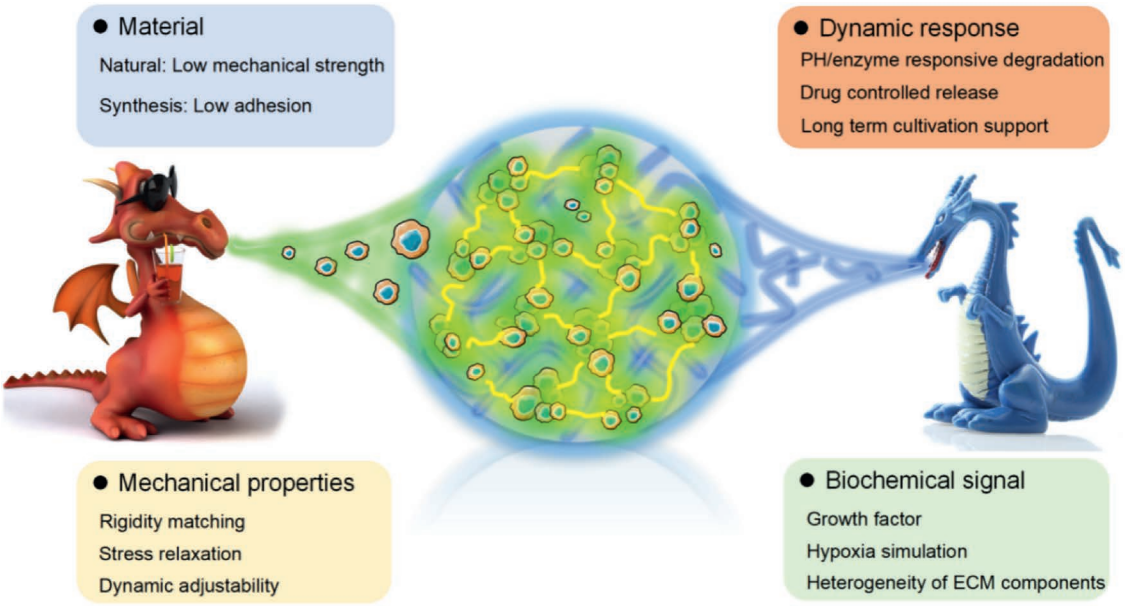

Figure 10 Key factors in hydrogels that mimic the TME integrate material selection (balancing natural polymers' stimuli-responsive degradation and drug release with synthetic polymers' long-term stability), dynamic responsiveness to pH/enzymatic cues, mechanical properties including rigidity matching and stress relaxation, and biochemical signaling through growth factor presentation and ECM component heterogeneity.

chemical equilibrium controlling the rate of hydrogel network reorganisation. This dynamic bonding behaviour allows macromolecular adaptation and structural reconfiguration at the molecular level to dissipate stress during deformation. These hydrogels were further shown to enhance glioblastoma invasion phenotypes, including cell spreading, migratory capacity, and expression of glioma stem cell markers[361].

However, the most significant limitation of current 3D hydrogel models for mimicking the TME is their inability to dynamically and sustainably recapitulate the highly heterogeneous cellular composition and the precise spatial gradients of nutrients, oxygen, and cytokines found *in vivo*[362,363]. Specifically, while these models can encapsulate multiple cell types, they often represent static snapshots. They fail to simulate the spatiotemporal evolution of ECM composition, stiffness, and vascularization status during tumor progression, as well as critical pathological dynamics, such as the expansion of hypoxic regions and patterns of immune infiltration[364–366]. Regarding spatial gradients, oxygen gradients merely form simple hypoxic zones in the deep layers of the hydrogel due to diffusion limitations, lacking the complex, dynamic oxygen distribution resulting from a heterogeneous vascular network[348]. Nutrient gradients, dependent on passive diffusion, struggle to maintain long-term stability[367]. The boundary between the central necrotic zone and the proliferative zone is often blurred, and it is particularly challenging to establish stable chemokine gradients necessary to guide the directional migration of immune cells[368,369]. The simulation of the immune system is also highly fragmented. Most models co-culture only a single type of immune cell, failing to recreate the complex network of T/B cells, dendritic cells, and NK cells, and cell functionality frequently diminishes over time[370]. Furthermore, the absence of a functional vascular network severely limits research into drug perfusion and immune evasion mechanisms[371]. In conclusion, while superior to 2D cultures, hydrogel models are fundamentally limited by their static and homogeneous nature, which contrasts starkly with the dynamic, heterogeneous, and vascularized characteristics of a real TME. Overcoming these limitations urgently requires integrating advanced technologies such as microfluidics, 3D bioprinting, and AI-driven dynamic regulation systems.

6. AI and hydrogels

Although hydrogels have attracted extensive attention, the development of novel hydrogel systems has progressed relatively slowly. This is mainly attributed to the complexity of the design process, which involves the integrated influence of multiple factors, including material composition, formulation parameters, and environmental stimuli[372,373]. Traditional hydrogel design often relies on extensive experimental exploration and empirical experience, which is time-consuming and costly, making it challenging to achieve rapid and precise modulation of specific properties and functions. In recent years, with the rapid advancement of AI, the field of materials science has undergone a significant transformation. The integration of AI and machine learning (ML) technologies with materials science has led to substantial progress in understanding the underlying physical principles of materials. Leveraging advanced algorithms such as artificial neural networks and convolutional neural networks (Table 8), researchers can extract key patterns from vast experimental datasets, predict material properties, and optimize formulation combinations. This approach significantly shortens the design cycle while enhancing design efficiency and success rates[374,375]. AI-based design strategies have not only accelerated the pace of innovation in hydrogels but also facilitated their widespread applications in biomedical engineering, environmental remediation, flexible electronics, and other fields.

6.1. ML

ML, a core branch of AI, enables computer systems to learn and improve from data without explicit programming automatically. Through algorithms, ML allows computers to learn from

Table 8 Classification and applications of common algorithms in machine learning.

Abbreviation	Full name	Category	Function	Applications in hydrogel design	Ref.
GBT	Gradient boosting Tree	Ensemble learning (boosting family)	Build strong learners by sequentially fitting residuals	Construct "formulation−structure −property" relationships	373
ANN	Artificial neural network	Neural network (classification/ regression)	Nonlinear mapping, multi-parameter modeling	Construct "formulation−structure −property" relationships	373
BO	Bayesian optimization	Sequential surrogate optimization	Black-box multi-objective formulation search	Rapidly identify optimal ratios from multi-round experiments	375
SVR	Support vector regression	Regression algorithm (regression extension of SVM)	Predict continuous variables	Predict elastic modulus, swelling ratio, degradation time, etc.	380
RF	Random forest	Ensemble learning (classification/ regression)	Feature importance analysis	Enable rapid inverse design and formulation screening	381
XGBoost	Extreme gradient boosting	Ensemble learning (classification/ regression)	High-precision regression, nonlinear modeling	Predict drug release profiles and adsorption performance	382
SVM	Support vector machine	Supervised classification/regression	Small sample, nonlinear classification	Classify formulations based on target hydrogel properties	383
DT	Decision Tree	Supervised classification/regression	Single tree rule extraction	Classify formulations based on target hydrogel properties	384
KNN	K-Nearest Neighbors	Supervised learning (lazy learning)	Direct classification/regression *via* distance metric	Classify formulations based on target hydrogel properties	385
SMOTE	Synthetic Minority over-sampling Technique	Data augmentation	Address class imbalance	Expand the representative formulation database	386
GAN	Generative Adversarial network	Deep learning - generative	Generate synthetic data	Build generative models for "formulation/process parameters → structure/properties"	387
CNN	Convolutional neural network	Deep learning (image/signal classification)	Image/spectral signal processing	Build correlation models for "image/ spectral signals → biological parameters"	388
LSTM	Long short-Term memory	Deep learning (time-series modeling)	Dynamic response modeling, time-series prediction	Analyze volume change trajectories of hydrogels in temperature cycles	389
FNN	Feedforward neural network	Nonlinear classification/regression	One-time forward computation from input to output	Enable rapid detection based on hydrogel platforms	390
RNN	Recurrent neural network	Deep learning (image/signal classification)	Process sequential data (*e.g.*, time series, text, or spectral signals) with memory and association capabilities	Achieve perception and task classification without building sensor networks	391

experience, recognize patterns, and make predictions or decisions[376]. In hydrogel design, machine learning enables the optimization of materials and properties, the precise programming of dynamic response behavior, the regulation of structure-function relationships, the control of responsiveness, and the analysis of macroscopic response signals. These capabilities confer predictability and programmability to smart hydrogels. In brief, the application of ML to hydrogel design can be summarized as follows. First, a high-quality, multidimensional training dataset is constructed, primarily through experimental data, literature mining, and high-throughput experimental platforms. Next, data preprocessing and feature engineering are performed to filter the data, select and extract relevant hydrogel features, and normalize the dataset. Subsequently, model selection and training are carried out. This step commonly uses some regression algorithms (SVR, RF, XGBoost, ANN, CNN, LSTM), classification algorithms (SVM, DT, RF, CNN), and optimization algorithms (BO) to estimate the mechanical properties and responsiveness of hydrogels. Finally, BO, combined with surrogate models such as Gaussian processes or random forests, is used to infer optimal formulations or structures from target performance, followed by experimental validation and iterative model refinement (Fig. 11)[377,378]. For example, to develop hydrogels with "ultra-strong adhesion" properties, Liao et al.[377] collected extensive data on adhesive proteins from the NCBI protein database, spanning proteins from various species, from bacteria to humans. Through statistical analysis, they identified common adhesive functional sequence motifs within these proteins and performed simulated sequence

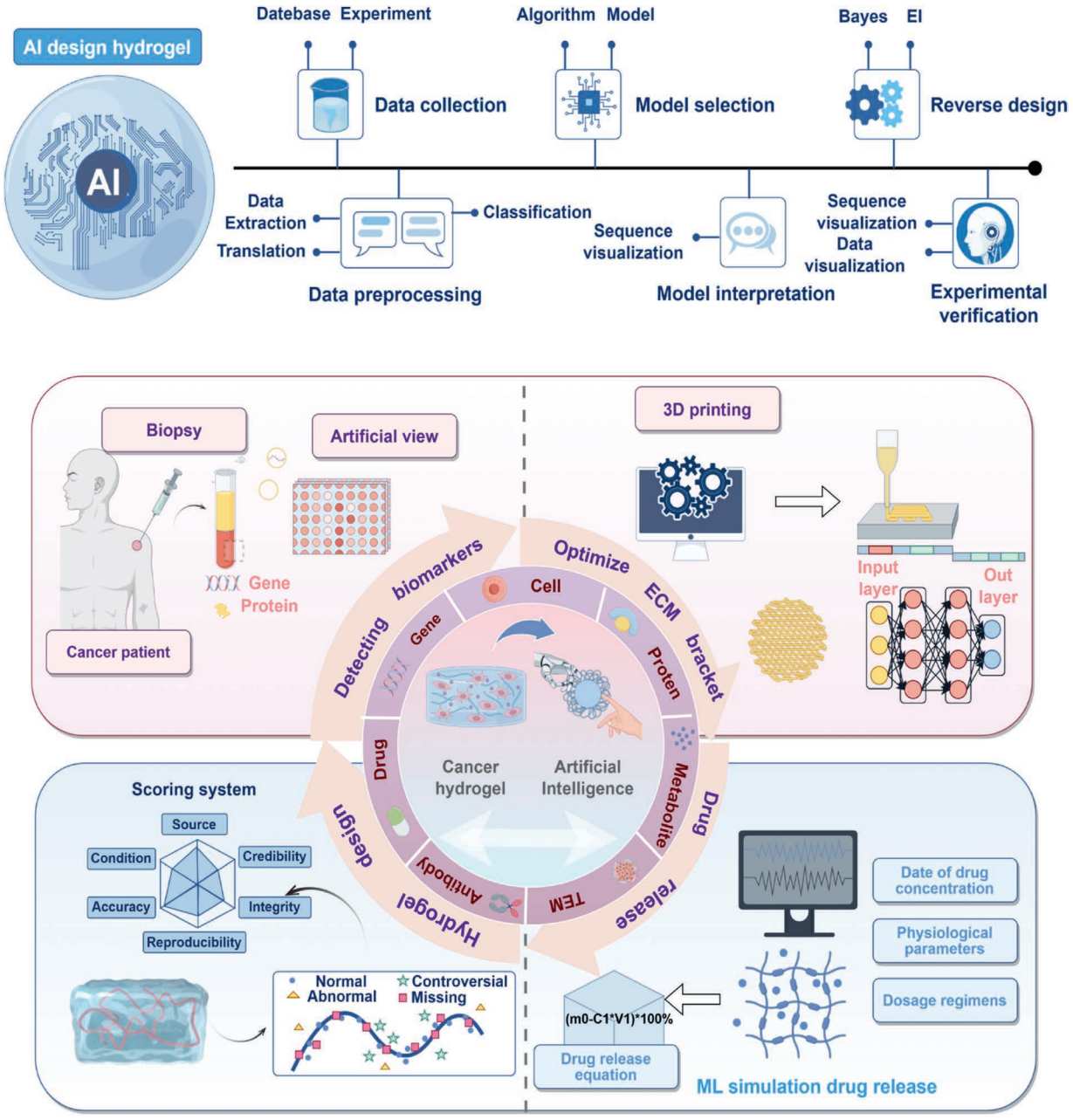

Figure 11 Basic workflow of AI/ML-assisted hydrogel design and its applications in cancer therapy: biomarker detection, ECM simulation, drug release, and formulation design.

recombination using 20 amino acids. Subsequently, multiple machine learning models, including Gaussian process regression and random forest regression, were employed to analyze the adhesion performance of the recombined hydrogel sequences. By integrating sequential model-based optimization and the expected improvement acquisition function, the team iteratively proposed new hydrogel formulations. Ultimately, the optimized hydrogel exhibited an adhesion strength exceeding 1 MPa. To rapidly screen and optimize hydrogels with specific photodegradation properties, Seifermann et al.[379] employed a miniaturized high-throughput synthesis platform to fabricate and screen 918 hydrogel compositions quickly, while simultaneously monitoring their degradation under UVC irradiation in real time. Subsequently, a Gaussian process regression model was used to map material composition to performance metrics, including initial size, fluorescence intensity, and degradation lifetime. By incorporating BO, the platform actively recommended 79 new compositions over 13 experimental rounds, leading to the discovery of hydrogels with enhanced fluorescence intensity and prolonged degradation lifetimes. This AI-driven hydrogel design platform enables precise tuning and optimization of photodegradation performance with minimal resource consumption, providing a novel paradigm for the intelligent design of functional materials.

Developing machine learning models for hydrogels in cancer therapy often poses significant challenges: selecting an appropriate model architecture and adapting it to the specific problem. Although there is no universal solution, experimental screening remains a viable approach to identifying the optimal model. Nevertheless, following certain guiding principles can help streamline the search for suitable models. Below are several case studies of ML models applied to hydrogels in cancer treatment, which generally follow a strategy of starting with simple algorithms and progressively moving to more complex ones if the simpler models fail to meet performance expectations.

Studies have shown that AI-driven optimization algorithms, by tuning key parameters in hydrogel synthesis processes, can significantly enhance both yield and performance. For example, predictive investigations of swelling behavior and gelation kinetics under varying conditions have expanded the applications of hydrogels in drug delivery systems, tissue engineering, and wound healing[392]. ML techniques can uncover latent patterns within multidimensional experimental data to guide the design of high-performance hydrogels. Xu et al.[393] optimized the design and fabrication process of polyacrylamide/sodium ALG double-network hydrogels using machine learning, focusing on five key performance indicators: strain sensitivity, elongation at break, fracture energy, hysteresis, and electrical resistivity. The study established a three-stage ML framework comprising BO, classification screening, and regression prediction. Iterative experimental designs were guided by a BO function, yielding an optimal formulation after 14 iterations. Subsequently, a classification algorithm (random forest classifier) identified the "invalid parameter space" where gelation failed and revealed that the concentrations of acrylamide, crosslinker MBA, and initiator APS had the most significant impact on gel formation. Finally, a regression algorithm (random forest regressor) was employed to build a composition-performance prediction model that accurately forecasts trends in electrical resistivity, elongation at break, and fracture energy. This approach resulted in an ultra-strong hydrogel exhibiting a maximum elongation of 2999%, a strain sensitivity gauge factor of 11.85, and a fracture energy of 0.43 J. The hydrogel's high strain sensitivity and conductivity enable its application as a flexible sensor for real-time monitoring of tumor-related physiological changes when attached to the skin surface or implanted in tissues. Qiu et al.[394] combined backpropagation neural networks with multi-population genetic algorithms to rapidly design hydrogel-based metamaterials exhibiting specific adverse hygroscopic expansion effects. The approach introduced several dimensionless design parameters to characterize the structural features of the metamaterials. An initial dataset was constructed from finite element simulation results, in which the backpropagation neural networks mapped the relationship between design parameters and equivalent linear strain. Subsequently, the multi-population genetic algorithm was employed to optimize metamaterials for targeted expansion effects efficiently. This method demonstrated high accuracy and efficiency, significantly reducing computational complexity while effectively avoiding local optima.

In precision oncology, accurate detection of key biomarkers within the TME is crucial for cancer classification, early diagnosis, and personalized treatment decision-making[395]. Leveraging its powerful data-mining and pattern-recognition capabilities, ML can not only optimize biomarker enrichment and quantification but also significantly enhance diagnostic and classification accuracy through multi-feature fusion modeling. For instance, to accurately identify and quantify various types and expression levels of serum miRNAs associated with different lung cancer subtypes. Chen et al.[396] employed a size-encoded hydrogel microbead technology for extraction-free quantification of serum miRNAs. Specifically, the expression levels of miR-21, miR-205, and miR-375 were used as feature parameters. Characteristic signals were obtained *via* flow cytometry, and models were constructed using principal component analysis and other methods. This study achieved an 80% classification accuracy for lung cancer subtypes across 108 samples, demonstrating the significant potential of ML-enabled multi-biomarker analysis in precise cancer classification. Early tumor detection can be achieved by isolating CTCs from peripheral blood samples and analyzing their characteristic molecular profiles. Li et al.[397] developed a functionalized hydrogel magnetic nanoparticle for the specific enrichment of CTCs from peripheral blood. RNA was then extracted from the enriched CTCs, and the levels of six particular genes (TGM2, EpCAM, DPEP1, MMP14, TM4SF1, ETV4) and serum carcinoembryonic antigen were quantified using droplet digital PCR. Subsequently, the XGBoost algorithm was employed to construct a colorectal cancer score by integrating five CTC mRNA biomarkers and CEA levels. To enhance model interpretability, the LIME and SHAP algorithms were applied to clarify each feature's contribution to the prediction. Finally, the colorectal cancer score was combined with patient age, sex, and CA125/CA199 levels to generate a personalized colorectal cancer risk score to assist clinical decision-making.

Machine learning can accurately predict and optimize drug release kinetics of hydrogels, enabling on-demand controlled release and personalized drug delivery design. Boztepe et al.[398] employed ML to predict the release kinetics of doxorubicin. By designing the hydrogel's microstructure through interpenetrating networks, they modulated swelling behavior and porosity, which significantly influenced the diffusion pathways and release rates of doxorubicin. Furthermore, ML accurately predicted release profiles under varying pH and temperature conditions, revealing that structural parameters such as crosslinking density and hydrophilic-hydrophobic balance govern the release kinetics. The AL-Rajabi team employed a random forest model to analyze the multidimensional coupling among temperature-responsive parameters,

polymer composition, and geometric factors, uncovering the pivotal regulatory role of macroscopic structure in the drug release process. Increasing the hydrogel thickness extended the diffusion pathway. Additionally, ML quantified the critical impact of temperature-induced phase transition, drug release efficiency at 32 °C in the gel state was enhanced by 256% compared to the sol state at 18 °C[399].

The analytical and recognition capabilities of ML make it particularly well-suited for optimizing the biomaterial composition, mechanical properties, and structural parameters of ECM scaffolds[400]. The integration of ML with computational fluid dynamics enhances the simulation of fluid flow, shear stress, and nutrient gradients. Furthermore, AI-driven adaptive control systems enable real-time modulation of ECM stiffness, biochemical gradients, and cell-cell interactions, thereby improving the physiological relevance of *in vitro* tumor models[401]. By integrating AI-assisted 3D bioprinting technology, real-time parameter adjustments can be achieved, which not only enhances printing accuracy and reproducibility but also reduces the need for trial-and-error experiments[402,403]. For example, Lee et al.[403] proposed a machine-learning-based strategy for designing 3D bioprinting bioinks. By analyzing the rheological properties of acellular collagen, HA, and fibrin, and applying ML combined with multivariate regression for feature analysis, they identified high elastic modulus and low yield stress as key factors influencing bioink printability. Based on these findings, the research team successfully developed multiple efficient bioink formulations. Cadamuro et al.[404] selected Gel derived from porcine skin and HA as biopolymer components, with PEG star-shaped molecules serving as crosslinkers. They covalently constructed a three-dimensional hydrogel network *via* azide-alkyne cycloaddition and Diels-Alder click chemistry reactions. By integrating rheological data with synthesis datasets and material usage constraints, they developed a machine learning model that accurately predicts hydrogel formulations based on target storage and loss moduli, thereby overcoming the limitations of traditional trial-and-error approaches. Gel and HA effectively mimic ECM components, while click chemistry enables precise control over crosslinking structure and properties. This predictive tool significantly enhances biomaterial design efficiency, reduces time and material waste, and maintains high accuracy even with limited datasets.

6.2. *AI simulation of microscopic property changes in hydrogels*

The "structure-property-function" relationships of hydrogels are highly complex. Their macroscopic properties are determined collectively by the chemical structure of polymer chains, crosslinking methods, network topology, and interactions with the environment. These intrinsic mechanisms are complex to elucidate at the molecular or atomic scale, significantly limiting the targeted design and development of high-performance hydrogels. Although experimental techniques, such as electron microscopy, nuclear magnetic resonance, and spectroscopy, provide valuable structural information, they often struggle to resolve multi-component synergistic effects, dynamic processes (*e.g.*, gelation, drug release, degradation), and interfacial behaviors. Against this backdrop, computational simulation technologies have emerged as a vital bridge linking microscopic structures to macroscopic properties, offering novel perspectives and powerful tools for the rational design of hydrogels[405,406].

The multiscale simulation methods applied in hydrogel research primarily include quantum mechanics (QM), molecular dynamics (MD), dissipative particle dynamics (DPD), and continuum modeling (Table 9). QM is employed to analyze electronic-level molecular energies, conformational behaviors, and interactions. While offering high accuracy, QM entails substantial computational costs and is typically limited to systems of approximately 100 atoms. It is beneficial for studying functional group design, crosslinking mechanisms, and drug release mechanisms in hydrogels[407,408]. Kocaaga et al.[409] employed QM as a theoretical screening tool to validate the compatibility and controlled release behavior of the lidocaine-pectin system at the molecular level. By calculating the interaction energies of 16 lidocaine-pectin complexes, the results indicated that hydrogen bonding (−17 kcal/mol) contributes to slow drug release at low concentrations. Furthermore, $\pi-\pi$ stacking interactions weakened as pH decreased, thereby helping to prevent drug-molecule self-aggregation.

MD simulations are categorized into all-atom molecular dynamics (AAMD) and coarse-grained molecular dynamics (CGMD). AAMD explicitly describes all atoms and solvent interactions, making it suitable for precise simulations at small scales. It is widely used to analyze hydrogel hydration, swelling behavior, and intermolecular interactions[410]. Kaufman et al.[411] investigated the temperature-responsive behavior of methyl acrylate-modified elastin-like polypeptides (ELP-MA) through AAMD simulations. They found that when the temperature exceeds the transition temperature, significant structural contraction occurs, with the polypeptides folding along their principal axis into more compact conformations. This modification alters the local conformation near lysine residues in elastin-like polypeptides, resulting in a lower glass transition temperature for ELP-MA and a concomitant reduction in optical crosslinking capability. CGMD simplifies atomic groups into "beads", reducing degrees of freedom and enabling simulations of larger spatial and longer temporal scales. CGMD is well-suited for investigating large-scale gelation processes of hydrogels, as well as the evolution of the overall network structure, energy dissipation mechanisms, and fracture points under stretching and compression[399]. Wang et al.[412] employed CGMD simulations to investigate the self-assembly process of diphenylalanine and azobenzene-grafted phenylalanyl-alanine, as well as their photoresponsive behavior. Experimental results demonstrated that the formed lamellar micelles transform into a network structure upon UV irradiation, and revert to the lamellar structure when the light stimulus is removed. These findings confirm the photoresponsive and reversible characteristics of the diphenylalanine/azobenzene-grafted phenylalanyl-alanine system.

Dissipative particle dynamics (DPD), combined with Flory-Huggins mean-field theory, enables the simulation of multicomponent complex systems. This approach is beneficial for analyzing hydrogel degradation and erosion behaviors, as well as drug release kinetics[413]. Lei et al.[414] employed DPD to construct a coarse-grained model of polyacrylamide hydrogels and systematically investigated their large deformation and fracture behaviors. The study revealed that the initial length ratios of effective network chains at the mesoscale follow a Maxwell distribution, resulting in asynchronous straightening of different chains during stretching. This heterogeneity underlies the dispersed macroscopic stress-strain response of hydrogels and explains the failure of conventional continuum mechanics theories under large strains.

Continuum mechanics simulations, such as those based on the fast Lagrangian analysis of continua (FLAC) method, utilize continuity equations to model macroscopic mechanical behavior.

Table 9 Comparison of features of multiscale simulation methods for hydrogel.

Method	Scale range	Time scale	Basic principle	Advantages	Disadvantages	Applications	Ref
QM	<100 atoms	Picosecond	Based on the Hohenberg-Kohn theorem, describing many-body systems *via* the electron density	High accuracy, good reliability; no empirical parameters required	Extremely high computational cost; severely limited number of atoms and time scales	Conformational behavior, charge distribution, intermolecular forces	407,408
AAMD	Atomic level	Femtosecond → Nanosecond	Newton's laws of motion explicitly describe interactions of all atoms (including solvent)	Atomic-level accuracy	High computational cost; limited length and time scales	Accurate simulation of small systems	410,417
CGMD	Nanometer → larger scales	Microsecond → Millisecond	Newton's laws of motion; groups of atoms treated as beads to reduce degrees of freedom	Suitable for large-scale, long-time simulations	Lower accuracy than all-atom simulations	Hydrogel formation process, physical properties, interactions	418,419
DPD	Nanometer → millimeter	Nanosecond → second	Mesoscopic simulation; coarse-grained beads; combined with Flory-Huggins mean-field theory	Fast computation; can handle complex multi-component systems	Relatively low accuracy	Degradation and erosion behavior of hydrogels, drug release kinetics	420,421
FLAC	Micrometer level and above	Millisecond level and above	Based on continuum equations (*e.g.*, finite element method)	Can handle engineering-scale problems	Long simulation times; complex model equations	Hydrogel sensor design, macroscopic mechanical behavior	422

This approach is well-suited for predicting stress distribution and tribological performance of hydrogel components under complex loading conditions[415]. Xu et al.[416] employed FLAC simulations to investigate the mechanical deformation behavior of PCBMA hydrogels with varying crosslinking densities (0.2% to 1.6%, *w*/*w*) under small applied pressures. They found that hydrogels with higher crosslinking density exhibited smaller displacements and faster responses (~38 ms), attributed to lower energy dissipation and quicker attainment of equilibrium. This study, using FLAC, validated the correlation between mesoscale mechanisms (force-induced ion generation) and macroscopic performance (response time), demonstrating that network crosslinking density is the key structural parameter influencing response speed, rather than elastic modulus, water content, or external ions.

AI and ML, through data-driven model construction and performance prediction, have enabled the optimization of hydrogel formulations, precise regulation of responsive behaviors, and accelerated functional design, significantly enhancing the efficiency and success rate of material development. Meanwhile, AI technologies demonstrate broad application prospects in fields such as precision oncology, bioprinting, and drug delivery. By integrating multiscale computational methods, including quantum mechanics, molecular dynamics, dissipative particle dynamics, and continuum mechanics, researchers have gained in-depth insights into the intrinsic mechanisms linking molecular structure to macroscopic performance. This integration offers a theoretical foundation and technical support for the rational design of high-performance hydrogels. Overall, the convergence of AI and multiscale simulation technologies is driving hydrogel research from empirical approaches toward intelligent, precise methodologies, greatly facilitating translational applications in biomedicine and other cutting-edge fields.

7. Challenges and prospects

Cancer hydrogel-based therapeutic platforms hold great potential; however, these innovative concepts emerging from the laboratory continue to face challenges in translational medicine. These challenges include material biocompatibility, long-term safety, scalable manufacturing, and regulatory standardization. Synthetic polymer hydrogels may release degradation products during *in vivo* breakdown, which, if accumulated or poorly metabolized, could exert toxic effects on surrounding tissues and compromise overall health[423,424]. The incorporation of metal ions (*e.g.*, Cu^{2+}, Fe^{3+}) into certain functionalized hydrogels can confer therapeutic effects; however, their long-term accumulation may lead to metal ion overload, resulting in cytotoxicity, oxidative stress, and tissue damage[425]. Furthermore, repeated implantation of hydrogels may activate the immune system, triggering local or systemic immune responses, such as inflammation, fibrosis, or immune rejection[426]. These reactions not only compromise therapeutic efficacy but also limit the long-term safety of hydrogel applications. Current laboratory assays commonly used to evaluate biocompatibility, such as CCK-8 viability tests, hemolysis assays, and H&E staining of major organs, are insufficient[427,428]. *In vitro* cell experiments cannot fully replicate the complex *in vivo* microenvironment, and the indicators employed in these assays are relatively limited, making it difficult to comprehensively assess the multidimensional biosafety of hydrogels[429]. Moreover, these evaluations predominantly focus on short-term biocompatibility, lacking a systematic assessment of the toxicity of long-term degradation

products and chronic immune responses. Therefore, a thorough and systematic investigation into biocompatibility is imperative. The development of safe, efficient, and controllable material systems is critical to advancing the clinical translation of hydrogels in cancer therapy.

The translation from laboratory research to clinical application involves overcoming multiple critical challenges, including quality control, process scale-up, stability validation, and complex regulatory approvals. The intricate composition of hydrogels poses significant difficulties in establishing material reference standards and scalable manufacturing protocols[430]. Typically composed of various synthetic polymers, biomacromolecules, and functional additives, hydrogels exhibit complex inter-component interactions that result in variability in their physicochemical properties and biological performance, thereby complicating quality control efforts[431]. Hydrogel properties are susceptible to preparation parameters such as crosslinking methods, crosslink density, temperature, and pH; even minor variations can markedly influence their structure and functionality, making batch-to-batch consistency difficult to achieve[432]. Critical attributes, including three-dimensional network architecture, mechanical properties, degradation rate, and drug release profiles, require precise characterization[433]. However, current analytical techniques remain insufficient for comprehensive and high-throughput quality assessment. Additionally, some hydrogel materials may undergo performance changes during storage and transportation, necessitating further research and standardization to ensure long-term stability and shelf life[434].

Regulatory agencies such as the U.S. Food and Drug Administration (https://www.fda.gov) and the European Medicines Agency (https://www.ema.europa) are increasingly focusing on emerging technologies like hydrogels. The Food and Drug Administration regulates hydrogel-based medical materials under the medical device framework, classifying products into Class I, II, or III based on their intended use, mechanism of action, and risk level. Low-risk physical barrier products, such as topical wound dressings, generally fall under Class I and are exempt from premarket notification[435]. Class II products, which may contain animal-derived components or are absorbable, require 510 (k) clearance demonstrating substantial equivalence[436]. High-risk Class III products, including injectable implants or those containing bioactive components (*e.g.*, growth factors), are subject to the more stringent premarket approval process. All products must comply with ISO 10993 series biocompatibility standards, as well as sterility and stability testing requirements, and be manufactured under GMP[437]. Products containing drugs or cellular components are regulated as combination products and are subject to even stricter oversight.

However, current regulatory frameworks face significant challenges. The lack of quantitative criteria makes it difficult for companies to define clear compliance pathways. Lagging technical standards result in the absence of unified testing methods for critical parameters such as core component quantification, swelling, and degradation profiles[438]. Furthermore, combination products with coupled catalytic activity and drug release functions often experience protracted approval timelines of 7-10 years, far exceeding initial expectations[439]. Emerging fields like injectable fillers and 3D bioprinting lack dedicated guidance, making it challenging to keep pace with rapid technological advances[440,441]. On the industrialization front, the absence of detailed GMP implementation guidelines leads to a disconnect between process validation and cost control[442]. These limitations collectively hinder the innovation, translation, and clinical accessibility of hydrogels and other advanced biomaterials.

AI-enhanced simulation techniques enable researchers to predict and optimize microenvironmental conditions, effectively reducing experimental variability and accelerating model development[443]. However, several limitations remain, including limited data availability, insufficient model interpretability, challenges in interdisciplinary integration, and translational feasibility issue[444,445]. The most prominent bottleneck lies in the lack of high-resolution spatial experimental datasets, which are critical for training accurate AI models[446]. Therefore, it is imperative to standardize and comprehensively document experimental conditions, including solvent type, temperature, pH, concentration, detection methods, and instrumentation. On a positive note, although data and code availability often pose challenges in interdisciplinary research, recent studies employing machine learning for self-assembly have begun to openly share datasets, with some also providing free access to developed software tools. This openness facilitates validation and reproducibility of research findings[447,448]. Nonetheless, there remains room for improvement, such as public sharing of finalized models to allow researchers to utilize them directly without repeating the entire training and optimization process. Moreover, there is an urgent need to establish a unified, open-access database of hydrogel formulations to address data scarcity and standardization issues. Such a platform would foster interdisciplinary collaboration and expedite machine learning-driven materials innovation.

Most hydrogel-based cancer therapies rely primarily on single intratumoral or peritumoral injections. However, such local strategies exhibit apparent limitations when addressing multifocal, metastatic, or unresectable tumors. For instance, conventional injectable hydrogels are administered directly into or around the cancer *via* puncture needles or catheters. Yet, metastatic lesions are often disseminated throughout deep organs, each only a few millimeters in diameter and numerous in number, making individual puncture infeasible[449]. Even with multipoint delivery, traditional hydrogels typically serve only as drug reservoirs. They may fail to replicate vascular networks necessary to support deep cell survival, resulting in rapid necrosis at the injection core and impaired immune cell function[450−452]. To overcome these challenges, hydrogel therapies are evolving towards systemic regulation. Nanoscale hydrogels can accumulate in tumors *via* the enhanced permeability and retention (EPR) effect and respond to TME-specific stimuli such as low pH or elevated MMP[453−456]. Additionally, supramolecular self-assembly triggered by α-cyclodextrin host−guest interactions and enzyme-activated crosslinking enables catheter-based delivery, offering potential for multipoint intervention in occult metastatic lesions[457,458]. Nevertheless, clinical translation is hindered by bottlenecks in circulatory stability and targeting precision. Hydrogel precursors must avoid premature crosslinking or clearance in the bloodstream and incorporate active targeting ligands, such as RGD peptides, to overcome EPR limitations, while precisely controlling *in situ* gelation kinetics within the TME to prevent capillary embolism[459,460]. Research on intravenous injection of hydrogel precursors with TME-specific assembly remains nascent, necessitating greater focus from the research community.

Furthermore, current hydrogel applications in tumor immunotherapy predominantly depend on chemokine-mediated immune cell recruitment. Hydrogels could potentially serve as “immune cell reservoirs”, evolving beyond inert scaffolds to become self-sustaining immune micro-organs[461,462]. By co-encapsulating

CAR-T/NK effector cells, dendritic cells/macrophages, fibroblast matrices, and signaling factors such as CCL21 and IL-15 within 3D porous gels, a "metabolic-immune dual circulation architecture" can be established[463,464]. Compared to the simple delivery of immunomodulatory drugs, this living reservoir imparts dynamic adaptability to the therapeutic system. However, to avoid immune rejection, these cells must be cultured autologously, which presents another challenge[465]. Moreover, immune cell reservoir hydrogels must establish microvascular connections within 48−72 h before cell necrosis occurs, potentially requiring "prevascularized" gels or rapid pro-angiogenic molecular[466].

8. Conclusions

In summary, functionalised hydrogels exemplify the convergence of innovation and practicality in oncology. By harmonising material intelligence with biological complexity, these systems have unparalleled potential to redefine cancer treatment and transform aggressive malignancies into manageable chronic conditions. With continuous advances in biomaterials, the development of machine learning and AI in materials science represents a potential area of expansion for hydrogel-based cancer therapies. Although preclinical experiments with hydrogels have made some progress, the successful translation of hydrogel technology into clinical treatments remains challenging. Issues such as safety, controllability of drug release, and long-term efficacy assessment need to be fully addressed in the preclinical research phase.

Acknowledgments

This work was supported by the National Natural Science Foundation of China (82474197), the Program for Professor of Special Appointment (Eastern Scholar) at Shanghai Institutions of Higher Learning (TP2020054, China), and the Program for Shanghai High-Level Local University Innovation Team (SZY20220315, China). Additionally, all figures in this paper were meticulously crafted using Microsoft PowerPoint, Chem Draw software, Figdraw (https://www.figdraw.com) and Biorender (https://www.biorender.com).

Author contributions

Wang Qingquan: Conceptualization, Writing-original draft. Li Jiaqi: Validation, Supervision. Feng Nianping: Methodology, Software, Resources. Zhang Yongtai: Conceptualization, Validation, Writing-review & editing, Project administration, Funding acquisition.

Conflicts of interest

The authors declare no conflicts of interest.

Declaration of generative AI and AI-assisted technologies in the manuscript preparation process

During the preparation of this work, the authors utilized ChatGPT and Kimi for information organization. After using this tool, the authors reviewed and edited the content as needed and take full responsibility for the content of the published article.

References

1. Arnold M, Sierra MS, Laversanne M, Soerjomataram I, Jemal A, Bray F. Global patterns and trends in colorectal cancer incidence and mortality. *Gut* 2017;**66**:683−91.
2. Siegel DA, O'Neil ME, Richards TB, Dowling NF, Weir HK. Prostate cancer incidence and survival, by stage and race/ethnicity-united states, 2001−2017. *MMWR Morb Mortal Wkly Rep* 2020;**69**:1473−80.
3. Wagle NS, Nogueira L, Devasia TP, Mariotto AB, Yabroff KR, Islami F, et al. Cancer treatment and survivorship statistics, 2025. *CA Cancer J Clin* 2025;**75**:308−40.
4. Yang L, Ran L, Li Y, Tan Ya, Xia D, Huang T, et al. Cancer cell membrane camouflaged metal-organic framework for enhanced multi-model therapies of prostate tumor *via* cisplatin prodrug delivery. *Colloids Surf* 2025;**725**:137603.
5. Bray F, Laversanne M, Sung H, Ferlay J, Siegel RL, Soerjomataram I, et al. Global cancer statistics 2022: globocan estimates of incidence and mortality worldwide for 36 cancers in 185 countries. *CA Cancer J Clin* 2024;**74**:229−63.
6. Miller KD, Nogueira L, Devasia T, Mariotto AB, Yabroff KR, Jemal A, et al. Cancer treatment and survivorship statistics, 2022. *CA Cancer J Clin* 2022;**72**:409−36.
7. Haider T, Pandey V, Banjare N, Gupta PN, Soni V. Drug resistance in cancer: mechanisms and tackling strategies. *Pharmacol Rep* 2020;**72**:1125−51.
8. Poland S, Ebina W, Muggia F, Guth A. Breast radiation-associated secondary malignancies: a review. *Clin Surg Oncol* 2023;**2**:100010.
9. Shi J, Kantoff PW, Wooster R, Farokhzad OC. Cancer nanomedicine: progress, challenges and opportunities. *Nat Rev Cancer* 2017;**17**:20−37.
10. Diamantis N, Banerji U. Antibody−drug conjugates-an emerging class of cancer treatment. *Br J Cancer* 2016;**114**:362−7.
11. Zhang Z, He C, Chen X. Designing hydrogels for immunomodulation in cancer therapy and regenerative medicine. *Adv Mater* 2024;**36**:e2308894.
12. Delgado-Pujol EJ, Martínez G, Casado-Jurado D, Vázquez J, León-Barberena J, Rodríguez-Lucena D, et al. Hydrogels and nanogels: pioneering the future of advanced drug delivery systems. *Pharmaceutics* 2025;**17**:215.
13. Li X, Xu X, Xu M, Geng Z, Ji P, Liu Y. Hydrogel systems for targeted cancer therapy. *Front Bioeng Biotechnol* 2023;**11**:1140436.
14. Cao H, Duan L, Zhang Y, Cao J, Zhang K. Current hydrogel advances in physicochemical and biological response-driven biomedical application diversity. *Signal Transduct Targeted Ther* 2021;**6**:426.
15. Gutierrez AM, Frazar EM, Mv XK, Paul P, Hilt JZ. Hydrogels and hydrogel nanocomposites: enhancing healthcare through human and evironmental treatment. *Adv Healthcare Mater* 2022;**11**:e2101820.
16. Wei L, Huang J. Recent progress in hydrogel synthesis and biomedical applications. *Gels* 2025;**11**:456.
17. Nanda D, Behera D, Pattnaik SS, Behera AK. Advances in natural polymer-based hydrogels: synthesis, applications, and future directions in biomedical and environmental fields. *Discover Polymers* 2025;**2**:6.
18. Liu LC, Chen YH, Lu DW. Overview of recent advances in nano-based ocular drug delivery. *Int J Mol Sci* 2023;**24**:15352.
19. Chelu M, Popa M, Calderón Moreno JM. Applications of hydrogels in emergency therapy. *Gels* 2025;**11**:234.
20. Di Modugno F, Colosi C, Trono P, Antonacci G, Ruocco G, Nisticò P. 3D models in the new era of immune oncology: focus on T cells, CAF and ECM. *J Exp Clin Cancer Res* 2019;**38**:117.

21. Dai B, Liang X, Dai Y, Ding X. Artificial intelligence medical image-aided diagnosis system for risk assessment of adjacent segment degeneration after lumbar fusion surgery. *SLAS Technol* 2025;**32**: 100283.
22. Gao L, Ye M, Wu C. Cancer classification based on support vector machine optimized by particle swarm optimization and artificial bee colony. *Molecules* 2017;**22**:2086.
23. Li J, Carayon P. Health care 4.0: a vision for smart and connected health care. *IISE Trans Healthc Syst Eng* 2021;**11**:171−80.
24. Baldea I, Grosu IG, Ghafury S, Golat C, Doubali D, Vestemean AM, et al. Biological models for evaluating hydrogel-based formulations in wound healing. *Gels* 2025;**11**:705.
25. Zhou B, Li X, Pan Y, He B, Gao B. Artificial intelligence-assisted next-generation biomaterials: from design and preparation to medical applications. *Colloids Surf B Biointerfaces* 2025;**255**:114970.
26. Ejeromedoghene O, Kumi M, Akor E, Zhang Z. The application of machine learning in 3D/4D printed stimuli-responsive hydrogels. *Adv Colloid Interface Sci* 2025;**336**:103360.
27. Sheng W, Cao S, Qin H, Liu P, Wang D, Weng J, et al. Hydrogel in musculoskeletal diseases: unraveling trends, research foci, and future trajectories *via* bibliometric insights (from 2000 to 2025). *Regen Ther* 2025;**30**:544−57.
28. Marques AC, Costa PJ, Velho S, Amaral MH. Stimuli-responsive hydrogels for intratumoral drug delivery. *Drug Discov Today* 2021; **26**:2397−405.
29. Zhang Y, Lu Y, Li S, Zheng F, Dong Y, Tang H, et al. Precision theranostics in cervical cancer: harnessing stimuli-responsive hydrogels for tumor microenvironment-targeted therapy and diagnosis. *Mater Today Bio* 2025;**35**:102392.
30. Tan W, Chen S, Xu Y, Chen M, Liao H, Niu C. Temperature-sensitive nanocarbon hydrogel for photothermal therapy of tumors. *Int J Nanomed* 2023;**18**:6137−51.
31. Zhao J, Su H, Vansuch GE, Liu Z, Salaita K, Dyer RB. Localized nanoscale heating leads to ultrafast hydrogel volume-phase transition. *ACS Nano* 2019;**13**:515−25.
32. Wu Y, Wang Y, Long L, Hu C, Kong Q, Wang Y. A spatiotemporal release platform based on pH/ROS stimuli-responsive hydrogel in wound repairing. *J Control Release* 2022;**341**:147−65.
33. Piergentili I, Hilberath T, Klemm B, Hollmann F, Eelkema R. Enhancing the ROS sensitivity of a responsive supramolecular hydrogel using peroxizyme catalysis. *Biomacromolecules* 2023;**24**: 3184−92.
34. Xian S, Webber MJ. Temperature-responsive supramolecular hydrogels. *J Mater Chem B* 2020;**8**:9197−211.
35. Wang X, Mafukidze D, Zheng Y. Microalgae aggregation induced by thermoresponsive polymers. *Bioresour Technol* 2025;**415**:131650.
36. Haq MA, Su Y, Wang D. Mechanical properties of PNIPAM based hydrogels: a review. *Mater Sci Eng C* 2017;**70**:842−55.
37. Hanyková L, Krakovský I, Šestáková E, Šťastná J, Labuta J. Poly(*N,N'*-diethylacrylamide)-based thermoresponsive hydrogels with double network structure. *Polymers* 2020;**12**:2502.
38. Işıklan N, Tokmak Ş. Development of thermo/pH-responsive chitosan coated pectin-*graft*-poly(*N,N*-diethyl acrylamide) microcarriers. *Carbohydr Polym* 2019;**218**:112−25.
39. Jo S, Roh S, Shim J, Yu JW, Jung Y, Jang WY, et al. Modulating the thermoresponsive characteristics of PLGA-PEG-PLGA hydrogels *via* manipulation of PLGA monomer sequences. *Biomacromolecules* 2024;**25**:5374−86.
40. Rahmani F, Atabaki R, Behrouzi S, Mohamadpour F, Kamali H. The recent advancement in the PLGA-based thermo-sensitive hydrogel for smart drug delivery. *Int J Pharm* 2023;**631**:122484.
41. Cao Z, Yuan G, Zeng L, Bai L, Liu X, Wu M, et al. Macrophage-targeted sonodynamic/photothermal synergistic therapy for preventing atherosclerotic plaque progression using CuS/TiO_2 heterostructured nanosheets. *ACS Nano* 2022;**16**:10608−22.
42. Xu S, Qian Z, Zhao N, Yuan W. Thermoresponsive injectable self-healing hydrogel containing polydopamine-coated Fe/Mo-doped TiO_2 nanoparticles for efficient synergistic sonodynamic-chemodynamic-photothermal-chemo therapy. *J Colloid Interface Sci* 2024;**654**:1431−46.
43. Kim S, Shin Y, Han J, Kim HJ, Sunwoo SH. Introductory review of soft implantable bioelectronics using conductive and functional hydrogels and hydrogel nanocomposites. *Gels* 2024;**10**:614.
44. Qin D, Zhang A, Wang N, Yao Y, Chen X, Liu Y. Hydroxybutyl chitosan/oxidized glucomannan self-healing hydrogels as BMSCs-derived exosomes carriers for advanced stretchable wounds. *Appl Mater Today* 2022;**26**:101342.
45. Beaudoin G, Lasri A, Zhao C, Liberelle B, De Crescenzo G, Zhu X-X. Making hydrophilic polymers thermoresponsive: the upper critical solution temperature of copolymers of acrylamide and acrylic acid. *Macromolecules* 2021;**54**:7963−9.
46. Kreuzer LP, Widmann T, Geiger C, Wang P, Vagias A, Heger JE, et al. Salt-dependent phase transition behavior of doubly thermoresponsive poly(sulfobetaine)-based diblock copolymer thin films. *Langmuir* 2021;**37**:9179−91.
47. Zhang J, Qian S, Chen L, Chen L, Zhao L, Feng J. Highly antifouling double network hydrogel based on poly(sulfobetaine methacrylate) and sodium alginate with great toughness. *J Mater Sci Technol* 2021; **85**:235−44.
48. Sennakesavan G, Mostakhdemin M, Dkhar LK, Seyfoddin A, Fatihhi SJ. Acrylic acid/acrylamide based hydrogels and its properties-A review. *Polym Degrad Stabil* 2020;**180**:109308.
49. Zhang L, Wang S, Wang Z, Liu Z, Xu X, Liu H, et al. Temperature-mediated phase separation enables strong yet reversible mechanical and adhesive hydrogels. *ACS Nano* 2023;**17**:13948−60.
50. Moon SH, Park SJ, Lee YW, Yang YJ. LCST/UCST behavior of polysaccharides for hydrogel fabrication. *RSC Adv* 2024;**14**: 35754−68.
51. Du W, Sun S, Zhao Z, Zhao B, Zhang X. Controllable transformation of UCST and LCST behaviors in polyampholyte hydrogels enabled by an association-disassociation theory-based switch mechanism. *Mater Horiz* 2025;**12**:587−98.
52. Xi S, Zhang HJ, Liu X, Zhu X, Guo H, Chang BP, et al. Effect of hydrogen bonding strength on the structure and properties of phase-separated hydrogel from gelatin. *Polymer* 2025;**316**:127870.
53. Wan X, Lin J, Bai J, Li J, Wang K, Cao Z, et al. Interception of RCONCl2: late-stage hydrolysis and esterification of primary amides††electronic supplementary information (ESI) available: experimental procedures, spectroscopic data, and NMR spectra. *Org Chem Front* 2023;**11**:183−93.
54. Russo E, Villa C. Poloxamer hydrogels for biomedical applications. *Pharmaceutics* 2019;**11**:671.
55. Kong S, Lv L, Guo J, Yang X, Liao M, Zhao T, et al. Preparation of cod skin collagen peptides/chitosan-based temperature-sensitive gel and its anti-photoaging effect in skin. *Drug Des Dev Ther* 2023;**17**: 419−37.
56. Wang Q, Wang X, Feng Y. Chitosan hydrogel as tissue engineering scaffolds for vascular regeneration applications. *Gels* 2023;**9**:373.
57. Qu C, Bao Z, Zhang X, Wang Z, Ren J, Zhou Z, et al. A thermosensitive RGD-modified hydroxybutyl chitosan hydrogel as a 3D scaffold for BMSCs culture on keloid treatment. *Int J Biol Macromol* 2019;**125**:78−86.
58. Riziotis IG, Lamprou P, Papachristou E, Mantsou A, Karolidis G, Papi R, et al. *De novo* synthesis of elastin-like polypeptides (ELPs): an applied overview on the current experimental techniques. *ACS Biomater Sci Eng* 2021;**7**:5064−77.
59. Liu J, Debuigne A, Detrembleur C, Jérôme C. Poly(*N*-vinylcaprolactam): a thermoresponsive macromolecule with promising future in biomedical field. *Adv Healthcare Mater* 2014;**3**:1941−68.
60. Choi H, Choi WS, Jeong JO. A review of advanced hydrogel applications for tissue engineering and drug delivery systems as biomaterials. *Gels* 2024;**10**:693.
61. Lin CX, Yang K, Li PC, Gao LT, Aziz Y, Li JH, et al. Self-healing and injectable chitosan/konjac glucomannan hydrogel with pH response for controlled protein release. *Colloids Surf B Biointerfaces* 2024;**242**:114089.

62. Zhao L, Feng Z, Lyu Y, Yang J, Lin L, Bai H, et al. Electroactive injectable hydrogel based on oxidized sodium alginate and carboxymethyl chitosan for wound healing. *Int J Biol Macromol* 2023;**230**: 123231.
63. Park J, Kim TY, Kim Y, An S, Kim KS, Kang M, et al. A mechanically resilient and tissue-conformable hydrogel with hemostatic and antibacterial capabilities for wound care. *Adv Sci* 2023;**10**: e2303651.
64. Syrén PO. Enzymatic hydrolysis of tertiary amide bonds by anti nucleophilic attack and protonation. *J Org Chem* 2018;**83**:13543−8.
65. Longo GS, Pérez-Chávez NA, Szleifer I. How protonation modulates the interaction between proteins and pH-responsive hydrogel films. *Curr Opin Colloid In* 2019;**41**:27−39.
66. Feng YH, Zhang XP, Hao YY, Ren GY, Guo XD. Simulation study of the pH sensitive directed self-assembly of rheins for sustained drug release hydrogel. *Colloids Surf B Biointerfaces* 2020;**195**:111260.
67. Lin Q, Lim CC, Owh C, Wong JHM, Ow V, Sim B, et al. PEG-free ph-responsive thermogels containing amphiphilic polycationic polyethylenimine copolymers. *Macromolecules* 2023;**56**:9368−78.
68. Liu C, Yang P, Li J, Cao S, Shi J. NIR/pH-responsive chitosan hydrogels containing Ti(3)C(2)/AuNRs with NIR-triggered photothermal effect. *Carbohydr Polym* 2022;**295**:119853.
69. Tian Y, Wu D, Wu D, Cui Y, Ren G, Wang Y, et al. Chitosan-based biomaterial scaffolds for the repair of infected bone defects. *Front Bioeng Biotechnol* 2022;**10**:899760.
70. Tyo KM, Duan J, Kollipara P, Dela Cerna MVC, Lee D, Palmer KE, et al. pH-responsive delivery of Griffithsin from electrospun fibers. *Eur J Pharm Biopharm* 2019;**138**:64−74.
71. Liu H, Wei X, Peng H, Yang Y, Hu Z, Rao Y, et al. LysSYL-loaded pH-switchable self-assembling peptide hydrogels promote methicillin-resistant staphylococcus aureus elimination and wound healing. *Adv Mater* 2024;**36**:e2412154.
72. Li N, Liu W, Zheng X, Wang Q, Shen L, Hui J, et al. Antimicrobial hydrogel with multiple pH-responsiveness for infected burn wound healing. *Nano Res* 2023;**16**:11139−48.
73. Simeonov M, Kostova B, Vassileva E. Interpenetrating polymer networks of polyacrylamide with polyacrylic and polymethacrylic acids and their application for modified drug delivery-a flash review. *Pharm Nanotechnol* 2023;**11**:25−33.
74. Xiong M, Chen Y, Hu HJ, Cheng H, Li WX, Tang S, et al. Multifunctional pH-responsive hydrogel dressings based on carboxymethyl chitosan: synthesis, characterization fostering the wound healing. *Carbohydr Polym* 2024;**341**:122348.
75. Cheung EC, Vousden KH. The role of ROS in tumour development and progression. *Nat Rev Cancer* 2022;**22**:280−97.
76. Pu M, Cao H, Zhang H, Wang T, Li Y, Xiao S, et al. ROS-responsive hydrogels: from design and additive manufacturing to biomedical applications. *Mater Horiz* 2024;**11**:3721−46.
77. Shi G, Wu Z, Hao Z, Zhu M, Shu F, Yang Z, et al. Microenvironment-responsive hydrogels comprising engineering zeolitic imidazolate framework-8-anchored parathyroid hormone-related peptide-1 for osteoarthritis therapy. *ACS Nano* 2025;**19**:6529−53.
78. Zhai Z, Ouyang W, Yao Y, Zhang Y, Zhang H, Xu F, et al. Dexamethasone-loaded ROS-responsive poly(thioketal) nanoparticles suppress inflammation and oxidative stress of acute lung injury. *Bioact Mater* 2022;**14**:430−42.
79. Pei P, Sun C, Tao W, Li J, Yang X, Wang J. ROS-sensitive thioketal-linked polyphosphoester−doxorubicin conjugate for precise phototriggered locoregional chemotherapy. *Biomaterials* 2019;**188**:74−82.
80. Song W, Yang H, Wang Y, Chen S, Zhong W, Wang Q, et al. Glutathione-sensitive photosensitizer−drug conjugates target the mitochondria to overcome multi-drug resistance in cancer. *Adv Sci* 2024;**11**:e2307765.
81. Wang Y, Yu H, Wang L, Zhang L, Liu J, Chen D, et al. Intelligent microneedle patch based on functionalized alginate and chitosan for long-term self-regulated insulin delivery. *Carbohydr Polym* 2025; **348**:122885.
82. Yuan R, Fang Z, Liu F, He X, Du S, Zhang N, et al. Ferrocene-based antioxidant self-healing hydrogel *via* the biginelli reaction for wound healing. *ACS Macro Lett* 2024;**13**:475−82.
83. Xu H, Suzuki N, Takahashi A, Ohishi T, Goseki R, Xie XM, et al. Structural reorganization and crack-healing properties of hydrogels based on dynamic diselenide linkages. *Sci Technol Adv Mater* 2020; **21**:450−60.
84. Hu J, Zhang Q, Mu Q, Tang Y, Wu Z, Wang G. A ROS-sensitive diselenide-crosslinked polymeric nanogel for nir controlled release. *Chin J Polym Sci* 2023;**41**:386−93.
85. Ding X, Zang M, Zhang Y, Chen Y, Du J, Yan A, et al. A bioresponsive diselenide-functionalized hydrogel with cascade catalytic activities for enhanced local starvation-and hypoxia-activated melanoma therapy. *Acta Biomater* 2023;**167**:182−94.
86. Zhang Y, Tian S, Huang L, Li Y, Lu Y, Li H, et al. Reactive oxygen species-responsive and Raman-traceable hydrogel combining photodynamic and immune therapy for postsurgical cancer treatment. *Nat Commun* 2022;**13**:4553.
87. Robby AI, Yang JH, Jin EJ, Park SY. Tumor microenvironment-selective sol-gel mineralization of ROS-responsive stretchable and conductive hydrogel. *Adv Funct Mater* 2024;**34**:2402367.
88. Li Z, Li G, Xu J, Li C, Han S, Zhang C, et al. Hydrogel transformed from nanoparticles for prevention of tissue injury and treatment of inflammatory diseases. *Adv Mater* 2022;**34**:e2109178.
89. Gong B, Liu Y, Li H, Ju X, Li D, Zou Y, et al. A silk fibroin nanoparticle hydrogel loaded with NK1R antagonist has synergistic anti-inflammatory and reparative effects on dry eye disease. *Adv Sci* 2025;**12**:e2404835.
90. Mastella P, Todaro B, Luin S. Nanogels: recent advances in synthesis and biomedical applications. *Nanomaterials* 2024;**14**:1300.
91. Zhou Z, Li K, Guo Y, Liu P, Chen Q, Fan H, et al. ROS/electro dual-reactive nanogel for targeting epileptic foci to remodel aberrant circuits and inflammatory microenvironment. *ACS Nano* 2023;**17**: 7847−64.
92. Dong S, An S, Saiding Q, Chen Q, Liu B, Kong N, et al. Therapeutic hydrogels: properties and biomedical applications. *Chem Rev* 2025; **125**:8835−920.
93. Martin JR, Howard MT, Wang S, Berger AG, Hammond PT. Oxidation-responsive, tunable growth factor delivery from polyelectrolyte-coated implants. *Adv Healthcare Mater* 2021;**10**:e2001941.
94. Canton M, Sánchez-Rodríguez R, Spera I, Venegas FC, Favia M, Viola A, et al. Reactive oxygen species in macrophages: sources and targets. *Front Immunol* 2021;**12**:734229.
95. Abbasi M, Sohail M, Minhas MU, Mahmood A, Shah SA, Munir A, et al. Folic acid-decorated alginate nanoparticles loaded hydrogel for the oral delivery of diferourylmethane in colorectal cancer. *Int J Biol Macromol* 2023;**233**:123585.
96. Wang M, Prachyathipsakul T, Silva CA, Xiong C, Goel S, Goel HL, et al. Therapeutic induction of ferroptosis in tumors using PD-L1 targeting antibody nanogel conjugates. *Cell Chem Biol* 2024;**31**: 2039−51.
97. Wu Y, Chang X, Yang G, Chen L, Wu Q, Gao J, et al. A physiologically responsive nanocomposite hydrogel for treatment of head and neck squamous cell carcinoma *via* proteolysis-targeting chimeras enhanced immunotherapy. *Adv Mater* 2023;**35**:e2210787.
98. Hussain S, Peng B, Cherian M, Song JW, Ahirwar DK, Ganju RK. The roles of stroma-derived chemokine in different stages of cancer metastases. *Front Immunol* 2020;**11**:598532.
99. Bickenbach K, David N, Koudelka T, Joos C, Scharfenberg F, Rüffer M, et al. Targeted approach to determine the impact of cancer-associated protease variants. *Sci Adv* 2025;**11**:eadp5958.
100. Mondal S, Adhikari N, Banerjee S, Amin SA, Jha T. Matrix metalloproteinase-9 (MMP-9) and its inhibitors in cancer: a minireview. *Eur J Med Chem* 2020;**194**:112260.
101. He L, Kang Q, Chan KI, Zhang Y, Zhong Z, Tan W. The immunomodulatory role of matrix metalloproteinases in colitis-associated cancer. *Front Immunol* 2022;**13**:1093990.

102. Liu W, Gao R, Yang C, Feng Z, Ou-Yang W, Pan X, et al. ECM-mimetic immunomodulatory hydrogel for methicillin-resistant Staphylococcus aureus-infected chronic skin wound healing. *Sci Adv* 2022;**8**:eabn7006.
103. Poreba M. Protease-activated prodrugs: strategies, challenges, and future directions. *FEBS J* 2020;**287**:1936−69.
104. Vizovisek M, Ristanovic D, Menghini S, Christiansen MG, Schuerle S. The tumor proteolytic landscape: a challenging frontier in cancer diagnosis and therapy. *Int J Mol Sci* 2021;**22**:2514.
105. Lin C, Hu Y, Lin Z, Du L, Hu Y, Ouyang L, et al. MMP-9 responsive hydrogel promotes diabetic wound healing by suppressing ferroptosis of endothelial cells. *Bioact Mater* 2025;**43**:240−54.
106. Zhang Z, Long M, Zheng N, Deng Y, Wang Q, Osire T, et al. Microstructural, physicochemical properties, and interaction mechanism of hydrogel nanoparticles modified by high catalytic activity transglutaminase crosslinking. *Food Hydrocoll* 2024;**147**:109384.
107. Davis NE, Ding S, Forster RE, Pinkas DM, Barron AE. Modular enzymatically crosslinked protein polymer hydrogels for *in situ* gelation. *Biomaterials* 2010;**31**:7288−97.
108. Tang R, Zhang Z, Liu X, Zhu L, Xu Y, Chai R, et al. Fibroblast growth factor receptor 1-specific dehydrogelation to release its inhibitor for enhanced lung tumor therapy. *ACS Nano* 2024;**18**:29223−32.
109. Coulter SM, Pentlavalli S, An Y, Vora LK, Cross ER, Moore JV, et al. *In situ* forming, enzyme-responsive peptoid-peptide hydrogels: an advanced long-acting injectable drug delivery system. *J Am Chem Soc* 2024;**146**:21401−16.
110. Zhao F, Liu M, Guo H, Wang Y, Zhang Y, He M, et al. Stimuli-responsive hydrogels based on protein/peptide and their sensing applications. *Prog Mater Sci* 2025;**148**:101355.
111. Zhang Q, Chen W, Li G, Ma Z, Zhu M, Gao Q, et al. A factor-free hydrogel with ros scavenging and responsive degradation for enhanced diabetic bone healing. *Small* 2024;**20**:e2306389.
112. Cañizares-Espada E, Pérez de Bustos G, Naoda K, Osuka A, Torres T, Rodríguez-Morgade MS. A green-to-near-infrared photoswitch based on a blended subporphyrazine-dithienylethene system. *Org Lett* 2024;**26**:955−9.
113. Austin E, Geisler AN, Nguyen J, Kohli I, Hamzavi I, Lim HW, et al. Visible light. part I: properties and cutaneous effects of visible light. *J Am Acad Dermatol* 2021;**84**:1219−31.
114. Dash P, Panda PK, Su C, Lin YC, Sakthivel R, Chen SL, et al. Near-infrared-driven upconversion nanoparticles with photocatalysts through water-splitting towards cancer treatment. *J Mater Chem B* 2024;**12**:3881−907.
115. Guo X, Sheng W, Pan H, Guo L, Zuo H, Wu Z, et al. Tuning shortwave-infrared j-aggregates of aromatic ring-fused aza-bodipys by peripheral substituents for combined photothermal and photodynamic therapies at ultralow laser power. *Angew Chem Int Ed Engl* 2024;**63**:e202319875.
116. Hu S, Fang Y, Liang C, Turunen M, Ikkala O, Zhang H. Thermally trainable dual network hydrogels. *Nat Commun* 2023;**14**:3717.
117. Yao H, Wang J, Mi S. Photo processing for biomedical hydrogels design and functionality: a review. *Polymers* 2018;**10**:11.
118. Soh W, Li J. Cyclodextrin-based pseudocopolymers and their biomedical applications for drug and gene delivery. *Small* 2025;**21**:e01304.
119. Steen JD, Duijnstee DR, Sardjan AS, Martinelli J, Kortekaas L, Jacquemin D, et al. Electrochemical ring-opening and-closing of a spiropyran. *J Phys Chem A* 2021;**125**:3355−61.
120. Shen W, Zheng J, Zhou Z, Zhang D. Approaches for the synthesis of *o*-nitrobenzyl and coumarin linkers for use in photocleavable biomaterials and bioconjugates and their biomedical applications. *Acta Biomater* 2020;**115**:75−91.
121. Kharkar PM, Scott RA, Olney LP, LeValley PJ, Maverakis E, Kiick KL, et al. Controlling the release of small, bioactive proteins *via* dual mechanisms with therapeutic potential. *Adv Healthcare Mater* 2017;**6**:1700713.
122. Huang Y, Wang Z, Zhang G, Ren J, Yu L, Liu X, et al. A pH/redox-dual responsive, nanoemulsion-embedded hydrogel for efficient oral delivery and controlled intestinal release of magnesium ions. *J Mater Chem B* 2021;**9**:1888−95.
123. Liang Y, Li M, Yang Y, Qiao L, Xu H, Guo B. pH/glucose dual responsive metformin release hydrogel dressings with adhesion and self-healing *via* dual-dynamic bonding for athletic diabetic foot wound healing. *ACS Nano* 2022;**16**:3194−207.
124. Pareek A, Bhatt B, Parmar V, Alasiri G, Alsaidan OA, Kapoor DU, et al. pH-sensitive hydrogels for breast cancer therapy: targeted drug delivery and controlled release approaches. *Int J Pharm* 2025;**682**:125899.
125. Karakaya M, Karataş RB, Ayaz F, Aydemir E. Hydrogel applications in tumor microenvironment modeling. *Discover Biotechnology* 2025;**2**:21.
126. Jaiswal MK, De M, Chou SS, Vasavada S, Bleher R, Prasad PV, et al. Thermoresponsive magnetic hydrogels as theranostic nanoconstructs. *ACS Appl Mater Interfaces* 2014;**6**:6237−47.
127. Dethe MR,AP, Ahmed H, Agrawal M, Roy U, Alexander A. PCL-PEG copolymer based injectable thermosensitive hydrogels. *J Control Release* 2022;**343**:217−36.
128. Cheng Q, Hao A, Xing P. Stimulus-responsive luminescent hydrogels: design and applications. *Adv Colloid Interface Sci* 2020;**286**:102301.
129. Amirthalingam S, Rajendran AK, Moon YG, Hwang NS. Stimuli-responsive dynamic hydrogels: design, properties and tissue engineering applications. *Mater Horiz* 2023;**10**:3325−50.
130. Luo R, Xiang X, Jiao Q, Hua H, Chen Y. Photoresponsive hydrogels for tissue engineering. *ACS Biomater Sci Eng* 2024;**10**:3612−30.
131. Li L, Scheiger JM, Levkin PA. Design and applications of photoresponsive hydrogels. *Adv Mater* 2019;**31**:e1807333.
132. Giliomee J, Toit LC, Kumar P, Klumperman B, Choonara YE. Evaluation of composition effects on the physicochemical and biological properties of polypeptide-based hydrogels for potential application in wound healing. *Polymers* 2021;**13**:1828.
133. Harun-Or-Rashid M, Aktar MN, Hossain MS, Sarkar N, Islam MR, Arafat ME, et al. Recent advances in micro- and nano-drug delivery systems based on natural and synthetic biomaterials. *Polymers* 2023;**15**:4563.
134. Karakuş NR, Türk S, Guney Eskiler G, Syzdykbayev M, Appazov NO, Özacar M. Investigation of tannic acid crosslinked pva/pei-based hydrogels as potential wound dressings with self-healing and high antibacterial properties. *Gels* 2024;**10**:682.
135. Gomez JC, Zakaria R, Aung MM, Mokhtar MN, Yunus R. Synthesis and characterization of polyurethanes from residual palm oil with high poly-unsaturated fatty acid oils as additive. *Polymers* 2021;**13**:4214.
136. Chiangnoon R, Karawak P, Eamsiri J, Nuchdang S, Thamrongsiripak N, Neramitmansook N, et al. Antibacterial hydrogel sheet dressings composed of poly(vinyl alcohol) and silver nanoparticles by electron beam irradiation. *Gels* 2023;**9**:80.
137. Li X, Gong JP. Design principles for strong and tough hydrogels. *Nat Rev Mater* 2024;**9**:380−98.
138. Jia Y, Zhou Z, Jiang H, Liu Z. Characterization of fracture toughness and damage zone of double network hydrogels. *J Mech Phys Solid* 2022;**169**:105090.
139. Zhang L, Lee W, Li X, Jiang Y, Fang NX, Dai G, et al. 3D direct printing of mechanical and biocompatible hydrogel meta-structures. *Bioact Mater* 2022;**10**:48−55.
140. Lin M, Wang G, Li Y. Structure, rheology and antioxidant properties of a polysaccharide from *Atractylodes macrocephala* in Pan'an. *Carbohydr Res* 2025;**552**:109464.
141. Krishnan BP, Saalwaechter K, Adjedje VKB, Binder WH. Design, synthesis and characterization of vitrimers with low topology freezing transition temperature. *Polymers* 2022;**14**:2456.
142. Zuliani A, Rapisarda M, Chelazzi D, Baglioni P, Rizzarelli P. Synthesis, characterization, and soil burial degradation of biobased polyurethanes. *Polymers* 2022;**14**:4948.
143. Perez-Puyana V, Jiménez-Rosado M, Romero A, Guerrero A. Fabrication and characterization of hydrogels based on gelatinised

collagen with potential application in tissue engineering. *Polymers* 2020;**12**:1146.
144. Boffito M, Torchio A, Tonda-Turo C, Laurano R, Gisbert-Garzarán M, Berkmann JC, et al. Hybrid injectable sol−gel systems based on thermo-sensitive polyurethane hydrogels carrying ph-sensitive mesoporous silica nanoparticles for the controlled and triggered release of therapeutic agents. *Front Bioeng Biotechnol* 2020;**8**:384.
145. Lee R, Hall EK, Aljohani BA, McClements J, Peeters M, Geoghegan M. Elastic modulus of hyaluronic acid hydrogels by compression testing. *J Mater Sci Mater Med* 2025;**36**:59.
146. Chen Y, Lu K, Song Y, Han J, Yue Y, Biswas SK, et al. A skin-inspired stretchable, self-healing and electro-conductive hydrogel with a synergistic triple network for wearable strain sensors applied in human-motion detection. *Nanomaterials* 2019;**9**:1737.
147. Ermis M, Falcone N, Roberto de Barros N, Mecwan M, Haghniaz R, Choroomi A, et al. Tunable hybrid hydrogels with multicellular spheroids for modeling desmoplastic pancreatic cancer. *Bioact Mater* 2023;**25**:360−73.
148. Kushibiki T, Mayumi Y, Nakayama E, Azuma R, Ojima K, Horiguchi A, et al. Photocrosslinked gelatin hydrogel improves wound healing and skin flap survival by the sustained release of basic fibroblast growth factor. *Sci Rep* 2021;**11**:23094.
149. Herrada-Manchón H, Rodríguez-González D, Fernández MA, Kucko NW, Barrère-de Groot F, Aguilar E. Effect on rheological properties and 3d printability of biphasic calcium phosphate microporous particles in hydrocolloid-based hydrogels. *Gels* 2022;**8**:28.
150. Yueqi L, Jie X, Ya S, Huan F, Jiaqi L, Siyao L, et al. A biocompatible double-crosslinked gelatin/sodium alginate/dopamine/quaterniazed chitosan hydrogel for wound dressings based on 3D bioprinting technology. *Int J Bioprint* 2023;**9**:689.
151. Aigoin J, Payré B, Minvielle Moncla J, Escudero M, Goudouneche D, Ferri-Angulo D, et al. Comparative analysis of electron microscopy techniques for hydrogel microarchitecture characterization: SEM, Cryo-SEM, ESEM, and TEM. *ACS Omega* 2025;**10**:14687−98.
152. Jin H, Chen J, Zhang J, Sheng L. Impact of phosphates on heat-induced egg white gel properties: texture, water state, micro-rheology and microstructure. *Food Hydrocoll* 2020;**110**:106200.
153. Guo J, Jiang Y. Submolecular insights into interfacial water by hydrogen-sensitive scanning probe microscopy. *Acc Chem Res* 2022; **55**:1680−92.
154. Long M, Li J, Zhu Y, Ruan H, Li J, Xu F, et al. Microneedle-facilitated *portulaca oleracea L.*-derived nanovesicles ameliorate atopic dermatitis by modulating macrophage M1/M2 polarization and inhibiting NF-κB and STING signaling pathways. *Acta Pharm Sin B* 2025;**15**:5966−87.
155. Sun Y, Ku BJ, Moon MJ. Microstructure of the silk fibroin-based hydrogel scaffolds derived from the orb-web spider Trichonephila clavata. *Appl Microsc* 2024;**54**:3.
156. Shirazaki P, Varshosaz J, Kharazi AZ. Electrospun gelatin/poly(glycerol sebacate) membrane with controlled release of antibiotics for wound dressing. *Adv Biomed Res* 2017;**6**:105.
157. Koetting MC, Peters JT, Steichen SD, Peppas NA. Stimulus-responsive hydrogels: theory, modern advances, and applications. *Mater Sci Eng R Rep* 2015;**93**:1−49.
158. Nishida M, Tanaka T, Miki T, Shigematsu I, Kanayama K. Variable temperature solid-state NMR spectral and relaxation analyses of the impregnation of polyethylene glycol (PEG) into coniferous wood. *RSC Adv* 2019;**9**:15657−67.
159. O'Neill H, Pingali SV, Petridis L, He J, Mamontov E, Hong L, et al. Dynamics of water bound to crystalline cellulose. *Sci Rep* 2017;**7**: 11840.
160. Dzyhovskyi V, Romani A, Pula W, Bondi A, Ferrara F, Melloni E, et al. Characterization methods for nanoparticle−skin interactions: an overview. *Life* 2024;**14**:599.
161. Cao Z, Li Z, Mooney M, Do C, Hong K, Rondeau-Gagné S, et al. Uncovering backbone conformation for rigid dpp-based donor−acceptor conjugated polymer using deuterium labeling and neutron scattering. *Macromolecules* 2024;**57**:10379−88.
162. Miclotte MPJ, Varlas S, Reynolds CD, Rashid B, Chapman E, O'Reilly RK. Thermoresponsive block copolymer core−shell nanoparticles with tunable flow behavior in porous media. *ACS Appl Mater Interfaces* 2022;**14**:54182−93.
163. Wang C, Chi H, Zhang F, Wang X, Wang J, Zhang H, et al. Temperature-responsive Pickering high internal phase emulsions for recyclable efficient interfacial biocatalysis. *Chem Sci* 2022;**13**:8766−72.
164. Rudyak VY, Kozhunova EY, Chertovich AV. Towards the realistic computer model of precipitation polymerization microgels. *Sci Rep* 2019;**9**:13052.
165. Gao K, Xu K. Advancements and prospects of pH-responsive hydrogels in biomedicine. *Gels* 2025;**11**:293.
166. Patel P, Ibrahim NM, Cheng K. The Importance of apparent pka in the development of nanoparticles encapsulating siRNA and mRNA. *Trends Pharmacol Sci* 2021;**42**:448−60.
167. Ow V, Lin Q, Wong JHM, Sim B, Tan YL, Leow Y, et al. Understanding the interplay between pH and charges for theranostic nanomaterials. *Nanoscale* 2025;**17**:6960−80.
168. Zhou T, Xiong H, Yao SY, Wang S, Li S, Chang J, et al. Hypoxia and matrix metalloproteinase 13-responsive hydrogel microspheres alleviate osteoarthritis progression *in vivo*. *Small* 2024;**20**:e2308599.
169. Moon YE, Jeong JO, Choi H. Inflammation-responsive hydrogels in perioperative pain and wound management: design strategies and emerging potential. *Gels* 2025;**11**:691.
170. Somsesta N, Chamamporn C, Wongsopanakun N, Sonaka P, Hongrattanavichit I. Surface-coated paper packaging with nanocellulose modified with quaternary ammonium organosilane and precipitated calcium carbonate for improved water repellency and antibacterial activity. *Sci Rep* 2025;**15**:25723.
171. Desai N, Pande S, Vora LK, Kommineni N. Nanofibrous microspheres: a biomimetic platform for bone tissue regeneration. *ACS Appl Bio Mater* 2024;**7**:4270−92.
172. Meng H, Su J, Shen Q, Hu W, Li P, Guo K, et al. A smart MMP-9-responsive hydrogel releasing M2 macrophage-derived exosomes for diabetic wound healing. *Adv Healthcare Mater* 2025;**14**:e2404966.
173. Ptáčková R, Ječmen T, Novák P, Hudeček J, Stiborová M, Šulc M. The application of an emerging technique for protein-protein interaction interface mapping: the combination of photo-initiated cross-linking protein nanoprobes with mass spectrometry. *Int J Mol Sci* 2014;**15**:9224−41.
174. Bryant SJ, Vernerey FJ. Programmable hydrogels for cell encapsulation and neo-tissue growth to enable personalized tissue engineering. *Adv Healthcare Mater* 2018;**7**:1700605.
175. Demirci S, Sahiner M, Yilmaz S, Karadag E, Sahiner N. Enhanced enzymatic activity and stability by *in situ* entrapment of α-Glucosidase within super porous p(HEMA) cryogels during synthesis. *Biotechnol Rep* 2020;**28**:e00534.
176. Vang JY, Breceda C, Her C, Krishnan VV. Enzyme kinetics by real-time quantitative NMR (qNMR) spectroscopy with progress curve analysis. *Anal Biochem* 2022;**658**:114919.
177. Zhu Y, Xiu Z, Jiang X, Zhang H, Li X, Feng Y, et al. Injectable hydrogels with ROS-triggered drug release enable the co-delivery of antibacterial agent and anti-inflammatory nanoparticle for periodontitis treatment. *J Nanobiotechnol* 2025;**23**:205.
178. Yang J, Tan Q, Li K, Liao J, Hao Y, Chen Y. Advances and trends of photoresponsive hydrogels for bone tissue engineering. *ACS Biomater Sci Eng* 2024;**10**:1921−45.
179. Yu H, Gao R, Liu Y, Fu L, Zhou J, Li L. Stimulus-responsive hydrogels as drug delivery systems for inflammation targeted therapy. *Adv Sci* 2024;**11**:e2306152.
180. Lerra L, Farfalla A, Sanz B, Cirillo G, Vittorio O, Voli F, et al. Graphene oxide functional nanohybrids with magnetic nanoparticles for improved vectorization of doxorubicin to neuroblastoma cells. *Pharmaceutics* 2018;**11**:3.
181. Sun G, Wu X, Liu R. A comprehensive investigation of acrylates photopolymerization shrinkage stress from micro and macro

perspectives by real time MIR-photo-rheology. *Prog Org Coating* 2021;**155**:106229.
182. Wu Z, Shang C, Zeng Q, Liu H, He F, Feng Y, et al. Photo-electrically responsive dual - network alginate-based composite hydrogels for the controlled release of plant essential nutrients. *Int J Biol Macromol* 2025;**305**:141161.
183. Li X, Lovell JF, Yoon J, Chen X. Clinical development and potential of photothermal and photodynamic therapies for cancer. *Nat Rev Clin Oncol* 2020;**17**:657−74.
184. Kong C, Chen X. Combined photodynamic and photothermal therapy and immunotherapy for cancer treatment: a review. *Int J Nanomed* 2022;**17**:6427−46.
185. Cui X, Ruan Q, Zhuo X, Xia X, Hu J, Fu R, et al. Photothermal nanomaterials: a powerful light-to-heat converter. *Chem Rev* 2023; **123**:6891−952.
186. Hu J, Chen Y, Li Y, Zhou Z, Cheng Y. A thermo-degradable hydrogel with light-tunable degradation and drug release. *Biomaterials* 2017; **112**:133−40.
187. Mei E, Chen C, Li C, Ding X, Chen J, Xi Q, et al. Injectable and biodegradable chitosan hydrogel-based drug depot contributes to synergistic treatment of tumors. *Biomacromolecules* 2021;**22**: 5339−48.
188. Yu Y, Wang T, Meng X, Jiang T, Zhao X. Chitosan thermosensitive hydrogel based on dna damage repair inhibition and mild photothermal therapy for enhanced antitumor treatment. *Biomacromolecules* 2023;**24**:3755−66.
189. Han X, Shen S, Fan Q, Chen G, Archibong E, Dotti G, et al. Red blood cell-derived nanoerythrosome for antigen delivery with enhanced cancer immunotherapy. *Sci Adv* 2019;**5**:eaaw6870.
190. Fei Z, Fan Q, Dai H, Zhou X, Xu J, Ma Q, et al. Physiologically triggered injectable red blood cell-based gel for tumor photoablation and enhanced cancer immunotherapy. *Biomaterials* 2021;**271**:120724.
191. Almeida SN, Elliott R, Silva ER, Sales CMD. Fear of cancer recurrence: a qualitative systematic review and meta-synthesis of patients' experiences. *Clin Psychol Rev* 2019;**68**:13−24.
192. Wang S, Zheng H, Zhou L, Cheng F, Liu Z, Zhang H, et al. Injectable redox and light responsive MnO_2 hybrid hydrogel for simultaneous melanoma therapy and multidrug-resistant bacteria-infected wound healing. *Biomaterials* 2020;**260**:120314.
193. Mehrabi T, Mesgar AS, Mohammadi Z. Bioactive glasses: a promising therapeutic ion release strategy for enhancing wound healing. *ACS Biomater Sci Eng* 2020;**6**:5399−430.
194. Liu X, Shen M, Bing T, Zhang X, Li Y, Cai Q, et al. A bioactive injectable hydrogel regulates tumor metastasis and wound healing for melanoma *via* NIR-light triggered hyperthermia. *Adv Sci* 2024;**11**: e2402208.
195. Wang H, Yang L, Yang Y. A review of sodium alginate-based hydrogels: structure, mechanisms, applications, and perspectives. *Int J Biol Macromol* 2025;**292**:139151.
196. Abbasi AR, Sohail M, Minhas MU, Khaliq T, Kousar M, Khan S, et al. Bioinspired sodium alginate based thermosensitive hydrogel membranes for accelerated wound healing. *Int J Biol Macromol* 2020;**155**:751−65.
197. Zhang Y, Wang T, Zhuang Y, He T, Wu X, Su L, et al. Sodium alginate hydrogel-mediated cancer immunotherapy for postoperative *in situ* recurrence and metastasis. *ACS Biomater Sci Eng* 2021;**7**:5717−26.
198. Musaie K, Abbaszadeh S, Nosrati-Siahmazgi V, Qahremani M, Wang S, Eskandari MR, et al. Metal-coordination synthesis of a natural injectable photoactive hydrogel with antibacterial and blood-aggregating functions for cancer thermotherapy and mild-heating wound repair. *Biomater Sci* 2023;**11**:2486−503.
199. Xu L, Tong G, Song Q, Zhu C, Zhang H, Shi J, et al. Enhanced intracellular Ca^{2+} nanogenerator for tumor-specific synergistic therapy *via* disruption of mitochondrial Ca^{2+} homeostasis and photothermal therapy. *ACS Nano* 2018;**12**:6806−18.
200. Yang WJ, Ma R, Wei S, Sun W, Xu W, Wang L. An injectable nanocomposite alginate-Ca^{2+} hydrogel for melittin-assisted Ca^{2+}-overload and photothermal cancer therapy. *Chem Commun* 2023;**59**: 8568−71.
201. Ceremuga M, Stela M, Janik E, Gorniak L, Synowiec E, Sliwinski T, et al. Melittin—a natural peptide from bee venom which induces apoptosis in human leukaemia cells. *Biomolecules* 2020;**10**:247.
202. Yi X, Duan QY, Wu FG. Low-temperature photothermal therapy: strategies and applications. *Research* 2021;**2021**:9816594.
203. Liu Y, Bhattarai P, Dai Z, Chen X. Photothermal therapy and photoacoustic imaging *via* nanotheranostics in fighting cancer. *Chem Soc Rev* 2019;**48**:2053−108.
204. Chang R, Zhao D, Zhang C, Liu K, He Y, Guan F, et al. PMN-incorporated multifunctional chitosan hydrogel for postoperative synergistic photothermal melanoma therapy and skin regeneration. *Int J Biol Macromol* 2023;**253**:126854.
205. Huang H, Wang X, Wang W, Qu X, Song X, Zhang Y, et al. Injectable hydrogel for postoperative synergistic photothermal-chemodynamic tumor and anti-infection therapy. *Biomaterials* 2022;**280**:121289.
206. Xing J, Yang Y, Zhang W, Yan J, Qian H, Hao J, et al. Injectable hydrogel containing TiO nanosheets for synergistic photothermal/thermodynamic therapy. *ACS Appl Mater Interfaces* 2023; **15**:34436−50.
207. Ding M, Fan Y, Lv Y, Liu J, Yu N, Kong D, et al. A prodrug hydrogel with tumor microenvironment and near-infrared light dual-responsive action for synergistic cancer immunotherapy. *Acta Biomater* 2022; **149**:334−46.
208. Zhou L, Zhao J, Chen Y, Zheng Y, Li J, Zhao J, et al. MoS_2-ALG-Fe/GOx hydrogel with Fenton catalytic activity for combined cancer photothermal, starvation, and chemodynamic therapy. *Colloids Surf B Biointerfaces* 2020;**195**:111243.
209. He PP, Du X, Cheng Y, Gao Q, Liu C, Wang X, et al. Thermal-responsive mxene-dna hydrogel for near-infrared light triggered localized photothermal-chemo synergistic cancer therapy. *Small* 2022;**18**:e2200263.
210. Hu X, Lei S, Song S, Xia X, Qi J, Liu J, et al. Guanosine-based hydrogel integrating photothermal effect of PDA-AuNPs through dynamic borate bond for photothermal therapy of cancer. *Chem Asian J* 2022;**17**:e202200302.
211. Yang X, Gao L, Wei Y, Tan B, Wu Y, Yi C, et al. Photothermal hydrogel platform for prevention of post-surgical tumor recurrence and improving breast reconstruction. *J Nanobiotechnol* 2021;**19**: 307.
212. Rostaminejad B, Karimi AR, Dinari M, Hadizadeh M. Photosensitive chitosan-based injectable hydrogel chemically cross-linked by perylene bisimide dopamine with robust antioxidant and cytotoxicity enhancer properties for *in vitro* photodynamic therapy of breast cancer. *ACS Appl Bio Mater* 2023;**6**:1242−51.
213. Chen X, Wang H, Shi J, Chen Z, Wang Y, Gu S, et al. An injectable and active hydrogel induces mutually enhanced mild magnetic hyperthermia and ferroptosis. *Biomaterials* 2023;**298**:122139.
214. Qian KY, Song Y, Yan X, Dong L, Xue J, Xu Y, et al. Injectable ferrimagnetic silk fibroin hydrogel for magnetic hyperthermia ablation of deep tumor. *Biomaterials* 2020;**259**:120299.
215. Su L, Zhu X, Ding H, Hu L, Chen J, Qi S, et al. Intraoperative tumor mapping using pyridine-carbazole based multifunctional fluorescent probes for precise resection and photodynamic therapeutics. *Sensor Actuator B Chem* 2024;**412**:135792.
216. Correia JH, Rodrigues JA, Pimenta S, Dong T, Yang Z. Photodynamic therapy review: principles, photosensitizers, applications, and future directions. *Pharmaceutics* 2021;**13**:1332.
217. Ostańska E, Aebisher D, Bartusik-Aebisher D. The potential of photodynamic therapy in current breast cancer treatment methodologies. *Biomed Pharmacother* 2021;**137**:111302.
218. Gunaydin G, Gedik ME, Ayan S. Photodynamic therapy—current limitations and novel approaches. *Front Chem* 2021;**9**:691697.
219. Liu H, Sun R, Wang L, Chen X, Li G, Cheng Y, et al. Biocompatible iron oxide nanoring-labeled mesenchymal stem cells: an innovative

magnetothermal approach for cell tracking and targeted stroke therapy. *ACS Nano* 2022;**16**:18806−21.
220. Xue F, Zhu S, Tian Q, Qin R, Wang Z, Huang G, et al. Macrophage-mediated delivery of magnetic nanoparticles for enhanced magnetic resonance imaging and magnetothermal therapy of solid tumors. *J Colloid Interface Sci* 2023;**629**:554−62.
221. Yang Z, Li P, Chen Y, Gan Q, Feng Z, Jin Y, et al. Construction of pH/glutathione responsive chitosan nanoparticles by a self-assembly/self-crosslinking method for photodynamic therapy. *Int J Biol Macromol* 2021;**167**:46−58.
222. Yue L, Li H, Sun Q, Luo X, Wu F, Zhu X. Organic nanoparticles based on D-A-D small molecule: self-assembly, photophysical properties, and synergistic photodynamic/photothermal effects. *Materials* 2022;**15**:502.
223. Xin J, Deng C, Aras O, Zhou M, Wu C, An F. Chemodynamic nanomaterials for cancer theranostics. *J Nanobiotechnol* 2021;**19**: 192.
224. Deng X, Shao Z, Zhao Y. Solutions to the drawbacks of photothermal and photodynamic cancer therapy. *Adv Sci* 2021;**8**:2002504.
225. Yang J, Wang Y, Wang Z, Wang J, Zhang C, Gu X, et al. Multifunctional lipid droplet probes for observing the polarity change of ferroptosis, inflammation, fatty liver and evaluating the efficacy of drugs. *Anal Chim Acta* 2024;**1312**:342747.
226. Khan S, Sharifi M, Hasan A, Attar F, Edis Z, Bai Q, et al. Magnetic nanocatalysts as multifunctional platforms in cancer therapy through the synthesis of anticancer drugs and facilitated Fenton reaction. *J Adv Res* 2021;**30**:171−84.
227. Gan L, Lin X, Zhong Z, Zheng Y, Chen X, Chen J, et al. Ferroptosis meets cancer immunotherapy: overcoming the crosstalk challenges through advanced drug delivery strategies. *Acta Pharm Sin B* 2025; **15**:6307−41.
228. Wang X, Zhong X, Liu Z, Cheng L. Recent progress of chemodynamic therapy-induced combination cancer therapy. *Nano Today* 2020;**35**:100946.
229. Sang Y, Cao F, Li W, Zhang L, You Y, Deng Q, et al. Bioinspired construction of a nanozyme-based H_2O_2 homeostasis disruptor for intensive chemodynamic therapy. *J Am Chem Soc* 2020;**142**: 5177−83.
230. Andrews LP, Yano H, Vignali DAA. Inhibitory receptors and ligands beyond PD-1, PD-L1 and CTLA-4: breakthroughs or backups. *Nat Immunol* 2019;**20**:1425−34.
231. Zhuang H, Xue P, Shao S, Zeng X, Yan S. *In situ* generation of hybrid alginate hydrogels for enhanced breast tumor ferrotherapy through multiplex magnifying redox imbalances. *Int J Biol Macromol* 2024;**258**:128952.
232. Sui X, Zhang R, Liu S, Duan T, Zhai L, Zhang M, et al. RSL3 drives ferroptosis through GPX4 inactivation and ros production in colorectal cancer. *Front Pharmacol* 2018;**9**:1371.
233. Chen K, Gu L, Zhang Q, Luo Q, Guo S, Wang B, et al. Injectable alginate hydrogel promotes antitumor immunity through glucose oxidase and Fe^{3+} amplified RSL3-induced ferroptosis. *Carbohydr Polym* 2024;**326**:121643.
234. Fan W, Lu N, Huang P, Liu Y, Yang Z, Wang S, et al. Glucose-responsive sequential generation of hydrogen peroxide and nitric oxide for synergistic cancer starving-like/gas therapy. *Angew Chem Int Ed Engl* 2017;**56**:1229−33.
235. Zhu X, Ji X, Kong N, Chen Y, Mahmoudi M, Xu X, et al. Intracellular mechanistic understanding of 2D MoS_2 nanosheets for anti-exocytosis-enhanced synergistic cancer therapy. *ACS Nano* 2018;**12**: 2922−38.
236. Bokare AD, Choi W. Review of iron-free fenton-like systems for activating H_2O_2 in advanced oxidation processes. *J Hazard Mater* 2014;**275**:121−35.
237. Liu Y, Wu J, Jin Y, Zhen W, Wang Y, Liu J, et al. Copper (I) phosphide nanocrystals for *in situ* self-generation magnetic resonance imaging-guided photothermal-enhanced chemodynamic synergetic therapy resisting deep-seated tumor. *Adv Funct Mater* 2019;**29**:1904678.
238. Kim S, Seo JH, Jeong DI, Yang M, Lee SY, Lee J, et al. Fenton-like reaction, glutathione reduction, and photothermal ablation-built-in hydrogels crosslinked by cupric sulfate for loco-regional cancer therapy. *Biomater Sci* 2021;**9**:847−60.
239. Dang W, Chen WC, Ju E, Xu Y, Li K, Wang H, et al. 3D printed hydrogel scaffolds combining glutathione depletion-induced ferroptosis and photothermia-augmented chemodynamic therapy for efficiently inhibiting postoperative tumor recurrence. *J Nanobiotechnol* 2022;**20**:266.
240. Cheng Y, Mo Q, Zeng F, Wang Y, Liu M, Li Y, et al. *In situ* generation of hydroperoxide-rich-peptide-based nano-assemblies for self-amplified magnetic resonance imaging-guided synergistic tumor chemo/chemodynamic/ferroptotic therapy. *J Colloid Interface Sci* 2026;**703**:139050.
241. Xu Y, Zhang K, Ye Z, Huang Z, Chen R, Zhang Y, et al. Nanomedicine initiates ferroptosis for enhanced lung cancer therapy. *Drug Deliv* 2025;**32**:2527752.
242. Edwards IA, De Carlo F, Sitta J, Varner W, Howard CM, Claudio PP. Enhancing targeted therapy in breast cancer by ultrasound-responsive nanocarriers. *Int J Mol Sci* 2023;**24**:5474.
243. Chang Y, Lim YG, Park K. Synergistic photodynamic and chemodynamic therapy using hypoxia-adaptive Ce6@Co nanoparticles for enhanced tumor suppression. *Int J Pharm X* 2025;**10**: 100348.
244. Han X, Zhong Y, Mi C, He Z, Gu J, Dai X, et al. NIR-IIb fluorescence-image guided synergistic surgery/starvation/chemodynamic therapy: an innovative treatment paradigm for malignant non-small cell lung cancers. *Theranostics* 2023;**13**:2176−91.
245. He X, Zhu H, Shang J, Li M, Zhang Y, Zhou S, et al. Intratumoral synthesis of transformable metal-phenolic nanoaggregates with enhanced tumor penetration and retention for photothermal immunotherapy. *Theranostics* 2022;**12**:6258−72.
246. Chen X, Jiang T, Li Y, Zhang Y, Chen J, Zhao X, et al. Carrageenan-ferrocene-eicosapentaenoic acid composite hydrogel induce ferroptosis and apoptosis for anti-tumor recurrence and metastasis. *Int J Biol Macromol* 2024;**276**:133942.
247. Blass E, Ott PA. Advances in the development of personalized neoantigen-based therapeutic cancer vaccines. *Nat Rev Clin Oncol* 2021;**18**:215−29.
248. Liang X, Li X, Wu R, He T, Liu F, Li L, et al. Breaking the tumor chronic inflammation balance with a programmable release and multi-stimulation engineering scaffold for potent immunotherapy. *Adv Sci* 2024;**11**:e2401377.
249. Kuai R, Yuan W, Son S, Nam J, Xu Y, Fan Y, et al. Elimination of established tumors with nanodisc-based combination chemoimmunotherapy. *Sci Adv* 2018;**4**:eaao1736.
250. Sahin U, Türeci Ö. Personalized vaccines for cancer immunotherapy. *Science* 2018;**359**:1355−60.
251. Francis DM, Manspeaker MP, Schudel A, Sestito LF, O'Melia MJ, Kissick HT, et al. Blockade of immune checkpoints in lymph nodes through locoregional delivery augments cancer immunotherapy. *Sci Transl Med* 2020;**12**:3575.
252. Zhou M, Zuo Q, Huang Y, Li L. Immunogenic hydrogel toolkit disturbing residual tumor "seeds" and pre-metastatic "soil" for inhibition of postoperative tumor recurrence and metastasis. *Acta Pharm Sin B* 2022;**12**:3383−97.
253. Zhang D, Li Q, Chen X, Nie X, Xue F, Xu W, et al. An injectable hydrogel to modulate T cells for cancer immunotherapy. *Small* 2022; **18**:e2202663.
254. Tian L, Shao M, Gong Y, Wei T, Zhu Y, Chao Y, et al. Epigenetic platinum complexes breaking the "eat me/don't eat me" balance for enhanced cancer chemoimmunotherapy. *Bioconjug Chem* 2022;**33**: 343−52.
255. Zhao M, Shao T, Ren Y, Zhou C, Tang W. Identifying optimal PD-1/PD-L1 inhibitors in first-line treatment of patients with advanced squamous non-small cell lung cancer in China: updated systematic review and network meta-analysis. *Front Pharmacol* 2022;**13**: 910656.

256. Zhao CX, Liu JN, Li BQ, Ren D, Chen X, Yu J, et al. Multiscale construction of bifunctional electrocatalysts for long-lifespan rechargeable zinc-air batteries. *Adv Funct Mater* 2020;**30**: 2003619.
257. Chen Q, Zhou S, Ding Y, Chen D, Dahiru NS, Tang H, et al. A bio-responsive, cargo-catchable gel for postsurgical tumor treatment *via* ICD-based immunotherapy. *J Control Release* 2022; **346**:212−25.
258. Kornepati AVR, Vadlamudi RK, Curiel TJ. Programmed death ligand 1 signals in cancer cells. *Nat Rev Cancer* 2022;**22**:174−89.
259. Zhu Y, Jin L, Chen J, Su M, Sun T, Yang X. Promoting the recruitment, engagement, and reinvigoration of effector T cells *via* an injectable hydrogel with a supramolecular binding capability for cancer immunotherapy. *Adv Mater* 2023;**35**:e2309667.
260. Liang JL, Jin XK, Luo GF, Zhang SM, Huang QX, Lin YT, et al. Immunostimulant hydrogel-guided tumor microenvironment reprogramming to efficiently potentiate macrophage-mediated cellular phagocytosis for systemic cancer immunotherapy. *ACS Nano* 2023; **17**:17217−32.
261. Shriky B, Kelly A, Isreb M, Babenko M, Mahmoudi N, Rogers S, et al. Pluronic F127 thermosensitive injectable smart hydrogels for controlled drug delivery system development. *J Colloid Interface Sci* 2020;**565**:119−30.
262. Fan Y, Li Y, Yao X, Jin J, Scott A, Liu B, et al. Epithelial SOX9 drives progression and metastases of gastric adenocarcinoma by promoting immunosuppressive tumour microenvironment. *Gut* 2023; **72**:624−37.
263. Bassez A, Vos H, Van Dyck L, Floris G, Arijs I, Desmedt C, et al. A single-cell map of intratumoral changes during anti-PD1 treatment of patients with breast cancer. *Nat Med* 2021;**27**:820−32.
264. Kennedy LB, Salama AKS. A review of cancer immunotherapy toxicity. *CA Cancer J Clin* 2020;**70**:86−104.
265. Fu W, Li X, Li Y, Luo R, Ou C, Huang D, et al. A programmable releasing versatile hydrogel platform boosts systemic immune responses *via* sculpting tumor immunogenicity and reversing tolerogenic dendritic cells. *Biomaterials* 2024;**305**:122444.
266. Decout A, Katz JD, Venkatraman S, Ablasser A. The cGAS−STING pathway as a therapeutic target in inflammatory diseases. *Nat Rev Immunol* 2021;**21**:548−69.
267. Wang M, Hu Q, Huang J, Zhang F, Yao Z, Shao S, et al. *In situ* formed ROS-responsive hydrogel with sting agonist and gemcitabine to intensify immunotherapy against pancreatic ductal adenocarcinoma. *Adv Healthcare Mater* 2023;**12**:e2203264.
268. Wu J, Dobbs N, Yang K, Yan N. Interferon-independent activities of mammalian sting mediate antiviral response and tumor immune evasion. *Immunity* 2020;**53**:115−26.
269. Wang C, Wang J, Zhang X, Yu S, Wen D, Hu Q, et al. *In situ* formed reactive oxygen species-responsive scaffold with gemcitabine and checkpoint inhibitor for combination therapy. *Sci Transl Med* 2018; **10**:3682.
270. Cheng F, Su T, Zhou S, Liu X, Yang S, Lin S, et al. Single-dose injectable nanovaccine-in-hydrogel for robust immunotherapy of large tumors with abscopal effect. *Sci Adv* 2023;**9**:eade6257.
271. Qin G, Li P, Zhang M, Yu Z, Shen X, Zhang W, et al. Exopolysaccharide from *Rhizopus nigricans* modulates antitumor immune responses by promoting tumor-associated macrophage polarization toward the M1 phenotype in C57BL/6J mice. *Russ J Bioorg Chem* 2024;**50**:2519−28.
272. Chen S, Saeed A, Liu Q, Jiang Q, Xu H, Xiao GG, et al. Macrophages in immunoregulation and therapeutics. *Signal Transduct Targeted Ther* 2023;**8**:207.
273. Wang Y, Su X, Liu Y, Hu L, Kang L, Xu C, et al. Improved prebiotic-based "shield" equipped probiotics for enhanced colon cancer therapy by polarizing M1 macrophages and regulating intestinal microbiota. *Acta Pharm Sin B* 2025;**15**:4225−47.
274. Chen D, Zhang X, Li Z, Zhu B. Metabolic regulatory crosstalk between tumor microenvironment and tumor-associated macrophages. *Theranostics* 2021;**11**:1016−30.
275. Deng X, Liang H, Yang W, Shao Z. Polarization and function of tumor-associated macrophages mediate graphene oxide-induced photothermal cancer therapy. *J Photochem Photobiol, B* 2020;**208**: 111913.
276. Locati M, Curtale G, Mantovani A. Diversity, mechanisms, and significance of macrophage plasticity. *Annu Rev Pathol* 2020;**15**: 123−47.
277. Zhang R, Ye Y, Wu J, Gao J, Huang W, Qin H, et al. Immunostimulant *in situ* fibrin gel for post-operative glioblastoma treatment by macrophage reprogramming and photo-chemo-immunotherapy. *ACS Appl Mater Interfaces* 2023;**15**:17627−40.
278. Chao Y, Liu Z. Biomaterials tools to modulate the tumour microenvironment in immunotherapy. *Nat Rev Bioeng* 2023;**1**:125−38.
279. Feng L, Dong Z, Tao D, Zhang Y, Liu Z. The acidic tumor microenvironment: a target for smart cancer nano-theranostics. *Natl Sci Rev* 2018;**5**:269−86.
280. Hartupee C, Nagalo BM, Chabu CY, Tesfay MZ, Coleman-Barnett J, West JT, et al. Pancreatic cancer tumor microenvironment is a major therapeutic barrier and target. *Front Immunol* 2024;**15**:1287459.
281. Cheng Y, Gong Y, Chen X, Zhang Q, Zhang X, He Y, et al. Injectable adhesive hemostatic gel with tumor acidity neutralizer and neutrophil extracellular traps lyase for enhancing adoptive NK cell therapy prevents post-resection recurrence of hepatocellular carcinoma. *Biomaterials* 2022;**284**:121506.
282. Lanis MR, Kim S, Schneck JP. Hydrogels in the immune context: *in vivo* applications for modulating immune responses in cancer therapy. *Gels* 2025;**11**:889.
283. Wei J, Huang C, Zhou Z, Lan Y. Engineered hydrogels revolutionize locoregional cancer immunotherapy. *Adv Nanobiomed Res* 2025;**5**: 2500046.
284. Wang M, Hu D, Yang Y, Shi K, Li J, Liu Q, et al. Enhanced chemoimmunotherapy strategy utilizing injectable thermosensitive hydrogel for the treatment of diffuse peritoneal metastasis in advanced colorectal cancer. *Adv Sci* 2023;**10**:e2303819.
285. Chen J, Cui M, He L, Mu Y, Hu N, Guan X. Engineered elastin-like polypeptide-based hydrogel delivering chemotherapeutics and PD-L1 antibodies for potentiated cancer immunotherapy. *J Mater Chem B* 2023;**11**:10355−61.
286. Liu Q, Xu R, Shen J, Tao Y, Shao J, Ke Y, et al. *In situ* chemoimmunotherapy hydrogel elicits immunogenic cell death and evokes efficient antitumor immune response. *J Transl Med* 2024;**22**:341.
287. Wang B, Chen J, Caserto JS, Wang X, Ma M. An *in situ* hydrogel-mediated chemo-immunometabolic cancer therapy. *Nat Commun* 2022;**13**:3821.
288. Correa S, Meany EL, Gale EC, Klich JH, Saouaf OM, Mayer AT, et al. Injectable nanoparticle-based hydrogels enable the safe and effective deployment of immunostimulatory CD40 agonist antibodies. *Adv Sci* 2022;**9**:e2103677.
289. Li C, Liu Y, Li D, Wang Q, Zhou S, Zhang H, et al. Promising alternatives of CD47 monoclonal antibody: an injectable degradable hydrogel loaded with PQ912 for postoperative immunotherapy effectively blocks CD47−SIRPα signal. *Theranostics* 2022;**12**: 4581−98.
290. Chen M, Tan Y, Hu J, Jiang Y, Wang Z, Liu Z, et al. Injectable immunotherapeutic thermogel for enhanced immunotherapy post tumor radiofrequency ablation. *Small* 2021;**17**:e2104773.
291. Zhang K, Fang Y, He Y, Yin H, Guan X, Pu Y, et al. Extravascular gelation shrinkage-derived internal stress enables tumor starvation therapy with suppressed metastasis and recurrence. *Nat Commun* 2019;**10**:5380.
292. Nguyen QV, Lee MS, Lym JS, Kim YI, Jae HJ, Lee DS. pH-sensitive sulfamethazine-based hydrogels as potential embolic agents for transcatheter vascular embolization. *J Mater Chem B* 2016;**4**: 6524−33.
293. Wang H, Jin Y, Tan Y, Zhu H, Huo W, Niu P, et al. Photo-responsive hydrogel facilitates nutrition deprivation by an ambidextrous approach for preventing cancer recurrence and metastasis. *Biomaterials* 2021;**275**:120992.

294. Choi H, Choi B, Yu B, Li W, Matsumoto MM, Harris KR, et al. On-demand degradable embolic microspheres for immediate restoration of blood flow during image-guided embolization procedures. *Biomaterials* 2021;**265**:120408.
295. Rankin EB, Giaccia AJ. Hypoxic control of metastasis. *Science* 2016; **352**:175−80.
296. Fan M, Liu Y, Ren Y, Gan L, Yang Y, Wang H, et al. Cascade reaction of "Mn^{2+} -catechol" triggered by H_2O_2 to integrate firm tumor vessel embolization and hypoxic response relief. *Adv Healthcare Mater* 2022;**11**:e2200544.
297. Liu X, Hu T, Jia Y, Yang S, Yang Y, Cui Z, et al. A MgAl-LDH-CuS nanosheet-based thermo-responsive composite hydrogel with nir-responsive angiogenesis inhibitor releasing capability for multi-mode starvation therapy. *J Nanobiotechnol* 2024;**22**:127.
298. Jing G, Yang L, Wang H, Niu J, Li Y, Wang S. Interference of layered double hydroxide nanoparticles with pathways for biomedical applications. *Adv Drug Deliv Rev* 2022;**188**:114451.
299. Hu T, Gu Z, Williams GR, Strimaite M, Zha J, Zhou Z, et al. Layered double hydroxide-based nanomaterials for biomedical applications. *Chem Soc Rev* 2022;**51**:6126−76.
300. Ajona D, Ortiz-Espinosa S, Lozano T, Exposito F, Calvo A, Valencia K, et al. Short-term starvation reduces IGF-1 levels to sensitize lung tumors to PD-1 immune checkpoint blockade. *Nat Cancer* 2020;**1**:75−85.
301. Bian Y, Li W, Kremer DM, Sajjakulnukit P, Li S, Crespo J, et al. Cancer SLC43A2 alters T cell methionine metabolism and histone methylation. *Nature* 2020;**585**:277−82.
302. Zhang S, Li Z, Wang Q, Liu Q, Yuan W, Feng W, et al. An NIR-II photothermally triggered "oxygen bomb" for hypoxic tumor programmed cascade therapy. *Adv Mater* 2022;**34**:e2201978.
303. Zhang C, Han ZY, Chen KW, Wang YZ, Bao P, Ji P, et al. *In situ* formed microalgae-integrated living hydrogel for enhanced tumor starvation therapy and immunotherapy through photosynthetic oxygenation. *Nano Lett* 2024;**24**:3801−10.
304. Wang P, Hou Z, Wang Z, Luo X. Multifunctional therapeutic nanodiamond hydrogels for infected-wound healing and cancer therapy. *ACS Appl Mater Interfaces* 2024;**16**:9656−68.
305. Yu D, Bu M, Yu P, Li Y, Chong Y. Regulation of wound healing and fibrosis by galectins. *J Mol Med* 2022;**100**:861−74.
306. Luan Q, Qiao R, Wu X, Shan J, Song C, Zhao X, et al. Plant-derived Chinese herbal hydrogel microneedle patches for wound healing. *Small* 2024;**20**:e2404850.
307. Yao Q, Lan QH, Jiang X, Du CC, Zhai YY, Shen X, et al. Bioinspired biliverdin/silk fibroin hydrogel for antiglioma photothermal therapy and wound healing. *Theranostics* 2020;**10**:11719−36.
308. Attia MS, Kijanka G, Nguyen NT, Zhang J, An H. Advances and prospects of RNA delivery nanoplatforms for cancer therapy. *Acta Pharm Sin B* 2025;**15**:52−96.
309. Zhang Y, Lu L, Song F, Zou X, Liu Y, Zheng X, et al. Research progress on non-protein-targeted drugs for cancer therapy. *J Exp Clin Cancer Res* 2023;**42**:62.
310. Zhao B, Zhou B, Shi K, Zhang R, Dong C, Xie D, et al. Sustained and targeted delivery of siRNA/DP7-C nanoparticles from injectable thermosensitive hydrogel for hepatocellular carcinoma therapy. *Cancer Sci* 2021;**112**:2481−92.
311. Lei S, Gao Y, Li J, Chen X, Zhou W, Wu J, et al. Dual-RNA controlled delivery system inhibited tumor growth by apoptosis induction and TME activation. *J Control Release* 2022;**344**:97−112.
312. Yin Y, Li X, Ma H, Zhang J, Yu D, Zhao R, et al. *In situ* transforming RNA nanovaccines from polyethylenimine functionalized graphene oxide hydrogel for durable cancer immunotherapy. *Nano Lett* 2021; **21**:2224−31.
313. Sun A, Li J, Wang J, Zhang S, Zhang X, Zhang Y, et al. Near-infrared lipid droplet polarity fluorescent probe based on phenothiazine derivative for diagnosis of non-alcoholic fatty liver and tumors. *Spectrochim Acta Mol Biomol Spectrosc* 2025;**341**:126430.
314. Sun S, Chen J. Recent advances in hydrogel-based biosensors for cancer detection. *ACS Appl Mater Interfaces* 2024;**16**:46988−7002.
315. Wang W, Rong Z, Wang G, Hou Y, Yang F, Qiu M. Cancer metabolites: promising biomarkers for cancer liquid biopsy. *Biomark Res* 2023;**11**:66.
316. Luan X, Gao Y, Pan Y, Huang Z, Zeng F, He G, et al. Bifunctional nanoassembly enables metabolism-driven microfluidic blood screening guided by MRI localization for cancer monitoring. *Anal Chem* 2025;**97**:3395−403.
317. Chen SE, Hu J, Yan P, Sun J, Jia W, Zhu S, et al. 12-Plex UHPLC−MS/MS analysis of sarcosine in human urine using integrated principle of multiplex tags chemical isotope labeling and selective imprint enriching. *Talanta* 2021;**224**:121788.
318. Alasiri G, Alaseem AM, El-Wekil MM, Hamdy AK, Ali ABH. Ratiometric fluorometric detection of urinary sarcosine *via* GSH@ Hg/carbon dots/sarcosine oxidase sensing platform: a non-invasive approach for prostate cancer diagnosis. *Talanta* 2026;**297**:128660.
319. Passornraprasit N, Hinestroza JP, Rodthongkum N, Potiyaraj P. Cellulose nanofibers/polyacrylic acid hydrogels integrated with a 3D printed strip: a platform for screening prostate cancer *via* sarcosine detection. *Carbohydr Polym* 2025;**352**:123134.
320. Masumoto M, Ohta S, Nakagawa M, Hiruta Y, Citterio D. Colorimetric paper-based sarcosine assay with improved sensitivity. *Anal Bioanal Chem* 2022;**414**:691−701.
321. Langer J, Jimenez de Aberasturi D, Aizpurua J, Alvarez-Puebla RA, Auguié B, Baumberg JJ, et al. Present and future of surface-enhanced Raman scattering. *ACS Nano* 2020;**14**:28−117.
322. Liu C, Liu T, Wei Y, Shi J, Deng L, Song M, et al. Interplay of serum taurine, *S*-adenosylmethionine, and cysteine levels in cancer risk: a prospective study. *Front Pharmacol* 2024;**15**:1507125.
323. Chen Z, Liu S. Hydrogel based flexible wearable sweat sensor for SERS-AI monitoring treatment effect of lung cancer. *Sensor Actuator B Chem* 2024;**427**:137155.
324. Gralewska P, Biegała Ł, Gajek A, Szymczak-Pajor I, Marczak A, Śliwińska A, et al. Olaparib combined with DDR inhibitors effectively prevents EMT and affects mirna regulation in TP53-mutated epithelial ovarian cancer cell lines. *Int J Mol Sci* 2025; **26**:693.
325. Peng J, Liu T, Guan L, Xu Z, Xiong T, Zhang Y, et al. A highly sensitive Lock-Cas12a biosensor for detection and imaging of miRNA-21 in breast cancer cells. *Talanta* 2024;**273**:125938.
326. Zhou Y, Ren H, Dai B, Li J, Shang L, Huang J, et al. Hepatocellular carcinoma-derived exosomal *miRNA-21* contributes to tumor progression by converting hepatocyte stellate cells to cancer-associated fibroblasts. *J Exp Clin Cancer Res* 2018;**37**:324.
327. Li F, Yan T, Wang S, Wen X. Exosome-associated *miRNA-99a-5p* targeting BMPR2 promotes hepatocyte apoptosis during the process of hepatic fibrosis. *Clin Exp Med* 2023;**23**:4021−31.
328. Masood N, Basharat Z, Khan T, Yasmin A. Entangling relation of micro RNA-let7, *miRNA-200* and *miRNA-125* with various cancers. *Pathol Oncol Res* 2017;**23**:707−15.
329. Seo SB, Lim J, Kim K, Maeng I, Rho HW, Son HY, et al. Nucleic acid amplification circuit-based hydrogel (NACH) assay for one-step detection of metastatic gastric cancer-derived exosomal miRNA. *Adv Sci* 2024;**11**:e2407621.
330. Wang C, Zhang Y, Liu C, Gou S, Hu S, Guo W. A portable colorimetric point-of-care testing platform for MicroRNA detection based on programmable entropy-driven dynamic DNA network modulated DNA-gold nanoparticle hybrid hydrogel film. *Biosens Bioelectron* 2023;**225**:115073.
331. Geng S, Guo P, Wang J, Zhang Y, Shi Y, Li X, et al. Ultrasensitive optical detection and elimination of residual microtumors with a postoperative implantable hydrogel sensor for preventing cancer recurrence. *Adv Mater* 2024;**36**:e2307923.
332. Li M, Pu J, Cao Q, Zhao W, Gao Y, Meng T, et al. Recent advances in hydrogel-based flexible strain sensors for harsh environment applications. *Chem Sci* 2024;**15**:17799−822.
333. Qi M, Han Y, Zhang W, Liu Y, Jiang D, Wu Z, et al. Advances and future perspectives in hydrogel-based sensing technologies: a comprehensive review. *Nanotechnology* 2025;**36**:342001.

334. Ou J, Zhang J, Alswadeh M, Zhu Z, Tang J, Sang H, et al. Advancing osteoarthritis research: the role of AI in clinical, imaging and omics fields. *Bone Res* 2025;**13**:48.
335. Ma Y, Yin Y, Ni L, Miao H, Wang Y, Pan C, et al. Thermo-responsive imprinted hydrogel with switchable sialic acid recognition for selective cancer cell isolation from blood. *Bioact Mater* 2021;**6**: 1308−17.
336. Hou M, Yin X, Jiang J, He J. DNAzyme-triggered sol−gel−sol transition of a hydrogel allows target cell enrichment. *ACS Appl Mater Interfaces* 2021;**13**:15031−9.
337. Surappa S, Multani P, Parlatan U, Sinawang PD, Kaifi J, Akin D, et al. Integrated "lab-on-a-chip" microfluidic systems for isolation, enrichment, and analysis of cancer biomarkers. *Lab Chip* 2023;**23**: 2942−58.
338. Sabirova A, Florica CF, Pisig Jr F, Syed A, Buttner U, Li X, et al. Nanoporous membrane fabrication by nanoimprint lithography for nanoparticle sieving. *Nanoscale Adv* 2022;**4**:1119−24.
339. Ye Q, Ling S, Zheng S, Xu X. Liquid biopsy in hepatocellular carcinoma: circulating tumor cells and circulating tumor DNA. *Mol Cancer* 2019;**18**:114.
340. Zhang Q, Rong Y, Yi K, Huang L, Chen M, Wang F. Circulating tumor cells in hepatocellular carcinoma: single-cell based analysis, preclinical models, and clinical applications. *Theranostics* 2020;**10**: 12060−71.
341. Sun W, You X, Zhao X, Zhang X, Yang C, Zhang F, et al. Precise capture and dynamic release of circulating liver cancer cells with dual-histidine-based cell imprinted hydrogels. *Adv Mater* 2024;**36**: e2402379.
342. Lin Y, Jiang L, Huang Y, Yang Y, He Y, Lu C, et al. DNA-mediated reversible capture and release of circulating tumor cells with a multivalent dual-specific aptamer coating network. *Chem Commun* 2019;**55**:5387−90.
343. Li L, Shen Y, Tang Z, Yang Y, Fu Z, Ni D, et al. Engineered nanodrug targeting oxidative stress for treatment of acute kidney injury. *Explorations* 2023;**3**:20220148.
344. Ye D, Li M, Zhai T, Song P, Song L, Wang H, et al. Encapsulation and release of living tumor cells using hydrogels with the hybridization chain reaction. *Nat Protoc* 2020;**15**:2163−85.
345. Song P, Ye D, Zuo X, Li J, Wang J, Liu H, et al. DNA hydrogel with aptamer-toehold-based recognition, cloaking, and decloaking of circulating tumor cells for live cell analysis. *Nano Lett* 2017;**17**: 5193−8.
346. Ostrom QT, Cote DJ, Ascha M, Kruchko C, Barnholtz-Sloan JS. Adult glioma incidence and survival by race or ethnicity in the United States from 2000 to 2014. *JAMA Oncol* 2018;**4**:1254−62.
347. Conte M, Casas-Tintò S, Soler J. Modeling invasion patterns in the glioblastoma battlefield. *PLoS Comput Biol* 2021;**17**:e1008632.
348. Khan ZM, Munson JM, Long TE, Vlaisavljevich E, Verbridge SS. Development of a synthetic, injectable hydrogel to capture residual glioblastoma and glioblastoma stem-like cells with CXCl12-mediated chemotaxis. *Adv Healthcare Mater* 2023;**12**:e2300671.
349. Zhu L, Lin H, Wan S, Chen X, Wu L, Zhu Z, et al. Efficient isolation and phenotypic profiling of circulating hepatocellular carcinoma cells *via* a combinatorial-antibody-functionalized microfluidic synergetic-chip. *Anal Chem* 2020;**92**:15229−35.
350. May AN, Crawford BD, Nedelcu AM. *In vitro* model-systems to understand the biology and clinical significance of circulating tumor cell clusters. *Front Oncol* 2018;**8**:63.
351. Zuo Y, Lu W, Xia Y, Meng J, Zhou Y, Xiao Y, et al. Glucometer readout for portable detection of heterogeneous circulating tumor cells in lung cancer captured on a dual aptamer functionalized wrinkled cellulose hydrogel interface. *ACS Sens* 2023;**8**:187−96.
352. Lin YN, Nasir A, Camacho S, Berry DL, Schmidt MO, Pearson GW, et al. Monitoring cancer cell invasion and T-cell cytotoxicity in 3D culture. *J Vis Exp* 2020;**23**:e61392.
353. Sabhachandani P, Sarkar S, McKenney S, Ravi D, Evens AM, Konry T. Microfluidic assembly of hydrogel-based immunogenic tumor spheroids for evaluation of anticancer therapies and biomarker release. *J Control Release* 2019;**295**:21−30.
354. Pun S, Prakash A, Demaree D, Krummel DP, Sciumè G, Sengupta S, et al. Rapid biofabrication of an advanced microphysiological system mimicking phenotypical heterogeneity and drug resistance in glioblastoma. *Adv Healthcare Mater* 2024;**13**:e2401876.
355. De Lorenzi F, Hansen N, Theek B, Daware R, Motta A, Breuel S, et al. Engineering mesoscopic 3D tumor models with a self-organizing vascularized matrix. *Adv Mater* 2024;**36**:e2303196.
356. Zhang Y, Peng L, Hu K, Gu N. Stress relaxation-induced colon tumor multicellular spheroid culture based on biomimetic hydrogel for nanoenzyme ferroptosis sensitization evaluation. *Adv Healthcare Mater* 2023;**12**:e2202009.
357. Xu R, Yin P, Wei J, Ding Q. The role of matrix stiffness in breast cancer progression: a review. *Front Oncol* 2023;**13**:1284926.
358. Nguyen HD, Lin CC. Viscoelastic stiffening of gelatin hydrogels for dynamic culture of pancreatic cancer spheroids. *Acta Biomater* 2024; **177**:203−15.
359. Najmina M, Ebara M, Ohmura T, Uto K. Viscoelastic liquid matrix with faster bulk relaxation time reinforces the cell cycle arrest induction of the breast cancer cells *via* oxidative stress. *Int J Mol Sci* 2022;**23**:14637.
360. Kölmel DK, Kool ET. Oximes and hydrazones in bioconjugation: mechanism and catalysis. *Chem Rev* 2017;**117**:10358−76.
361. Sinha S, Ayushman M, Tong X, Yang F. Dynamically crosslinked poly(ethylene-glycol) hydrogels reveal a critical role of viscoelasticity in modulating glioblastoma fates and drug responses in 3D. *Adv Healthcare Mater* 2023;**12**:e2202147.
362. Khan AH, Zhou SP, Moe M, Ortega Quesada BA, Bajgiran KR, Lassiter HR, et al. Generation of 3D spheroids using a thiol-acrylate hydrogel scaffold to study endocrine response in ER^+ breast cancer. *ACS Biomater Sci Eng* 2022;**8**:3977−85.
363. Balachander GM, Kotcherlakota R, Nayak B, Kedaria D, Rangarajan A, Chatterjee K. 3D tumor models for breast cancer: whither we are and what we need. *ACS Biomater Sci Eng* 2021;**7**: 3470−86.
364. Teer L, Yaddanapudi K, Chen J. Biophysical control of the glioblastoma immunosuppressive microenvironment: opportunities for immunotherapy. *Bioengineering* 2024;**11**:93.
365. Li W, Zhou Z, Zhou X, Khoo BL, Gunawan R, Chin YR, et al. 3D biomimetic models to reconstitute tumor microenvironment *in vitro*: spheroids, organoids, and tumor-on-a-chip. *Adv Healthcare Mater* 2023;**12**:e2202609.
366. Cassereau L, Miroshnikova YA, Ou G, Lakins J, Weaver VM. A 3D tension bioreactor platform to study the interplay between ECM stiffness and tumor phenotype. *J Biotechnol* 2015;**193**:66−9.
367. Bhattacharya S, Calar K, de la Puente P. Mimicking tumor hypoxia and tumor−immune interactions employing three-dimensional *in vitro* models. *J Exp Clin Cancer Res* 2020;**39**:75.
368. Li Y, Kumacheva E. Hydrogel microenvironments for cancer spheroid growth and drug screening. *Sci Adv* 2018;**4**:eaas8998.
369. Solbu AA, Caballero D, Damigos S, Kundu SC, Reis RL, Halaas Ø, et al. Assessing cell migration in hydrogels: an overview of relevant materials and methods. *Mater Today Bio* 2023;**18**:100537.
370. Wu Y, Xiao Y, Yin B, Wong SHD. Dynamic hydrogels: adaptive biomaterials for engineering tumor microenvironment and cancer treatment. *Int J Mol Sci* 2025;**26**:9502.
371. Dai G, Feinberg AW, Wan LQ. Recent advances in cellular and molecular bioengineering for building and translation of biological systems. *Cell Mol Bioeng* 2021;**14**:293−308.
372. Cui Y, Hu J, Dong Z, Li B, Chang C. Temperature-triggered inflatable hydrogel muscles with snap-through instability for untethered robots. *Nat Commun* 2025;**16**:3384.
373. Zhang J, Fu K, Wang D, Zhou S, Luo J. Refining hydrogel-based sorbent design for efficient toxic metal removal using machine learning-bayesian optimization. *J Hazard Mater* 2024; **479**:135688.

374. Boateng D, Li X, Wu W, Yang A, Gul A, Kang Y, et al. Air-writing recognition enabled by a flexible dual-network hydrogel-based sensor and machine learning. *ACS Appl Mater Interfaces* 2024;**16**: 54555−65.
375. Deng D, Liang L, Su K, Gu H, Wang X, Wang Y, et al. Smart hydrogel dressing for machine learning-enabled visual monitoring and promote diabetic wound healing. *Nano Today* 2025;**60**:102559.
376. Suwardi A, Wang F, Xue K, Han MY, Teo P, Wang P, et al. Machine learning-driven biomaterials evolution. *Adv Mater* 2022;**34**: e2102703.
377. Liao H, Hu S, Yang H, Wang L, Tanaka S, Takigawa I, et al. Data-driven *de novo* design of super-adhesive hydrogels. *Nature* 2025;**644**: 89−95.
378. Negut I, Bita B. Exploring the potential of artificial intelligence for hydrogel development—a short review. *Gels* 2023;**9**:845.
379. Seifermann M, Reiser P, Friederich P, Levkin PA. High-throughput synthesis and machine learning assisted design of photodegradable hydrogels. *Small Methods* 2023;**7**:e2300553.
380. Xu T, Wang J, Zhao S, Chen D, Zhang H, Fang Y, et al. Accelerating the prediction and discovery of peptide hydrogels with human-in-the-loop. *Nat Commun* 2023;**14**:3880.
381. Zhang W, Rao Y, Wong SH, Wu Y, Zhang Y, Yang R, et al. Transcriptome-optimized hydrogel design of a stem cell niche for enhanced tendon regeneration. *Adv Mater* 2025;**37**:e2313722.
382. Sikander R, Ghulam A, Ali F. XGB-DrugPred: computational prediction of druggable proteins using eXtreme gradient boosting and optimized features set. *Sci Rep* 2022;**12**:5505.
383. Ibrahim SMA, Fang Z, Park J. Phononic crystal-based pH sensing and its classification with machine learning. *Sensor Actuator Phys* 2025;**381**:116064.
384. Wang Z, Xu L, Liu W, Chen Y, Yang Q, Tang Z, et al. Tough, self-healing, adhesive double network conductive hydrogel based on gelatin-polyacrylamide covalently bridged by oxidized sodium alginate for durable wearable sensors. *Int J Biol Macromol* 2024;**276**: 133802.
385. Rajabinasab M, Pakdaman F, Zimek A, Gabbouj M. Randomized PCA forest for approximate k-nearest neighbor search. *Expert Syst Appl* 2025;**281**:126254.
386. Lee YW, Choi JW, Shin EH. Machine learning model for predicting malaria using clinical information. *Comput Biol Med* 2021;**129**: 104151.
387. Lavrentev FV, Rumyantsev IS, Ivanov AS, Shilovskikh VV, Orlova OY, Nikolaev KG, et al. Soft hydrogel actuator for fast machine-learning-assisted bacteria detection. *ACS Appl Mater Interfaces* 2022;**14**:7321−8.
388. Wang P, Wang G, Sun G, Bao C, Li Y, Meng C, et al. A flexible-integrated multimodal hydrogel-based sensing patch. *Nano-Micro Lett* 2025;**17**:156.
389. Cuéllar M, Lapresta-Fernández A, Herrera J, Salinas-Castillo A, Pegalajar Jiménez MdC, Titos-Padilla S, et al. Thermochromic sensor design based on Fe(II) spin crossover/polymers hybrid materials and artificial neural networks as a tool in modelling. *Sensors Actuat B-Chem* 2015;**208**:180−7.
390. Zeng S, Qiu Y, Peng Q, Lin J, Yi N, Wang Z, et al. Neural network-assisted carbon nanotube hydrogel-based dual-modal sensors for material perception. *J Alloys Compd* 2025;**1013**:178534.
391. Ameri A, Akhaee MA, Scheme E, Englehart K. Regression convolutional neural network for improved simultaneous EMG control. *J Neural Eng* 2019;**16**:036015.
392. Wang S, Zhaojia S. Hydrogel and machine learning for soft robots' sensing and signal processing: a review. *J Bionic Eng* 2022;**20**: 845−57.
393. Xu S, Chen X, Wang S, Chen Z, Pan P, Huang Q. Integrating machine learning for the optimization of polyacrylamide/alginate hydrogel. *Regen Biomater* 2024;**11**:rbae109.
394. Qiu Y, Ye H, Zhang H, Zheng Y. Machine learning-driven optimization design of hydrogel-based negative hydration expansion metamaterials. *Comput Aided Des* 2023;**166**:103631.
395. Zhou Y, Tao L, Qiu J, Xu J, Yang X, Zhang Y, et al. Tumor biomarkers for diagnosis, prognosis and targeted therapy. *Signal Transduct Targeted Ther* 2024;**9**:132.
396. Chen D, Wang Y, Wei Y, Lu Z, Ju H, Yan F, et al. Size-coded hydrogel microbeads for extraction-free serum multi-mirnas quantifications with machine-learning-aided lung cancer subtypes classification. *Nano Lett* 2025;**25**:453−60.
397. Li C, Wang Z, Ding P, Zhou Z, Chen R, Hu Y, et al. A digital score based on circulating-tumor-cells-derived mrna quantification and machine learning for early colorectal cancer detection. *ACS Nano* 2025;**19**:18117−28.
398. Boztepe C, Yuceer M, Kunkul A, Şölener M, Kabasakal O. Prediction of the deswelling behaviors of pH- and temperature-responsive poly(NIPAAm-*co*-AAc) IPN hydrogel by artificial intelligence techniques. *Res Chem Intermed* 2020;**46**:409−28.
399. Al-Rajabi MM, Alzyod S, Patel A, Teow YH. A hybrid machine learning framework for predicting drug-release profiles, kinetics, and mechanisms of temperature-responsive hydrogels. *Polym Bull* 2025; **82**:2911−32.
400. Parvin N, Joo SW, Jung JH, Mandal TK. Multimodal ai in biomedicine: pioneering the future of biomaterials, diagnostics, and personalized healthcare. *Nanomaterials* 2025;**15**:895.
401. Xiang Y, Shimoyama K, Shirasu K, Yamamoto G. Machine learning-assisted high-throughput molecular dynamics simulation of high-mechanical performance carbon nanotube structure. *Nanomaterials* 2020;**10**:2459.
402. Greener JG, Kandathil SM, Moffat L, Jones DT. A guide to machine learning for biologists. *Nat Rev Mol Cell Biol* 2022;**23**:40−55.
403. Lee J, Oh SJ, An SH, Kim WD, Kim SH. Machine learning-based design strategy for 3D printable bioink: elastic modulus and yield stress determine printability. *Biofabrication* 2020;**12**:035018.
404. Cadamuro F, Piazzoni M, Gamba E, Sonzogni B, Previdi F, Nicotra F, et al. Artificial intelligence tool for prediction of ecm mimics hydrogel formulations *via* click chemistry. *Biomater Adv* 2025;**175**:214323.
405. Jiang L, Wufang Y, Xie L, Liu Y, Wang X, Wu X, et al. Experimental study on mechanism of stable drag reduction with hydrogel interface. *Tribol Int* 2022;**178**:108013.
406. Liu Y, Li Y, Shang H, Zhong W, Wang Q, Mequanint K, et al. Underwater instant adhesion mechanism of self-assembled amphiphilic hemostatic granular hydrogel from andrias davidianus skin secretion. *iScience* 2022;**25**:105106.
407. Torres C, Quezada T, Kharissova O, Kharisov B, Gómez I. Carbon-based aerogels and xerogels: synthesis, properties, oil sorption capacities, and DFT simulations. *J Environ Chem Eng* 2021;**9**: 104886.
408. Ahadian S, Naito U, Velappa Jayaraman S, Darvishi S, Estili M, Liang X, et al. Fabrication of poly(ethylene glycol) hydrogels containing vertically and horizontally aligned graphene using dielectrophoresis: an experimental and modeling study. *Carbon* 2017;**123**: 460−70.
409. Kocaaga B, Inan T, Yasar N, Yalcin CE, Sungur FA, Kurkcuoglu O, et al. Innovative use of an injectable, self-healing drug-loaded pectin-based hydrogel for micro- and supermicro-vascular anastomoses. *Biomacromolecules* 2024;**25**:3959−75.
410. Dai X, Chen L, Liao Y, Sheng M, Qu Q, Shi Y, et al. Formulation design and mechanism study of hydrogel based on computational pharmaceutics theories. *J Mol Graph Model* 2022; **110**:108051.
411. Kaufman F, David M, Zaiden M, Shabat D, Amiram M. Imparting new stimuli-responsive behaviors in protein-polymers *via* self-immolative linker conjugation. *J Mater Chem B* 2025;**13**: 12276−92.
412. Wang X, Wang Y, Wang J, Li Z, Zhang J, Li J. *In silico* design of photoresponsive peptide-based hydrogel with controllable structural and rheological properties. *Colloids Surf* 2023;**663**:131020.
413. Yong X, Kuksenok O, Balazs AC. Modeling free radical polymerization using dissipative particle dynamics. *Polymer* 2015;**72**:217−25.

414. Lei J, Xu S, Li Z, Liu Z. Study on large deformation behavior of polyacrylamide hydrogel using dissipative particle dynamics. *Front Chem* 2020;**8**:115.
415. Sharifikia D, Salem Yafia M, Fradet G, Mohammadi H. Design and fabrication of a 3D scaffold for the aortic root tissue engineering application. *J Med Biol Eng* 2018;**38**:211−21.
416. Xu S, Yu JX, Guo H, Tian S, Long Y, Yang J, et al. Force-induced ion generation in zwitterionic hydrogels for a sensitive silent-speech sensor. *Nat Commun* 2023;**14**:219.
417. Song X, Lu G, Wang J, Zheng J, Sui S, Li Q, et al. Molecular dynamics-assisted design of high temperature-resistant polyacrylamide/poloxamer interpenetrating network hydrogels. *Molecules* 2022;**27**:5326.
418. Hagita K, Tominaga T, Hatazoe T, Sone T, Morita H, Takano H. Two dimensional scattering patterns analysis of coarse grained molecular dynamics simulation on filled composites of end modified SBR. *Int J Polym Sci* 2017;**44**:35−40.
419. Quesada-Pérez M, Martín-Molina A. Solute diffusion in gels: thirty years of simulations. *Adv Colloid Interface Sci* 2021;**287**:102320.
420. Ahmadi M, Aliabadian E, Liu B, Lei X, Khalilpoorkordi P, Hou Q, et al. Comprehensive review of the interfacial behavior of water/-oil/surfactant systems using dissipative particle dynamics simulation. *Adv Colloid Interface Sci* 2022;**309**:102774.
421. Mayoral E, Goicochea AG. Modeling of branched thickening polymers under poiseuille flow gives clues as to how to increase a solvent's viscosity. *J Phys Chem B* 2021;**125**:1692−704.
422. Lei J, Li Z, Xu S, Liu Z. Recent advances of hydrogel network models for studies on mechanical behaviors. *Acta Mech Sin* 2021;**37**:367−86.
423. Gao Y, Peng K, Mitragotri S. Covalently crosslinked hydrogels *via* step-growth reactions: crosslinking chemistries, polymers, and clinical impact. *Adv Mater* 2021;**33**:e2006362.
424. Smola-Dmochowska A, Lewicka K, Macyk A, Rychter P, Pamuła E, Dobrzyński P. Biodegradable polymers and polymer composites with antibacterial properties. *Int J Mol Sci* 2023;**24**:7473.
425. Huang H, Ge H, Ren Z, Huang Z, Xu M, Wang X. Controllable synthesis of biocompatible fluorescent carbon dots from cellulose hydrogel for the specific detection of Hg_2. *Front Bioeng Biotechnol* 2021;**9**:617097.
426. Peng S, Fu H, Li R, Li H, Wang S, Li B, et al. A new direction in periodontitis treatment: biomaterial-mediated macrophage immunotherapy. *J Nanobiotechnol* 2024;**22**:359.
427. Kao ECY, Seo J, McCanna DJ, Subbaraman LN, Jones LW. *In vitro* assessment of the biocompatibility of chemically treated silicone materials with human lens epithelial cells. *Sci Rep* 2022;**12**:4649.
428. Zhu P, Chen J, Li P, Xu S. Limitation of water-soluble tetrazolium salt for the cytocompatibility evaluation of zinc-based metals. *Materials* 2021;**14**:6247.
429. Feng S, Pan Y, Lu P, Li N, Zhu W, Hao Z. From bench to bedside: the application of cannabidiol in glioma. *J Transl Med* 2024;**22**:648.
430. Fu Z, Qu Y, Wu Y, Xu Y, Zhang H, Tang Y, et al. Piezoelectric poly(3-hydroxybutyrate-*co*-3-hydroxyhexanoate) (PHBHHx) microspheres for collagen regeneration and skin rejuvenation. *Front Bioeng Biotechnol* 2025;**13**:1554825.
431. Constantino VRL, Figueiredo MP, Magri VR, Eulálio D, Cunha VRR, Alcântara ACS, et al. Biomaterials based on organic polymers and layered double hydroxides nanocomposites: drug delivery and tissue engineering. *Pharmaceutics* 2023;**15**:413.
432. Kammona O, Tsanaktsidou E, Kiparissides C. Recent developments in 3d-(bio)printed hydrogels as wound dressings. *Gels* 2024;**10**:147.
433. Alshehri AM, Wilson OC. Biomimetic hydrogel strategies for cancer therapy. *Gels* 2024;**10**:437.
434. Chen Y, Wang X, Tao S, Wang Q, Ma PQ, Li ZB, et al. Research advances in smart responsive-hydrogel dressings with potential clinical diabetic wound healing properties. *Milit Med Res* 2023;**10**:37.
435. Levin L, Sheldon M, McDonough RS, Aronson N, Rovers M, Gibson CM, et al. Early technology review: towards an expedited pathway. *Int J Technol Assess Health Care* 2024;**40**:e13.
436. Köckerling F, Simon T, Hukauf M, Hellinger A, Fortelny R, Reinpold W, et al. The importance of registries in the postmarketing surveillance of surgical meshes. *Ann Surg* 2018;**268**:1097−104.
437. Satyamitra MM, Andres DK, Bergmann JN, Hoffman CM, Hogdahl T, Homer MJ, et al. Overlapping science in radiation and sulfur mustard exposures of skin and lung: consideration of models, mechanisms, organ systems, and medical countermeasures: overlapping science in radiation and sulfur mustard injuries to lung and skin. *Disaster Med Public Health Prep* 2023;**17**:e552.
438. Ding X, Fan L, Wang L, Zhou M, Wang Y, Zhao Y. Designing self-healing hydrogels for biomedical applications. *Mater Horiz* 2023;**10**:3929−47.
439. Correa S, Grosskopf AK, Lopez Hernandez H, Chan D, Yu AC, Stapleton LM, et al. Translational applications of hydrogels. *Chem Rev* 2021;**121**:11385−457.
440. Salamone M, Rigogliuso S, Nicosia A, Campora S, Bruno CM, Ghersi G. 3D collagen hydrogel promotes *in vitro* langerhans islets vascularization through ad-MVFs angiogenic activity. *Biomedicines* 2021;**9**:739.
441. Cong B, Zhang H. Innovative 3D printing technologies and advanced materials revolutionizing orthopedic surgery: current applications and future directions. *Front Bioeng Biotechnol* 2025;**13**:1542179.
442. Alonso JM, Andrade Del Olmo J, Perez Gonzalez R, Saez-Martinez V. Injectable hydrogels: from laboratory to industrialization. *Polymers* 2021;**13**:650.
443. Pezoulas VC, Zaridis DI, Mylona E, Androutsos C, Apostolidis K, Tachos NS, et al. Synthetic data generation methods in healthcare: a review on open-source tools and methods. *Comput Struct Biotechnol J* 2024;**23**:2892−910.
444. Zhang S, Wang H, Liu F, Su Y, Han K, Liu Y, et al. Artificial intelligence-enabled hydrogels: innovations and applications. *J Mater Chem B* 2025;**13**:14967−81.
445. Zheng S, Zhu Z, Sun D-W. From material-derived to artificial intelligence-empowered intelligent hydrogels. *Coord Chem Rev* 2026;**549**:217198.
446. Zhu M, Li S, Kuang Y, Hill VB, Heimberger AB, Zhai L, et al. Artificial intelligence in the radiomic analysis of glioblastomas: a review, taxonomy, and perspective. *Front Oncol* 2022;**12**:924245.
447. Benerradi J, Clos J, Landowska A, Valstar MF, Wilson ML. Benchmarking framework for machine learning classification from fNIRS data. *Front Neuroergon* 2023;**4**:994969.
448. Ren X, Wei J, Luo X, Liu Y, Li K, Zhang Q, et al. Hydrogelfinder: a foundation model for efficient self-assembling peptide discovery guided by non-peptidal small molecules. *Adv Sci* 2024;**11**:e2400829.
449. Saberian E, Jenča A, Petrášová A, Zare-Zardini H, Ebrahimifar M. Application of scaffold-based drug delivery in oral cancer treatment: a novel approach. *Pharmaceutics* 2024;**16**:802.
450. Wei L, Zhu J, Wang Q, He Y, Yan H, Gao L, et al. Injectable thermosensitive hydrogel co-loading with ATRi and doxorubicin for the treatment of triple-negative breast cancer. *RSC Adv* 2025;**15**:20385−96.
451. Lei D, Wang W, Zhao J, Zhou Y, Chen Y, Dai J, et al. An injectable gambogic acid loaded nanocomposite hydrogel enhances antitumor effect by reshaping immunosuppressive tumor microenvironment. *Mater Today Bio* 2025;**31**:101611.
452. Wu H, Liu Z, Zhang Z, Liu Z, Gao Z, Mamtilahun M, et al. Injectable micropore-forming microgel scaffold for neural progenitor cells transplantation and vascularization after stroke. *Nat Commun* 2025;**16**:9285.
453. Men W, Zhu P, Dong S, Liu W, Zhou K, Bai Y, et al. Layer-by-layer pH-sensitive nanoparticles for drug delivery and controlled release with improved therapeutic efficacy *in vivo*. *Drug Deliv* 2020;**27**:180−90.
454. Paik BA, Mane SR, Jia X, Kiick KL. Responsive hybrid (Poly)-peptide-polymer conjugates. *J Mater Chem B* 2017;**5**:8274−88.
455. Ma W, Wang X, Zhang D, Mu X. Research progress of disulfide bond based tumor microenvironment targeted drug delivery system. *Int J Nanomed* 2024;**19**:7547−66.

456. Bi Y, Xie S, Li Z, Dong S, Teng L. Precise nanoscale fabrication technologies, the "last mile" of medicinal development. *Acta Pharm Sin B* 2025;**15**:2372−401.
457. Parvin N, Joo SW, Mandal TK. Injectable biopolymer-based hydrogels: a next-generation platform for minimally invasive therapeutics. *Gels* 2025;**11**:383.
458. Hu W, Ye B, Yu G, Yang H, Wu H, Ding Y, et al. Dual-responsive supramolecular polymeric nanomedicine for self-cascade amplified cancer immunotherapy. *Adv Sci* 2024;**11**:e2305382.
459. Kim MH, Lin CC. Assessing monocyte phenotype in poly(γ-glutamic acid) hydrogels formed by orthogonal thiol-norbornene chemistry. *Biomed Mater* 2021;**16**:045027.
460. Thongpon P, Tang M, Cong Z. Peptide-based nanoparticle for tumor therapy. *Biomedicines* 2025;**13**:1415.
461. Mohammadzadeh V, Atapour-Mashhad H, Shahvali S, Salehi B, Shaban M, Shirzad M, et al. Hydrogels as advanced drug delivery platforms for cancer immunotherapy: promising innovations and future outlook. *J Nanobiotechnol* 2025;**23**:545.
462. Maheshwari S, Akram H, Bulstrode H, Kalia SK, Morizane A, Takahashi J, et al. Dopaminergic cell replacement for parkinson's disease: addressing the intracranial delivery hurdle. *J Parkinsons Dis* 2024;**14**:415−35.
463. Huang S, Zhao Y, Shen J. Advances in integrating biomaterials with CAR-T cells for enhancing solid tumor therapy. *Chin J Cancer Res* 2025;**37**:742−58.
464. Wang X, Luo W, Chen Z, Li C, Zhou J, Huang Z, et al. Co-expression of IL-15 and CCL21 strengthens CAR-NK cells to eliminate tumors in concert with T cells and equips them with PI3K/AKT/mTOR signal signature. *J Immunother Cancer* 2025;**13**:e010822.
465. Deuse T, Schrepfer S. Progress and challenges in developing allogeneic cell therapies. *Cell Stem Cell* 2025;**32**:513−28.
466. Kuan CH, Chang L, Ho CY, Tsai CH, Liu YC, Huang WY, et al. Immunomodulatory hydrogel orchestrates pro-regenerative response of macrophages and angiogenesis for chronic wound healing. *Biomaterials* 2025;**314**:122848.